Optical characterisation of the interaction between calcium-silicate based dental restorative materials and dentine

Atmeh, Amre

Awarding institution:
King's College London

Optical characterisation of the interaction between calcium-silicate based dental restorative materials and dentine

Amre Ragheb Atmeh

Biomaterials, Biomimetics and Biophotonics

Dental Institute, King's College London

April 2013

Thesis submitted for the degree of Doctor of Philosophy at King's College London, 2013

Abstract

Since their introduction to dentistry, calcium silicate based cements have been mainly used for endodontic applications, principally due to their long setting time. Recently, a new formulation of this cement was produced as a coronal restorative material. The aim of this project was to study the nature and dynamics of the interface between this calcium silicate based dental restorative material (Biodentine^{TM}) with human dentine in comparison with glass ionomer cement, and to investigate its capability to induce dentine remineralisation. Different optical, microscopic, and fluorescent labelling techniques have been applied; such as tandem scanning and laser scanning confocal microscopy, which were both used with cement labelling and micropermeability tests to evaluate the interfacial morphology and microscopic appearance along with scanning electron microscopy. Additionally, two-photon fluorescence microscopy was applied in conjugation with Tetracycline labelling to study dentine remineralisation induced by the Biodentine cement; this novel combination provided a useful technique for the observation of mineral formation inside the organic matrix of demineralised dentine when aged in an in-vitro model. Fluorescence lifetime imaging and second harmonic generation imaging were also used for the characterisation of re-mineralisaion and collagen denaturation respectively. For the chemical analysis, Raman spectroscopy was applied to analyse the chemical composition of the cement and the changes associated with its hydration and ageing in different conditions. Micro-Raman imaging was also applied to quantify and model the infiltration of the cement's hydration products into the dentine. Results indicated an interactive interface between the Biodentine and sound dentine, mediated by the alkaline caustic effect of the cement on the dentine's organic component, which was associated with mineral transfer, and led to the formation of what we described as a "Mineral Infiltration zone" (MIZ). This later explained the ability of Biodentine to induce remineralisation of dentine and the formation of apatite structures, which indicated the bioactivity of the cement.

Table of Contents

Table of Contents....3
Table of Figures....5
Table of Tables....11
Acknowledgements....12
Introduction....13
Chapter 1 Literature review....16
1.1 Dental Biomaterials....16
1.1.1 Calcium silicate cements:....16
1.1.2 Glass ionomer cements:....19
1.1.3 Dentine remineralisation:....21
1.2 Optics....24
1.2.1 Introduction to optics....24
1.2.2 Fluorescence and fluorophores....26
1.2.3 Non-linear optics:....28
1.3 Optical investigation techniques....30
1.3.1 Confocal microscopy....30
1.3.2 Two-photon fluorescence microscopy....32
1.3.3 Raman spectroscopy....34
1.4 Optical investigation techniques in dental research....36
1.4.1 Confocal microscopy and extrinsic fluorophores....36
1.4.2 Auto-fluorescence in dental research....36
1.4.3 Second harmonic generation microscopy....41
1.4.4 Backscattered electron-Scanning electron microscopy....42
1.4.5 Raman spectroscopy....42
1.5 Aims & Objectives:....44
Chapter 2 Raman spectroscopic characterisation of the Biodentine, and its surface carbonation rate.....45
1.1 Introduction:....45
1.2 Materials and Methods:....46
1.2.1 Sample preparation....46
1.2.2 Raman spectroscopy....47
1.3 Results:....49

1.4 Discussion: 53
1.5 Conclusions: 57
Chapter 3 Chemo-morphological characterization of the dentine Biodentine interface in comparison with glass ionomer cement. 58
2.1 Introduction: 58
2.2 Material and Methods: 59
2.2.1 Sample preparation 59
2.2.2 Imaging & data analysis 66
2.3 Results: 69
2.3.1 Tag like structures 69
2.3.2 Dye-infiltrated zone 71
2.3.3 Chemical mapping 76
2.3.4 Horizontal lines 76
2.4 Discussion: 79
2.5 Suggested model for the horizontal lines: 83
2.5.1 Dentinal tubule micro-branches: 85
2.5.2 Trans-tubular septa 86
2.6 Conclusions: 89
Chapter 3 Calcium silicate cement -induced remineralisation of totally demineralised dentine in comparison with glass ionomer cement: Tetracycline labelling and two-photon fluorescence microscopy. 90
3.1 Introduction: 90
3.2 Materials and Methods: 93
3.2.1 Sample preparation 93
3.2.2 Imaging: 94
3.3 Results: 97
3.3.1 Dentine degradation: 97
3.3.2 Two-photon fluorescence imaging 97
3.3.3 Raman spectroscopy 108
3.4 Discussion: 110
3.5 Conclusions: 116
Chapter 5 Discussion 117
Chapter 6 Future Work 121

Publications.....123
References.....129

Table of Figures

Figure 1: A Jablonski diagram demonstrating the changes in the energy states of molecules associated with different optical phenomena; **(a)** Rayleigh scattering occurs when incident photons are scattered in a different direction but at the same energy state, which does not affect the energy status of illuminated matter. Non-elastic scattering occurs when the incident photons are scattered with reduced **(b)** energy and described as Stokes shift, or increased **(c)** energy which is described as an anti-Stokes shift. **(d)** Fluorescence occurs when the photon energy is fully absorbed by the fluorophore, and re-emitted with different energy and wavelength. **(e)** Two-photon excitation requires two photons with half of the fluorescence excitation energy each to excite the fluorophore and induce fluorescence. 25

Figure 2: Nonlinear optics: This diagram demonstrates the linear (a) versus non-linear (b & c) optics. New G (2011). Introduction *In*: *Introduction to nolinear optics*. Cambridge Cambridge University Press, pp 4. 29

Figure 3: Second harmonic generation occurs as a result of the electron motion in non-centrosymmetric molecules when affected by the electromagnetic waves within the optical field of an intense laser (b), which does not occur in symmetric molecules (a). This interaction generates an additional frequency component with double the frequency (2ω) of the illuminating light, which is the SHG signal, beside the usual linear component that results in Rayleigh scattering. Mertz J. Applications of Second-Harmonic Generation Microscopy .in: Masters BR and So P (eds). Handbook of biomedical nonlinear optical microscopy. Oxford University Press 31

Figure 4: Averaged Raman spectra for the un-hydrated Biodentine powder (Red) and hydrated Biodentine cement (black) after 7 days. 50

Figure 5: Normalised Raman spectra of hydrated Biodentine cement showing the 1088 cm^{-1} peak, which represents the carbonate. The intensity of this peak increased overtime as the cement was stored in deionised water while exposed

to atmospheric conditions. This allowed the carbonation of the cement's hydration products, which explains this increase. 52

Figure 6: The change in the intensity of calcium carbonate forming on the surface of Biodentine cement blocks is demonstrated by the change in the intensity of the carbonate Raman peak at 1088 cm^{-1} relative to 470 cm^{-1} Raman peak, which represents ZrO_2 that was considered as the internal standard. This change was much faster in the samples that were stored in carbonate /bicarbonate buffer (red) in comparison with the samples stored in water (blue). 53

Figure 7: Micropermeability test. After sectioning their roots, filled teeth were mounted up-side down in a small water filled container. A fluorescent dye solution (Rhodamine-B) was added to the pulp chamber and maintained for 3 hours before it was washed away and crowns were sectioned and polished for imaging. 62

Figure 8:(a) Raman area maps were obtained for the dentine-cement interface in GIC and Biodentine filled teeth using the StreamLine™ scanning from point X to Y. Raman spectral maps were analysed with a curve fitting software which averaged each area map into a single line, where each point on that line was represented by an averaged Raman spectrum **(b)**. From the cements' Raman spectra **(c)**, representative characteristic peaks; 1082 cm^{-1} and 1262 cm^{-1} (marked with asterisks) were designated for Biodentine and GI cements respectively. **(d)** Intensity line profiles were generated for each of these Raman peak, intensity of these peaks were plotted against distance from the interface and the average penetration depth was measured. 68

Figure 9: (a) Reflection mode TSM image for the dentine-Biodentine interface showing the tag-like structures (arrows) X100/ 1.4 NA OI TSM **(b)** Fluorescence mode CLSM image showing the cement tags, which appear on the interfacial surface of the Fluorescein labelled Biodentine (above) after it was pulled away from dentine due to desiccation. 63x/1.4NA OI. **(c)** SEM micrograph of fractured dentine beneath a Biodentine restoration. Tag-like structures were detected forming within the dentinal tubules (arrows). **(d)** A fluorescence mode confocal image for a double labelled sample showing the formation of cement-tags (arrows) by Fluorescein labelled Biodentine (green) in the dentine. Composite image of fields taken at 488/530 and 546/600 nm x63/ 1.4 NA OI.CLSM. 70

Figure 10: (a) Reflection mode TSM image for the dentine-Biodentine interface, the mineral infiltration zone (MIZ) appears as a band of highly reflective dentine beneath the interface, indicating a change in the dentine's mineral content within this zone. The fluorescence mode image of the same area **(b)** shows the distribution of Rhodamine-B dye, which permeated from the pulp chamber into the interface and cement. X100/ 1.4 NA OI TSM. 546/600 nm. 71

Figure 11: **(a-c**). Fluorescence mode CLSM images for the Biodentine and GIC interfaces with dentine. (a1) Distribution of the Fluorescein dye labelling the Biodentine cement shows a band of dye-infiltrated dentine just beneath the interface, this band cannot be seen with Rhodamine-B micropermeability (b1).. Caption is continued next page. 72

Figure 12: (a) Interfacial dentine under Fluorescein labelled GIC. The scalloped appearance of the interfacial layer, which shows the deeper infiltration of the fluorescent dye towards the pulp in areas adjacent to the tubular lumina (arrows), this is caused by the acidic effect of the GIC, which affects the highly mineralised peri-tubular dentine to a greater extent compared with the inter-tubular dentine. **(b)** The interfacial dentine under Fluorescein labelled Biodentine, exhibited the inverse effect, where peri-tubular dark spaces appeared in the interfacial layer, due to the selective caustic etching effect of the alkaline cement, which spared the peri-tubular dentine, and affected the inter-tubular dentine that has much higher protein content. 74

Figure 13: SEM micrographs for fractured dentine discs that were exposed to Biodentine **(a)** or GIC **(b)**. A band of structurally altered dentine is extending along the interface, as can be seen by the obliterated dentine tubules above the dotted line in **(a),** when compared with dentine of the opposing surface where no cement was applied **(c). (b)**no structural changes can be detected in the dentine beneath GIC when compared with dentine of the opposing surface (**d**). 75

Figure 14: In confocal images obtained for Biodentine **(a, b, c)** and GIC (**d)** samples, it was observed that there were a. **(a)** and**(b)** fluorescence mode confocal images for dentine-Biodentine interface x100/1.4 NA OI TSM. Fig (b) shows clearly the presence of trans-tubular microstructures that cross the tubules (arrows). **(c)** A fluorescence mode image for a dentine-Biodentine interface showing the same horizontal lines (arrows) x63/1.4 NA OI CLSM. **(d)**

A fluorescence mode confocal image for dentine -glass ionomer interface under Fluorescein labelled cement (x63/1.4 NA OI CLSM).....77
Figure 15: Reconstructed z-stack image that was taken of mid-coronal dentine after it was soaked in a 0.25% Fluorescein solution for 3 hours, showing the horizontal lines crossing the dentinal tubules.....78
Figure 16: The dual effect of Biodentine on the interfacial dentine is mediated by the diffusion of calcium hydroxide into the intertubular dentine, which induces an alkaline caustic effect on the organic component of dentine, associated with mineral transfer. This diffusion is different than the tubular diffusion of hydration products that occur through the dentinal tubules towards the pulp chamber. ...83
Figure 17: When applying the fluorescent dye (green) inside the dentinal tubules, it infiltrates into these spaces to give the appearance of peri-tubular rings (PTR). In un-erupted or newly erupted teeth (lower ring), these rings do not appear due to the difference in the nature of the substance occupying these spaces, where the dye cannot infiltrate. **(b)** a schematic demonstration for the peri-tubular spaces that are confined within the peri-tubular matrix (yellow). These spaces extend between the tubular lumen (black) and the inter-tubular matrix (red) disturbing the continuity of the peri-tubular dentine. **(c):** Trans-tubular septa (TS), which are formed by central extensions of the lamina limitans (LL), extend towards the tubular space (TS) and attach the odontoblastic process membrane (OPM). These septa enclose the fibrous material (F) that is believed to extend from the inter-tubular matrix through the peri-tubular rings and the lumen of dentinal tubules. in un-erupted or newly erupted teeth. OBP: Odontoblastic process.....85
Figure 18: Sample preparation. Dentine discs (1.5 mm) cut from extracted third molars **(a)** and demineralised using EDTA **(b)**. Cement blocks of Biodentine (or GIC) were placed under the dentine discs **(d)** after the cement was mixed and packed in square shaped moulds for 30 min **(c).**.....94
Figure 19: Sample storage. Samples with Biodentine **(a)** or GIC **(b)** cements were stored for eight weeks in designated storage media. B: Biodentine™, G: GIC, T: Tetracycline, P: PBS, W: Water.....95
Figure 20: Samples sectioning. Before imaging, dentine discs were collected from the storage media and cleaned before they were included in light-cured

polymethyl-metharcylate sheets in order to section the discs and image the sectioned surface.....96
Figure 21: A photograph taken of the inner surface of the shell-like structure of the remineralised dentine after ageing in a phosphate rich medium with calcium silicate cement Biodentine. The inset shows the location of this remaining structure.....98
Figure 22: Comparing the fluorescence intensity of the demineralised dentine discs after storage with the Biodentine cement in: **(a)** Tetracycline and PBS solution (BTP). **(b)** Tetracycline and water (BTW). **(c)** Tetracycline and PBS without the cement (DTP)**. (d)** PBS alone (BP)**.** The fluorescence intensity of these images have been standardised to exhibit the real difference among the different groups. The insets show the same images after enhancing the fluorescence intensity. 99
Figure 23: The average fluorescence intensity of each dentine group after 8-week storage in different media with the Biodentine cement (BTP, BTW, BP), or without the cement (DTP). 100
Figure 24: Fluorescence intensity ratio between ageing of totally demineralised dentine in phosphate rich media and phosphate –free media with the Biodentine cement or GIC.....100
Figure 25: The average fluorescence lifetime of each dentine group after 8-week storage in different media with the Biodentine cement (BTP, BTW, BP), or without the cement (DTP). Fluorescence lifetime was also measured for sound and totally demineralised dentine, as well as for Tetracycline in its free or Ca^{2+} forms.....101
Figure 26: Two-photon fluorescence mode image for a demineralised dentine sample stored with Biodentine in PBS solution and Tetracycline. The mineralisation front (arrows) appears to separate between the highly fluorescent mineralising areas below, and the less fluorescent dentine matrix above.....105
Figure 27:Intra-tubular mineralisation: Highly fluorescent structures (black arrows) are aligned within the widely opened dentinal tubules indicating intra-tubular mineralisation. Micron sized spherules (Black arrow heads) can be detected between the tubules in the inter-tubular matrix.....105
Figure 28: Intertubular mineralisation**. (a)** Two-photon fluorescence mode image showing fluorescent spherules (arrow heads) within the intertubular

dentine matrix of demineralised dentine samples that were stored with the Biodentine cement in tetracycline and PBS (BTP group). **(b)** Higher magnification image shows the arrangement of these spherules in organized architecture. The dentinal tubules are totally obliterated with minerals. **(c)** A plot profile for the white line drawn in Figure-a showing the size of these spherules to be around 1 µm. 106

Figure 29: Inter-tubular mineralisation. Two-photon fluorescence intensity image showing highly fluorescent granular structures arranged in patterns along with acicular structures (arrow) in the inter-tubular matrix of dentine samples stored with the Biodentine cement in tetracycline and PBS. 107

Figure 30: Two-photon fluorescence mode image showing acicular microstructures (arrows) forming within the inter-tubular matrix of demineralised dentine after storage with Biodentine in a PBS solution and Tetracycline. 107

Figure 31: Back scattered electron SEM images for remineralised dentine discs after storage in phosphate rich media with Biodentine (BTP and BP). Micro-structural features of mineralisation; mineralisation lines (**a**), intra-tubular mineralisation (**b**), and intertubular mineralisation (**c**) were detectable with this imaging technique. The arrangement of intertubular mineralisation in regular patterns (**d**) might reflect the influence of the organic matrix in the deposition and arrangement of the forming minerals. Accelerating voltage=20 kV, current=626 pA. 108

Figure 32: Two-photon fluorescence mode images of demineralised dentine after storage with glass ionomer cement in a PBS solution and tetracycline (GTP), showing no signs of intra- or inter-tubular mineralisation, with no structural changes in the matrix except for the increased fluorescence induced by adsorbed Tetracycline **(a).** Adsorption of the tetracycline stain might be responsible for the appearance of annular patterns in these samples **(b),** as well as in the GTW, BTP and BTW. 109

Figure 33: Normalised Raman spectra obtained for demineralised dentine discs after storage for 8 weeks in PBS with the Biodentine (BP), in PBS with GIC (GP), in PBS without cement (DP), in addition to sound dentine (SD). The Raman peaks representing the phosphate's vibrational modes (v1, v2, v3, and v4) in sound dentine (SD) were only detectable in the BP group. No apatite peaks was detectable in the dentine of the other groups. 109

Table of Tables

Table 1: Numbers and ageing conditions for the samples prepared.....47

Table 2: Raman peaks of calcium silicate cements in the hydrated and un-hydrated forms with the designated vibrational modes and chemical bonds of each peak ……51

Table 3: List of the imaging techniques used in the study of the dentin-cement interfaces 60

Table 4: One-way ANOVA statistical analysis to compare the means of the fluorescence intensity among the different groups. (*) The mean difference is significant at the 0.05 level.....102

Table 5: One-way ANOVA statistical analysis to compare the means of the fluorescence lifetime (FLIM) among the different groups. TC: Tetracycline. (*) The mean difference is significant at the 0.05 level. 104

Acknowledgements

By the name of Allah, the most beneficent and the most merciful, to whom is all the praises and thanks for the grants I have been blessed with in my life.

I owe sincere thankfulness to Professor Timothy Watson, my first supervisor, for his support, without which this dissertation would not be possible. I am grateful to him for his guidance and help by all means throughout my PhD study. I would also like to express my gratitude to Dr Frederic Festy, my second supervisor, for the time, effort, and useful critiques, and most importantly his patience while explaining the science behind imaging and microscopy. I appreciate his encouragement and support. I am truly thankful to Professor Gordon Proctor, my coordinator, for his advice and assistance in keeping my progress on schedule.

It gives me great pleasure in acknowledging the help of Professor Alan Boyde from QMUL for his time and expertise in the BSE SEM imaging. I would like to express my very great appreciation to Professor Avijit Banerjee, Dr Sanjukta Deb, and Dr Richard Cook for their valuable opinions and suggestions for the progression of this work. I wish also to thank Dr Giuseppe Cama, Dr Salvatore Sauro, Dr Ee Zuahn Chong, Mr Peter Pilecki, and Mr Richard Mallet for their help and assistance in the lab, and the nice time I had there during the years of my study.

I wish to thank Septodont Company (Saint-Maur-des-fossés Cedex-France) for their generous funding of this project.

My sincere thanks to my parents, for their continuous support throughout the years; I will be always indebted to them. I owe my deepest gratitude to my dear wifefor her limitless support and encouragement, who shared with me all the difficult and pleasant times to finish this dissertation.

Introduction

Life around is all about interactions; from the level of atoms to complicated molecules, from organelles to cells, and from individuals to communities. It is all about the acts and responses between the elements comprising this existence, of which our awareness is pathetically limited by modest perceptual capabilities. Nevertheless, being privileged with much advanced intellectual ability and aptitude has been the key factor that enabled humans to develop, civilise, and most importantly seek understanding of their surroundings. The human mind is the mean that enabled us to surpass our limitations and explore the worlds hidden beyond our senses, which has driven humanity through eras of revolutions to the life we are living now.

A great example of the human mind creativity that contributed invaluably to our knowledge is the invention of the microscope. This remarkable device has disclosed whole worlds of unseen objects of micro- and nano-structures as small as atoms. Starting from a single low-magnification glass lens, microscopes have been developed into a wide range of complicated optical devices of massive magnification and resolution powers. Magnification and microstructural observation are not the only functions of microscopes; based on the variable modes of interaction between the light and matter, microscopes can be used to obtain different types of information such as the chemical composition, crystalline structure, or fluorescence lifetime.

As for all the other fields of research, dental research has extensively benefited from microscopes in the study of dental tissues and materials, and in the understanding of the relation between the two. This has had a remarkable influence on the dental profession and reflected positively on the quality and level of the dental care provided, which demonstrates the integral role of research in dentistry. Using microscopes as well as other advanced testing and exploratory devices in dental research has also synchronised its development with the other fields. Recruiting the latest technologies, which were the product

of research in other fields, for the study of teeth, microorganisms, or materials is a good example of this synchrony.

Despite the massive leaps that have been achieved, we are still vulnerable to a countless number of risks and factors that distress our daily life. Dental caries is among the most common diseases affecting humans, and the most challenging problem to manage for dentists. This is accounted by the complexity of the structure of the dental tissues on one hand, and the lack of a proper material to restore or replace the lost tissues on the other. In the search for a proper “ideal” material, a wide range of restorative materials have been introduced over the past years, and many more were discontinued, which created that dynamic action between development and research. In this context, an interesting development was the introduction of constructions cement, after proper modification, into the dental clinic. Since their first introduction in 1993 as mineral tri-oxide aggregates (MTA), calcium silicate based cements have had a growing attention and a widening range of clinical applications, such that recently a new formulation of this cement was developed as a coronal restorative material. Being of a relatively short initial setting time and a rich source of calcium ions, this type of restorative material could have a potential application for the management of dental caries by encouraging the remineralisation of carious dentine.

The aim of this work was to study and characterise the interface between calcium silicate based coronal restorative materials and dentine, and compare it with equivalent materials such as the glass ionomer cement. The experiments were divided into three main studies, where we firstly characterised the calcium silicate based restorative material before and after hydration using micro-Raman spectroscopy, and studied the chemical changes associated with ageing in deionised water. In the second study we examined the interface between the cements and sound dentine when aged in deionised water using confocal laser scanning microscopy (CLSM), scanning electron microscopy (SEM), micro-Raman spectroscopy, and second harmonic generation imaging. In the third study we examined the remineralisation potential of these cements on totally demineralised dentine when aged in a phosphate containing solution,

which was conducted using two-photon fluorescence and fluorescence lifetime imaging in conjugation with Tetracycline labelling. These studies were concluded with a suggested future work for potential areas of research continuation.

Chapter 1 Literature review

1.1 Dental Biomaterials

1.1.1 Calcium silicate cements:

Calcium silicate based cements were first introduced to dentistry in 1993 when Torabinejad developed a formula based on ordinary Portland cement (OPC) to produce the mineral trioxide aggregate, or the gray MTA (Lee *et al.* 1993). This material was basically composed of tri-calcium silicate, di-calcium silicate, tri-calcium aluminate, and tetra-calcium aluminoferrite, in addition to calcium sulphate, and bismuth oxide which was added as a radiopaqer to suit the clinical application of the MTA (Funteas *et al.* 2003, Song *et al.* 2006, Howard *et al.* 2008). In 2002, a white version of the MTA was developed, which had the same composition of gray MTA but lacking the tetra-calcium aluminoferrite (Asgary *et al.* 2005, Song *et al.* 2006) and having reduced aluminate levels (Camilleri 2007). Since their introduction, MTA has been principally used for endodontic applications such as repairing perforated roots, apexification, or pulp capping (Torabinejad & Chivian 1999, Dammaschke *et al.* 2005, Camilleri & Pitt Ford 2006).

Very recently, a short-setting calcium-silicate based dental cement called Biodentine™, was introduced by Septodont (*Saint Maur des Fosses- France)*. Henceforth this commercial name will be used for representation and brevity. Biodentine was developed as a dentine replacement material, with novel clinical applications to this family of materials such as coronal restorations. The relatively short setting time of the Biodentine, around 12 minutes, enabled the use of this cement for restorative procedures, which was not possible with the slower setting MTA that has an initial setting time of 3-4 hours (Torabinejad *et al.* 1995). Biodentine is principally composed of a highly purified tri-calcium silicate powder that is prepared synthetically in the lab rather than in a clinker. Additionally, Biodentine contains di-calcium silicate, calcium carbonate and zirconium dioxide which acts as a radiopaquer. The di-calcium and tri-calcium silicate phases form around 70% of the weight of Biodentine's un-hydrated powder, which is close to that percentage of WMTA and white Portland cement

(Camilleri 2008, Belío -Reyes *et al.* 2009). In contrary to MTA, Biodentine does not contain calcium sulphate, aluminate, or aluminoferrite. The powder is dispensed in a capsule with a standardised separate proportion of its own liquid that is composed of water, calcium chloride, and a water reducing agent.

Despite the fact that calcium silicate based dental cements share similar constituents, there is, however a variation in their manufacturing processes. This affects the purity of their constituents and hydration products, as well as their behaviour (Camilleri 2011). Studies have shown that cements such as ProRoot MTA (Dentsply, Tulsa Dental Products, Tulsa, OK) and MTA Angelus (Angelus Soluções Odontológicas, Londrina, Brazil) share almost the same composition with white OPC, except for the addition of bismuth oxide to the MTA for radiopacity (Funteas *et al.* 2003, Oliveira *et al.* 2007, Camilleri & Pitt Ford 2006). This includes some impurities and contaminating heavy metals such as chromium, arsenic, and lead (Schembri *et al.* 2010) indicating that both MTA and OPC were manufactured using the same process, but with cleaner and segregated conditions (Matsushita *et al.* 2000), and controlled particle size (Dammaschke *et al.* 2005). On the other hand, other calcium silicate based dental cements, such as Biodentine or MTA-bio (Angelus Indústria de Produtos Odontológicos Ltda, Londrina, Brazil) have been produced under controlled lab conditions from raw materials, in a step to avoid any potential contamination of the basic constituents, and to avoid the incorporation of aluminium oxide which was linked to some medical conditions such as Alzheimer's disease (Camilleri 2011).

Similar to OPC, calcium silicate based dental cements set through a hydration reaction (Camilleri 2007, 2008, 2011). Although the chemical reactions taking place during the hydration are more complex, the conversion of the anhydrous phases into corresponding hydrates can be simplified as follows:

$2Ca_3SiO_5 + 7H_2O \longrightarrow 3CaO.2SiO_2.4H_2O + 3Ca(OH)_2 + \text{energy}$

C3S + **Water** $\longrightarrow$ **CSH** + **CH**

$2Ca_2SiO_4 + 5H_2O \longrightarrow 3CaO.2SiO_2.4H_2O + Ca(OH)_2 + \text{energy}$

C2S + **Water** $\longrightarrow$ **CSH** + **CH**

This setting reaction is a dissolution-precipitation process that involves a gradual dissolution of the unhydrated calcium silicate phases (C3S and C2S) and formation of hydration products, mainly calcium silicate hydrate (CSH) and calcium hydroxide (CH). The CSH is a generic name for any amorphous calcium silicate hydrates that includes the particular type of CSH that results from the hydration of tri- and dicalcium silicate phases (Taylor 1997). The CSH precipitates as a colloidal material and grows on the surface of un-hydrated calcium silicate granules to form a matrix that holds all the other components together, and gradually replaces these granules. Meanwhile, calcium hydroxide is distributed throughout water filled spaces present in between the hydrating cement's components (Taylor 1997, Kjellsen & Justnes 2004). Compared with OPC, the hydration of MTA is affected by the bismuth oxide, which forms 20% of its weight and acts as a radiopaquer (Camilleri 2007, 2008). Hydrated MTA and tri-calcium silicate cements were found to release more calcium ions than hydrated OPC (Camilleri 2007, 2011).

For the Biodentine, the setting reaction is expected to be similar to the hydration of pure tri-calcium silicate cement (Camilleri 2011). Therefore, it is expected to produce the same hydration products as WMTA and OPC, except for the absence of alumina and gypsum hydration products. The zirconium oxide present in the Biodentine powder as a radiopaquer acts as an inert filler and is not involved in the setting reaction (Camilleri *et al.* 2011) unlike the bismuth oxide present in the MTA (Camilleri 2007). The hydration reaction starts with the fast dissolution of the tri-calcium silicate particles, which therefore can explain the fast setting of Biodentine (Taylor 1997), in addition to the presence of calcium chloride in the liquid, which is known to speed up the hydration reaction (Kjellsen & Justnes 2004), and the absence of calcium sulphate that acts as a retarder.

Although the different calcium silicate based cements currently available share their essential constituents (Camilleri 2005), these cements do, however, vary in the percentage, purity, and manufacturing process of their components. Therefore, it has been always important to study and characterise these cements individually, in order to understand their nature and clinical behaviour.

Such studies have been very limited for the Biodentine; with only one study in the literature that characterised the setting reaction, precisely the maturation time, using impedance spectroscopy (Villat *et al.* 2010). Therefore, further characterisation of the Biodentine and its setting reaction is still required. On the other hand, a number of studies have been conducted on the interaction of Biodentine with dental tissues (Han & Okiji 2011, Leiendecker *et al.* 2012, Sawyer *et al.* 2012) and pulpal tissues (Laurant *et al.* 2008, Pérard *et al.* 2011, Laurant *et al.* 2012). However, no comprehensive understanding has been provided for the nature and dynamics of the Biodentine's interface with dentine. Additionally, no correlation has been established between Biodentine's properties and its behaviour in contact with dentine.

1.1.2 Glass ionomer cements:

Glass ionomer cements (GICs) are another family of water-based dental materials. They were first introduced to dentistry in 1975 (Nicholson 1998), and since then they have been used in a wide range of clinical applications. Conventional GICs are dispensed in a powder form supplied with its own liquid. The powder is formed of fluoro-aluminosilicate glass, while the liquid is an aqueous solution of a polyalkenoic acid, such as polyacrylic acid, although in later formulations, the acid is added to the powder in a dried polymer form (Nicholson 1998). Strontium has been added in some commercial GICs, such as GC Fuji IX_{GP}, to substitute calcium due to its radiopaque properties (Billington *et al.* 2006). This substitution did not have any effect on the setting products (Deb & Nicholson 1999) or cement's remineralizing capability (Ngo *et al.* 2006).

Upon mixing, an acid-base reaction takes place between the polyalkenoic acid and the ion-leachable glass particles (Walls 1986), which occurs in two phases. The first phase is a dissolution phase, in which the acid attacks the surface of the glass particles to release ions such as aluminium, fluoride, and calcium or strontium. Following ion release, the polyacid molecules become ionised and adopt a more linear form. This renders the carboxylic groups within the polyacid to become more accessible for the ions, and leads to their cross linking in the

later stage of gelation (Walls 1986). Eventually, the set cement will be formed of a composite of un-reacted glass particles surrounded by a silicious gel on their surfaces while embedded in a polyacid-salt matrix which hold all the components together (Causton 1981, Walls 1986, Watson 1999). Within the polyacid-salt matrix of set GIC, water is distributed in two forms; loose water which can be removed through desiccation, or bound water which is binding chemically to the matrix (Nicholson 1998). Water plays an essential role during the maturation of the cement as well as the diffusion of ions (Billington *et al.* 2006).

When a freshly mixed GIC is placed on wet dentine, an interaction between the two substrates takes place in the form of an ion exchange (Sennou *et al.* 1999, Yiu *et al.* 2004). Aluminium, fluoride, and calcium or strontium leaches out of the cement as the glass is being dissolved by the polyacid, while calcium and phosphate ions move out of the underlying dentine as a result of the self-etching effect of the setting cement on mineralised dentine (Sennou *et al.* 1999, Tanumiharja *et al.* 2001). This ion exchange process creates an intermediate layer composed of ions leached out from both substrates (Watson 1999, Tanumiharja *et al.* 2001, Yiu *et al.* 2004). The release of fluoride and calcium/ strontium ions has provided GICs with the capability to remineralize carious tissues (ten Cate *et al.* 1995, Ngo *et al.* 2006), where ion exchange could take place to supply the demineralised tissues with the ions required to tip the balance in favour of apatite formation.

In our studies, glass ionomer cements have been chosen as a control material with which the Biodentine will be compared. This selection was based on the fact that GICs and calcium silicate based cements are both considered water based cements, hence they could share similar interfacial properties with wet dentine. In addition, GIC is the closest material to Biodentine in terms of their clinical applications, as GIC can be indicated as a provisional restoration, and has the potential to induce remineralisation of carious dentine.

1.1.3 Dentine remineralisation:

With the enhanced understanding of the dental caries process and the improvements that have been achieved in both dental materials and diagnostic devices, more interest has been directed towards minimally invasive approaches for the treatment of dental caries. Such approaches aim eventually to minimize the excavation of dental tissues, and encourage their recovery and repair instead. Dentine caries results from a bacteriogenic acid attack followed by enzymatic destruction of the organic matrix. These lesions are usually classified into caries -infected and -affected dentine (Fusayama 1979) based on the extent and reversibility of the damage induced. In the caries infected dentine, the organic matrix is irreversibly damaged, while the deeper caries affected dentine is hypomineralised with sound organic matrix, which could be repaired and remineralised. The slow progression of caries allows a reparative intervention, which can restore the mineralised architecture after excavating the infected layer.

Carious dentine remineralisation has been thoroughly studied using different in-vitro models. In these models, dentine caries was simulated through partial demineralisation of sound dentine using pH cycling (Liu *et al.* 2011c) or short duration application of phosphoric acids (Klont & ten Cate 1991) or ethylenediaminotetraacetic acid (EDTA) (Kawasaki *et al.* 1999), and in some studies total demineralisation was used (Arends *et al.* 1990, Inaba *et al.* 1996). These methods were actually aiming to simulate the caries affected "hypomineralised" dentine, which have the potential to be remineralised.

For the remineralisation process, different approaches have been applied, which can be classified as classical and non-classical (Cai & Tang 2009), or top-down and bottom-up approaches (Liu *et al.* 2011b). In the classical (top-down) approach (Klont & ten Cate 1991, Arends *et al.* 1990, Inaba *et al.* 1996, Kawasaki *et al.* 1999, Saito 2003), dentine remineralisation is based on the epitaxial growth of residual crystallites, which act as nucleation sites for the calcium phosphate minerals to precipitate when dentine is stored in a solution rich with calcium and phosphate ions (Liu *et al.* 2011b). However, recent studies have indicated that such an approach would result in an incomplete and non-

functional remineralisation of dentine (Tay & Pashley 2008, Liu *et al.* 2011a, Bertassoni*et al.* 2011, Zhang 2012). The classical remineralisation approach results in extra-fibrillar remineralisation of the collagen matrix of dentine, without the mineralisation of collagen's intra-fibrillar compartments (Liu *et al.* 2011a). This is due to the size of the apatite crystals forming during this process, in the absence of any control on their size and orientation.

The non-classical approach was suggested as an alternative in-vitro remineralisation technique, which attempted to achieve a hierarchical biomimetic remineralisation of the organic matrix of dentine (Tay & Pashley 2008). This approach involves the use of synthetic substitutes for certain dentine matrix proteins that play an essential role during the biomineralization process. Two types of analogs were suggested. The first is a sequestration analogue, which is a polyanionic molecule such as polyacrylic acid that allows the formation and stabilisation of amorphous calcium phosphate (ACP) (Tay & Pashley 2008, Liu *et al.* 2011a, Qi *et al.* 2012). These nano-aggregates of ACP are thought to form flowable nanoprecursers that can infiltrate the water filled gap zones in the dentinal collagen fibrils, where they precipitate as polyelectrolite-stabilised apatite nanocrystals (Tay & Pashley 2008). This precipitation is guided by the second analogue, which is a dentine matrix phosphoprotein substitute (Gu *et al.* 2011). This analogue is usually a polyphosphate molecule, such as sodium metaphosphate, which acts as an apatite template that encourages the crystalline alignment in the gap zones (Qi *et al.* 2012), and leads to a hierarchical dentine remineralisation (Liu *et al.* 2011a).

In the biomimetic bottom-up remineralisation approach, calcium silicate based cements, such as MTA, were used as the calcium source (Tay & Pashley 2008, Gu *et al.* 2011, Qi *et al.* 2012). Upon hydration, these cements release calcium in the form of calcium hydroxide over a long duration (Camilleri 2011). In addition to calcium release, these cements release silicon ions into underlying dentine (Han & Okiji 2011). Silica was found to be a stronger inducer of dentine matrix remineralization compared with fluoride (Saito *et al.* 2003). Furthermore, calcium silicate cements have the advantage of high alkalinity, which favour

apatite formation (Tay *et al.* 2007) and matrix phosphorylation (Zhang *et al.* 2012), and provide a potential caustic proteolytic effect that could enhance dentine remineralisation (Inaba *et al.* 1996). For the Biodentine, no studies have been conducted to evaluate its capability to induce dentine remineralisation, which would be valuable as one of the cement's clinical applications in carious dentine lesions.

The non-classical approach is alleged to be advantageous over the classical, as the former provides continuous replacement of water, which occupies the intra-fibrillar compartments, by apatite crystals. The non-classical approach also provides a self-assembly system that does not require the presence of nucleation sites (Liu *et al.* 2011b). However, the idea of using matrix protein analogues could be challenging clinically and difficult to apply. Recent attempts aimed to take this concept a further step into clinical application (Qi *et al.* 2012). Therefore, the classical approach remains a closer and more applicable approach to the clinical situation.

For the detection and evaluation of the mineralisation process, different techniques have been applied. Scanning and transmission electron microscopy (SEM) & (TEM) (Eisenmann & Yaeger 1972, Tay & Pashley 2008), Fourier transform infrared spectroscopy (FTIR) (Li & Chang 2008), Raman spectroscopy (Sauro *et al.* 2011), X-ray diffraction (XRD) (Saito *et al.* 2003), energy dispersive X-ray spectroscopy (EDX) (Zhang *et al.* 2012), microradiography (Arends *et al.* 1990, Kawasaki *et al.* 1999), Micro-CT scanning (Liu *et al.* 2011c), and nanoindentation (Bertassoni *et al.* 2011). However, the capability of these techniques in detecting the mineralisation process is limited to surface characterisation, whether morphological, chemical, or mechanical. Hence, they do not enable the observation of the mineralisation process and its morphological features deeply within the structure of the remineralising organic matrix. Therefore, other techniques seem to be required to allow the deep detection of mineralisation.

1.2 Optics

1.2.1 Introduction to optics

Optics is the study of light's propagation in space or matter as well as the interactions between the two (Baldwin 1974). This field of physical science aims to explain the phenomena associated with light's behaviour in different media; which is a very wide field that acknowledges the obscure nature of light on one hand and the variation in the structure and inner dynamism that govern the entity of the molecular systems on the other.

For the study of light's interaction with matter, optics differentiates between two levels of interactions; geometrical and physical optics. Geometrical optics deals with the matter at the level of large objects, in which light is treated as a cluster of rays; therefore it describes the behaviour of light rays when directed to surfaces, such as reflection and refraction (Morgan 1953). Physical optics, on the other hand, considers the interaction between light and matter on the molecular level, this type of interaction will be the subject of the following discussion.

Energy is the currency which all material systems use in their transactions between their molecules, rendering the stability or activity of these systems dependent on their energy status, which defines the way they can deal or interact with each other. This relation applies on the interaction between light and matter too. Based on the dual wave-particle theory, light propagates in the form of energy units called photons. Photon energy is expressed as waves of frequencies that is proportional to the energy, therefore, it is possible that light could interact with the matter and energy can be transferred between the two.

On illuminating a material system with light of a certain wavelength, photons are directed to that surface with an energy that is proportional to their frequency. When the photons bombard the surface, energy transfer can occur between the two in a process mediated by interference of the electric component of light's electromagnetic force with the electronic cloud distribution within the molecules. This interference could lead either to energy absorption by molecules or to

scattering of the photons in different directions. During energy absorption, the electrons of molecules within the optical field become excited up to a higher energy state, or excited state, while the bombarding photons vanish. Following the absorption, electrons soon re-emit the absorbed energy through non-radiative emission such as heat, or radiative emission such as fluorescence (Figure 1-d) (Xu 2001).

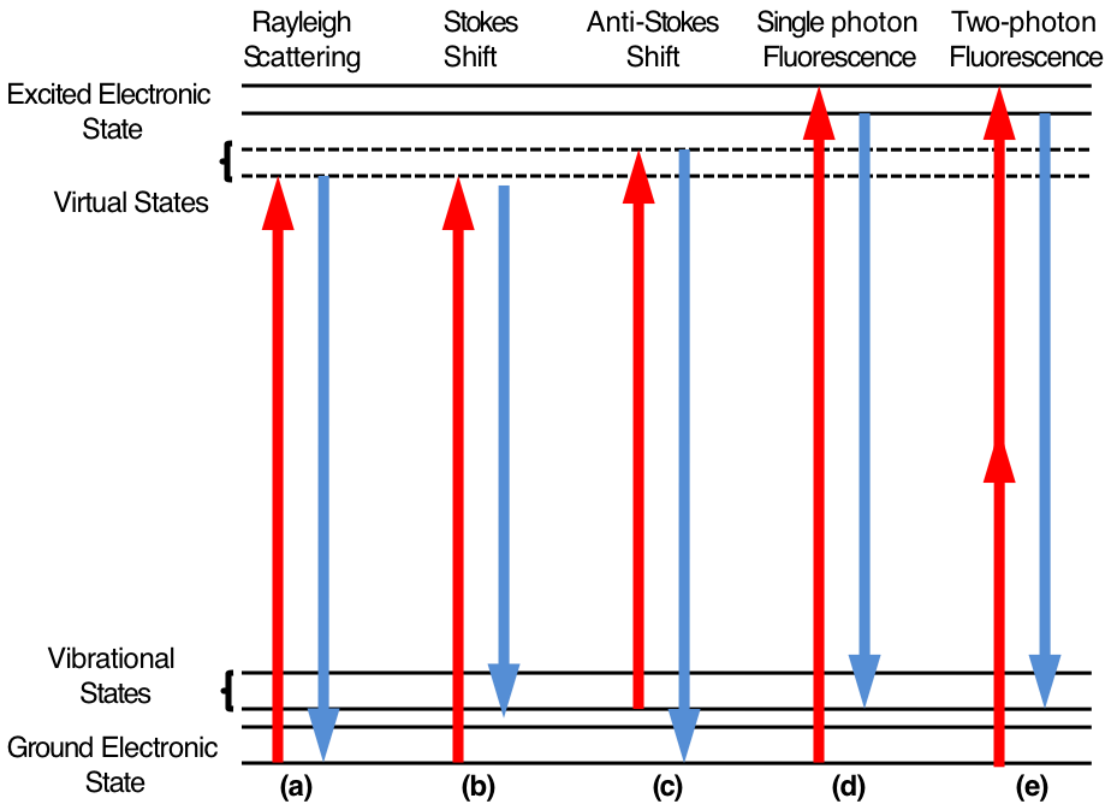

Figure 1: A Jablonski diagram demonstrating the changes in the energy states of molecules associated with different optical phenomena; **(a)** Rayleigh scattering occurs when incident photons are scattered in a different direction but at the same energy state, which does not affect the energy status of illuminated matter. Non-elastic scattering occurs when the incident photons are scattered with reduced **(b)** energy and described as Stokes shift, or increased **(c)** energy which is described as an anti-Stokes shift. **(d)** Fluorescence occurs when the photon energy is fully absorbed by the fluorophore, and re-emitted with different energy and wavelength. **(e)** Two-photon excitation requires two photons with half of the fluorescence excitation energy each to excite the fluorophore and induce fluorescence.

Scattering of the electromagnetic waves by molecular systems results in a scattered light that is principally of the same wavelength as the incident light. This type of scattering is called elastic scattering or Rayleigh scattering (Figure 1-a), where photon energy does not change. A small proportion of incident photons are scattered with a decrease or increase in their energy, which is described as non-elastic scattering, or Raman scattering (Figure 1-b,c) (Long 1977).

1.2.2 Fluorescence and fluorophores

- Fluorescence

Fluorescence is a radiative absorption process within a molecular system that leads to emission of light of a certain frequency range following its excitation with a higher light frequency (Figure 1-d). During this process, the energy of incident photons is totally absorbed by the molecular system causing them to vanish, while exciting the irradiated molecules into a higher electronic energy level (Learmonth *et al.* 2009). Following excitation of the electrons, they return back from their excited state into a more stable ground energy state, re-emitting the absorbed energy into the surrounding medium through radiative (fluorescence and phosphorescence) and non-radiative (heat) forms of decay. Therefore, we can define fluorescence as the emission of lower frequency photons by molecules as a result of electronic transmissions from excited to ground energy states after optical excitation with higher frequency photons (Boyd & Masters 2008).

Compared with light scattering, fluorescence involves the absorption of the incident photons' energy by the illuminated molecules, which causes the incident photons to vanish after their energy is totally absorbed. In light scattering however (Figure 1-a), incident photons do not vanish, instead they disseminate in different directions without any change in their energy in the case of elastic scattering, where the scattered light has the same wavelength as the incident light (Sathyanarayana 2005). In non-elastic scattering (Figure 1-b,c), incident photons might lose or gain relatively small amounts of their energy, which correspond to various vibrational or rotational energies within the

illuminated molecules. Additionally, for the fluorescence to occur it requires an illumination with a characteristic frequency called the “excitation wavelength”, which then leads to emission of light of a certain frequency called the “emission wavelength”, depending on the nature of the material. Scattering, on the other hand, occurs at any incident frequency, and the frequency of scattered light does not depend on the materials nature, rather it depends on the illumination frequency (Yadav 2005).

- Fluorophores

Fluorescence is a property of a specific molecular configuration, which usually occurs in organic molecules with conjugated double-bond systems (Learmonth *et al.* 2009). Fluorescent molecules are called “fluorophores”, and each fluorophore has its characteristic excitation and emission wavelengths or spectra. In addition, fluorophores are characterised by the ratio of photons they emit to the photons they absorb when excited, this is described as the quantum yield. Fluorescence lifetime is also another important characteristic of fluorophores (discussed below). All these characteristics could be used in the identification of fluorescent molecules. It is important to know that all these characteristics are the function of both the fluorophore’s structure and the surrounding environment, where any change on these would affect the fluorescence. Depending on their origin, fluorophores are usually classified as intrinsic or extrinsic.

- Intrinsic fluorophores and auto-fluorescence

In living tissues, some organic molecules have the ability to fluoresce under certain excitation wavelengths, these molecules are described as intrinsic fluorophores, and the process is described as auto-fluorescence or natural fluorescence. Auto-fluorescence originates from a range of molecules that could be either metabolites within the cell or extra-cellular structural components (Billinton & Knight 2001). Most common fluorescent metabolites are advanced glycation end-products (AEG), lipofuscins, flavins, and protoporphyrin. Collagen and elastin, on the other hand, are extracellular structures that contain fluorescent components responsible for their natural fluorescence, one of which is a cross linking tricarboxylic acid with a pyridinium ring (Deyl *et al.* 1980)

Auto-fluorescence could be undesirable and a source of background noise when examined specimens are labelled with extrinsic fluorophores (Billinton & Knight 2001). However, auto-fluorescence detection by itself could be a valuable source of information, especially when used in combination with other stain-free imaging techniques such as fluorescence lifetime imaging (FLIM) and second harmonic generation microscopy (SHG). Stain-free imaging enables the study of living tissues with minimal intervention, depending on the characteristic behaviour of their intrinsic components under optical excitation.

1.2.3 Non-linear optics:

Non-linearity, in general, refers to the change in the output or response when it is not proportional to the change in the input or stimulus (Figure 2). In optics, non-linearity refers to the "non-conventional" interaction between light and matter that occurs when the response of a material system changes in a non-linear manner upon the strength of the applied electromagnetic field or light (Boyd & Masters 2008). Therefore, it is the property of certain materials that have the susceptibility to behave non-linearly when illuminated with a very high intensity light source, namely a pulsed laser.

Materials vary in there susceptibility to react with light in a linear or non-linear way, this can be expressed through the following equation:

$$P = X^{(1)}E + X^{(2)}E^2 + X^{(3)}E^3 + \ldots$$

Where $\boldsymbol{P}$ is the dielectric polarisation within the molecular system, which depends on both the difference between net nuclear and electronic charges within molecules and the relative displacement between them. $\boldsymbol{E}$ is the strength of the electric/optical field that is related to the frequency and intensity of the illuminating light. While $\boldsymbol{X^{(1)}}$is the linear optical susceptibility, $\boldsymbol{X^{(2)}}$ and $\boldsymbol{X^{(3)}}$ are the second- and third-order non-linear optical susceptibilities respectively. Therefore, the linear and non-linear optical susceptibilities of any material determine its behavior with respect to light depending on the conditions (New 2011).

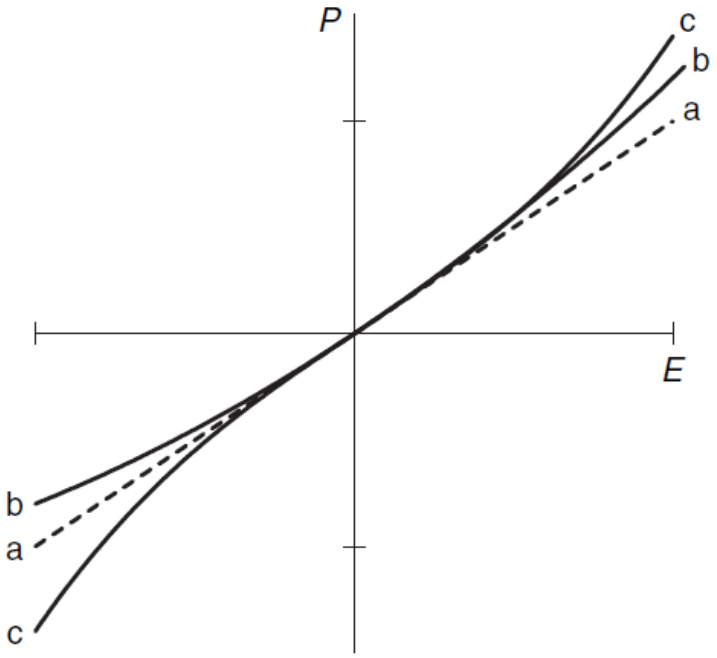

Figure 2: Nonlinear optics: This diagram demonstrates the linear (a) versus non-linear (b & c) optics. New G (2011). Introduction *In*: *Introduction to nolinear optics*. Cambridge Cambridge University Press, pp 4.

When illuminating a material with a laser source of any intensity, the electric component of the electromagnetic field interferes with the electron motion within these molecules. This ideally causes an elastic light scattering, described above as Rayleigh scattering, in which the frequency of the scattered light is similar to the illuminating (fundamental) laser frequency. However, in a non-linear material, when illuminated with a high intensity laser source, additional scattered frequencies of double or triple the fundamental frequency will result, this type of scattering is described as hyper-Rayleigh scattering, and includes the second and third harmonic generation described below (Figure 3).

- Second harmonic generation

Second harmonic generation (SHG), or frequency doubling, is a non-linear type of interaction between light and matter. It occurs when hyper-Rayleigh scattering is produced coherently by an organised collection of molecules when illuminated with a high intensity laser beam and leads to the emission of light

with double the frequency (half the wavelength) of the illuminating laser source; therefore it is considered a second-order non-linear interaction (Boyd 2003).

Second harmonic generation occurs as a result of the electron motion in non-centrosymmetric molecules when affected by the electromagnetic waves within the optical field of an intense laser. This interaction generates an additional frequency component with double the frequency (2ω) of the illuminating light, which is the SHG signal, beside the usual linear component that results in Rayleigh scattering (Mertz 2008) (Figure 3).

1.3 Optical investigation techniques

1.3.1 Confocal microscopy

Confocal microscopy is an optical imaging technique that increases the resolution and contrast of the images taken for samples under observation. In this type of microscope, an aperture located in the conjugate focal plane of the objective lens is used to eliminate the out of focus light beams directed to the sample or reflected by it, which reduces their contribution in the detected signal and therefore enhances the image quality (Webb 1996, Watson 1997, Inoué 2006). The confocal microscope, in addition, provides the optical sectioning feature, which enables the detection of subsurface features, up to 200 µm in depth without the need for real sample sectioning (Watson 1997).

A scanning confocal microscope is equipped with a scanning device, which is essential for a fast and efficient confocal image and helps in illuminating and detecting as many points as possible, in some cases, simultaneously. Scanning is performed by either using a moving laser beam e.g. the confocal laser scanning microscopes (CLSM) or through moving multiple pinholes such as the confocal tandem scanning microscope (TSM). In the CLSM, a laser beam scans the surface of the sample through moving galvanometer mirrors, this movement passes the laser beam over the whole surface of the sample in a raster pattern allowing a point by point illumination, while at the same time the conjugated aperture in the pathway of the reflected beam eliminates the out-of-focus beams to produce the confocal image (Webb 1996, Inoué 2006).

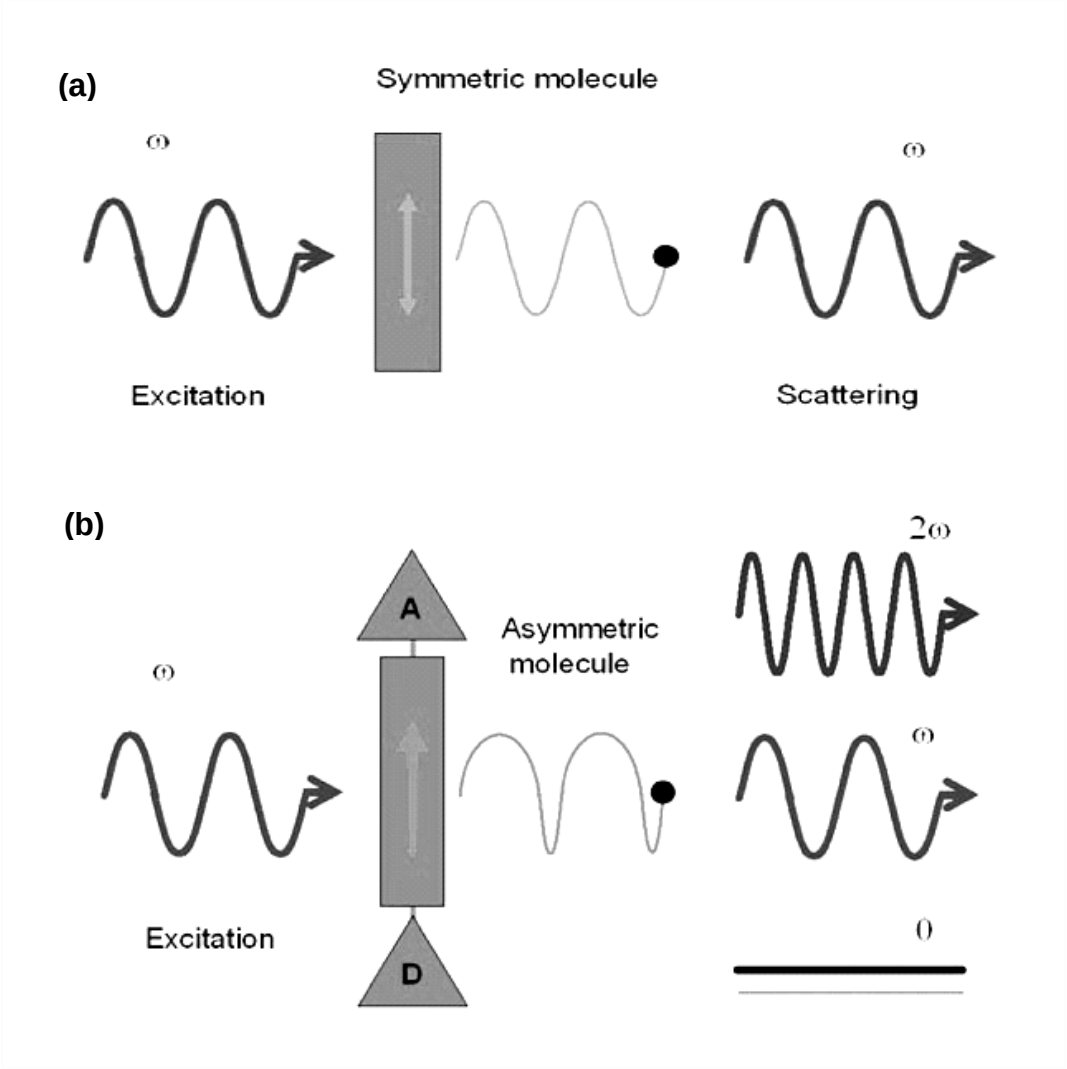

Figure 3: Second harmonic generation occurs as a result of the electron motion in non-centrosymmetric molecules when affected by the electromagnetic waves within the optical field of an intense laser (b), which does not occur in symmetric molecules (a). This interaction generates an additional frequency component with double the frequency (2ω) of the illuminating light, which is the SHG signal, beside the usual linear component that results in Rayleigh scattering. Mertz J. Applications of Second-Harmonic Generation Microscopy .in: Masters BR and So P (eds). Handbook of biomedical nonlinear optical microscopy. Oxford University Press

In the tandem-scanning confocal microscope (TSM), scanning is performed through a spinning disc that directs the light beam. The spinning disc, called a Nipkow disc, is located in a conjugate image plane and contains many pinholes that are arranged in a series of nested spirals (Inoué 2006). This structure provides moving points of illumination with synchronized moving points of

detection on the opposite side of the disc that allows the scanning of the sample and produces a real time confocal image.

1.3.2 Two-photon fluorescence microscopy

Two-photon excitation microscopy is an advanced fluorescence imaging technique, in which fluorophores are excited by simultaneous absorption of two photons to induce their electronic transition from ground to excited state (Figure 1-e) (So 2001, Boyd & Masters 2008). In this technique, specimens are illuminated with an intense laser source, but with twice the excitation wavelength required for the fluorophore emission. Therefore, for the fluorophore excitation, two photons are required transferring their energy, leading to non-linear excitation (quadratic) probability. With such excitation, the volume that has the highest photon intensity will have the sufficient probability for two photon excitation, which therefore confines the excitation field to a small volume at the focal plane of the objective lens within the specimen. A pulsating laser source is used for illumination, which with its high intensity it provides the peak power required for non-linear fluorescence.

Compared with the confocal microscope, no pinhole aperture is required to collimate illuminated and collected light. Conversely, the microscopic field is limited by the area irradiated simultaneously by two photons. This produces a minimal volume of signal generation and minimizes the signal loss resulting from fluorescence bleaching of the out-of-focus layers. Using higher excitation wavelength in the two photon microscope provides wider separation between the excitation and emission spectra, reduces scattering, and allows deeper penetration of the light, which enables deeper imaging within the specimen, up to 500 µm depending on the imaged tissue (So 2001, Boyd & Masters 2008).

- Second Harmonic generation microscopy

As described above, the second harmonic generation is an inherent property of the material that is determined by its second order non-linear susceptibility and structural arrangement. Therefore, the detection of this signal using second harmonic generation microscopy provides a highly specific stain-free imaging

technique for the study of living tissues, where structures producing the SHG signal are limited; mainly collagen, microtubules, and DNA (Zipfel *et al.* 2003). In addition to its selective capability in the imaging of living tissues, second harmonic generation microscopy could be used to detect conformational changes affecting these structures. Conditions such as heat, glycation, and enzymatic cleavage, which are known to alter the conformation of proteins, were found to suppress the SHG signal of collagen within excised tissues (Kim *et al.* 2000, Sun *et al.* 2006). This proved the ability of SHG microscopy in detecting and monitoring these changes effectively (Sun *et al.* 2006), in which the SHG was significantly reduced in the structurally modified collagen (Kim *et al.* 2000).

- Fluorescence Lifetime Imaging Microscopy (FLIM)

Fluorescence measurement is generally either conducted in a steady-state or time-resolved mode. In the steady-state fluorescence measurement, the sample is illuminated with a continuous beam of light and the fluorescence intensity is measured and averaged over time. Imaging using this mode depends on the spatial localization of fluorescence based on its intensity (Clegg & Schneider 1996, Lakowicz 2006,). This technique is beneficial in obtaining important information about the examined specimen such as morphology, status, and concentration of the fluorophores or fluorescently labelled targets in it (Chang *et al.* 2007). However, much of the information about the fluorescent dye molecules is lost from the detected fluorescence due to the averaging of the signal (Lakowicz 2006).

Time-resolved fluorescence measurement, on the contrary, records the decay of fluorescence intensity in real time without averaging. It uses a pulsed illumination light source, which is shorter in duration than the fluorescence decay time, to illuminate the specimen in conjugation with a high speed fluorescence detection system to measure the fluorescence lifetime. Fluorescence lifetime is the average time a fluorescent molecule spends in the electronic excited state prior its return to the ground state (Lakowicz 2006, Chang *et al.* 2007, Learmonth*et al.* 2009).

Using time-resolved imaging enables the recording of fluorescence lifetime for each of the excited fluorophores when illuminated, creating an image where each pixel's intensity is determined by the fluorescence lifetime, rather than fluorescence intensity of the fluorophores (Rietdorf & Gadella 2005). This imaging technique is described as Fluorescence Lifetime Imaging Microscopy or FLIM. FLIM produces spatially resolved images that map the distribution of nanosecond excited state lifetime of fluorophores (Rietdorf & Gadella 2005, Chang *et al.* 2007).

Compared with steady-state fluorescence imaging, FLIM enables the differentiation between different fluorophores of similar excitation and emission spectra based on their different fluorescence decay times and better contrast between materials of different fluorescence decay rates (Chang *et al.* 2007). FLIM provides much more information about the molecular structure of the fluorophores such as shape and conformational changes (Lakowicz 2006), as well as the micro-environment surrounding them such as the temperature, pH, and oxygen concentration (Chang *et al.* 2007). All this makes FLIM a very useful tool especially in samples where auto-fluorescence is taking place in the background of the optic field.

1.3.3 Raman spectroscopy

Raman spectroscopy is a spectroscopic technique that is used to study and identify materials depending on the vibrational and rotational modes of the chemical bonds forming their molecular structure. In this technique, a laser source illuminates the material under study with a monochromatic laser beam, through an objective lens. When the incident photons of the illuminating beam hit the sample they undergo scattering and produce a collection of reflected beams that have a variety of altered or unaltered direction, energy or both. While most of the interactions between the incident photons and the scattering material produce Rayleigh spectra, a small proportion of the incident photons undergo inelastic interactions to produce the Raman spectra (Figure 1-b, c). In these spectra, the scattered photons lose or gain energy from the interaction with the scattering molecules. The drop in the energy is called a Stokes shift

(Figure 1-b), while gain in the reflected photons' energy is called an anti-Stokes shift (Figure 1-c) (Long 1977, Tsuda *et al.* 1996).

The reflected laser beam is then collected through the same objective lens, and then filtered to exclude the Rayleigh spectra. Using a charge-coupled device (CCD), the collected Raman spectra are converted into spectral charts that can be displayed and analysed using a computer with special software. These spectra are displayed as a group of peaks characteristically allocated by their wave-number, where each peak represents a certain vibrational mode for one chemical bond in the molecular structure of the material; therefore each material has its own unique and characteristic Raman spectrum that can be used as a fingerprint to find out its identity.

- StreamLine^{TM} technology

The StreamLine^{TM} technology is a novel Raman imaging technique from Renishaw plc (Wotton-under-Edge, UK) that comprises distinctive hardware and sophisticated hardware/software integration (Evans 2008). This technique enables the performance of Raman mapping 200 times faster than the point to point mapping, and the acquisition of high resolution Raman maps with less than a micron spatial resolution (www.renishaw.com).

The StreamLine technique is a dynamic line-scanning Raman mapping, where the fast mapping is performed through combining a laser line-scanning of the sample with a motorized stage movement that allows the movement of the sample in both vertical and horizontal directions (Bernard *et al.* 2004). This combination allow the synchronization of the sample's movement and illumination in the Y direction only, and data read out, where they occur all at once, unlike the point mapping where these steps are done in sequence rather than simultaneously (Evans 2008, Bernard *et al.* 2004). The dynamic line-scanning process is performed through a laser source that illuminates a line over the sample; the length of this line is inversely proportional to the magnification of the objective length (Bernard *et al.* 2004), while the motorised microscope stage moves the sample beneath the objective lens so that the line is rastered across the region of interest (www.renishaw.com). The stage's

movement is synchronized with a CCD that records the back scattered beam from each point and projects it as a Raman spectrum for each designated point. At the end of the scanning process a Raman chemical image of the scanned area is produced, where every point is represented by its own Raman spectrum that indicates the chemical composition of the sample at that point.

1.4 Optical investigation techniques in dental research

1.4.1 Confocal microscopy and extrinsic fluorophores

Confocal scanning microscopy has been applied efficiently in studying the dynamic properties of the interfaces between hard dental tissues and different dental materials such as conventional glass ionomer (Watson *et al.* 1991), and resin modified glass ionomer cements (Sidhu & Watson 1996, Sidhu *et al.* 2002), and resin based adhesive materials (Griffiths *et al.*1999, Watson & de J Wilmot 1992). Confocal microscopy has the advantage of reduced artifacts and enables optical sectioning that can overcome the interference that might be caused by the smearing on the surface of the sample produced during the preparation process (Sidhu & Watson 1996) and therefore allows the acquisition of good quality reflection images. In addition, fluorescent dyes that can be used to facilitate the examination of these interfaces (Watson & Boyde 1991). In this context, a useful technique was developed by Sidhu and Watson (Sidhu & Watson 1996) that relied on tracking of the permeation of fluorescent dye solutions through the dentinal tubules into water filled micro spaces in the interfaces between the dentine and dental restorations when the dye is applied in the pulpal chamber. This technique has been used to examine interfacial properties of different materials such as resin based adhesives and glass ionomer cements (Sauro *et al.* 2010, Griffiths *et al.* 1999, Sidhu & Watson 1996, Sidhu *et al.* 2002, D'Alpino *et al.* 2006).

1.4.2 Auto-fluorescence in dental research

The detection and investigation of natural fluorescence in the dental tissues has been of a great importance and value since it was firstly reported by Stübel in 1911. This observation triggered several investigations over the years and

resulted in a wide range of studies that aimed to characterise the natural fluorescence in sound and carious teeth and to identify its origin (Bachmann *et al.* 2006). Despite their importance, these studies were inconsistent in their findings and interpretation of their results, with many missing links, mainly regarding the origin of auto-fluorescence in the dental tissues. One point, however, which all these studies have agreed on, is the anonymity and uncertainty of the origin of natural fluorescence in the dental tissues.

For studying the auto-fluorescence in dental tissues, several excitation wavelengths have been used, which ranged between 337 nm and 515 nm. On the other hand, multiple emission spectra were detected, which varied between studies depending on the excitation frequencies that were used. However they were all distributed around 400, 450, 500 and 550 nm wavelengths. No distinction has been made between the emission spectra of sound enamel and dentine, although higher fluorescence intensity has been reported for dentine compared with enamel (Hartles & Leaver 1953, Borisova *et al.* 2004) which supported the opinion of the role of the organic matrix as the source of auto-fluorescence in these tissues.

In the majority of studies, the organic dental components have been endorsed as the source of natural fluorescence in teeth (Tiede & Chomse 1934, Hartles & Leaver 1953, Armstrong 1963a, Spitzer & ten Bosch 1976), nevertheless, no exact substances were indisputably agreed on to be responsible for this phenomenon. Amino acids with aromatic rings such as tryptophan and tyrosine were suggested to be the source of dentine auto-fluorescence, as they can exist in the structure of collagen and they are known to exhibit fluorescence at 350 nm and 300 nm respectively upon ultra-violet (U.V) -excitation (Hoerman & Mancewicz 1964, Mancewicz & Hoerman 1964, Foreman 1980). However, because of the minimal percentage of these amino acids among others in the polypeptide structure of collagen (Hoerman & Mancewicz 1964), and due to their U.V. fluorescence, amino acids were excluded to be responsible for the visible fluorescence of teeth (Armstrong 1963b, Booij & Bosch 1982).

Through studying both demineralised dentine and hydrolysed extracts, it was speculated that dental auto-fluorescence should originate from independent organic molecules of high weight, which could exist in distinct entities and not as part of the collagenous matrix, but could bond strongly to it (Armstrong 1963a, Armstrong & Horsley 1972, Spitzer & ten Bosch 1976). Armstrong & Horsley (1972) isolated fluorescent compounds from hydrolysed dentine matrix which were not amino acids. This was consistent with other studies that suggested the potential role of collagen cross linking molecules in dentine auto-fluorescence (Hoerman & Balekjian 1966); such as dityrosine (LaBella*et al.* 1967, Booij & ten Bosch 1982) and pyridinoline (Fujimoto 1980, Rivera & Yamauchi 1993), results of these studies indicated a similarity between the characteristic excitation and fluorescence spectra of these molecules and those of dentine auto-fluorescence.

On the other hand, few studies have indicated the role of inorganic dental components in the auto-fluorescence of dental tissues. Glasser & Fonda first speculated this in 1938, which was supported by the later work of Hafström-Bjorkman *et al.* 1991, who studied fluorescence from sound and demineralised enamel and found that fluorescence intensity reduced in the latter. The same was also indicated by the results of Spitzer & ten Bosch (1977), and Borisova *et al.* (2004, 2006), although they excluded the role of the inorganic component of teeth in auto-fluorescence. Carious enamel was also detected to exhibit reduced auto-fluorescence compared with sound enamel (Sunderstorm *et al.* 1985, Borisova *et al.* 2004, Zezell *et al.* 2007). Moreover, auto-fluorescence was detected in synthetic hydroxyapatite (Hafström-Bjorkman *et al.* 1991, Zezell *et al.* 2007, Song *et al.* 2005), which exhibited fluorescence at 460 and 560 nm wavelengths when it was excited with 375 nm light source (Hafström-Bjorkman *et al.* 1991). Auto-fluorescence was also detected in deproteinised enamel (Hartles & Leaver 1953). From all these findings, it would be still possible to argue for a role of the inorganic component in the natural fluorescence of the dental tissues, which might originate from the mineral itself, or from components attached to it as suggested by Hafström-Bjorkman *et al.*(1991).

It is clear that the auto-fluorescence of dental tissues could be of multiple origins, where both organic and inorganic components participate in the characteristic excitation and emission spectra, but with variable degrees. Studies have indicated multiple fluorescent compounds (Hoerman & Mancewicz 1964, Foreman 1980). Some studies suggested the effect of certain compounds acting as inner filters, which could enhance or reduce the fluorescence of other fluorescent compounds depending on the location of their absorption and emission spectra with regards to intrinsic fluorophores (Armstrong 1963b). Studies that investigated the auto-fluorescence lifetime in dental tissues (Alfano & Yao 1981, König *et al.* 1993, Matsumoto *et al.* 1999, McConnell *et al.* 2007, Lin *et al.* 2011) have also indicated the multiplicity of the origin of natural fluorescence in these tissues. In these studies, the fluorescence decay curves of sound dental tissues appeared as multi-component exponential decay curves, where each component could be representing a different intrinsic fluorophore (Matsumoto *et al.* 1999). However, the number of these components varied among these studies.

Since the auto-fluorescence is the result of fluorescence activity of intrinsic compounds within tissues, then it could be conclusive that any change in the fluorescence characteristics may reflect structural changes affecting these tissues. In teeth, caries is a major pathological process, and therefore its effect on the auto-fluorescence of dental tissues has been of a great interest for both researchers and clinicians. Nonetheless, among the various studies that examined auto-fluorescence in carious enamel and dentine there has been no correlation or explanation for the discrepancy in the findings obtained from both tissues.

Studying the effect of caries on the natural fluorescence of enamel has been a subject of significance mainly for its clinical application as a non-invasive diagnostic technique for caries detection and observation (Stooky *et al.* 2005). Studies on this subject have agreed comprehensively on the suppressive effect of both demineralisation (Spitzer & ten Bosch 1977, Borisova *et al.* 2006 and 2004) and caries (Sundstrom *et al.* 1985, Borisova *et al.* 2004, Zezell *et al.* 2007) on the auto-fluorescence of enamel. Spitzer & ten Bosch 1977 reported

that caries can reduce the fluorescence quantum yield of enamel, which explained the reduced fluorescence signal in carious or hypomineralised enamel lesions (Al-Khateeb *et al.* 1998), except in the red region of the fluorescence spectrum, where auto-fluorescence is mainly from bacterial metabolic products (König *et al.* 1993). This reduction was mainly attributed either to the loss and/or changes in the organic matrix (Booij & ten Bosch 1982, Spitzer & ten Bosch 1977), or to the change in the optical properties of enamel caused by mineral loss, which reduces its transmittance and increases scattering and therefore causes the loss of the fluorescence signal (Spitzer & ten Bosch 1976, Booij & ten Bosch 1982). However, no clear evidence has been given to explain why the loss of minerals by itself would not be responsible for the reduction of auto-fluorescence signal in carious enamel lesions, despite the fact that these and other studies have clearly indicated a relation between the two.

The effect of caries and demineralisation on dentine auto-fluorescence was opposite to the effect upon enamel. Dentine exhibited increased fluorescence in demineralised (van der Veen & ten Bosch 1996, Banerjee & Boyde 1998) as well as carious lesions (Armstrong 1963a, Banerjee & Boyde 1998, Banerjee *et al.* 1999, Banerjee *et al.* 2010, McConnell *et al.* 2007). This inverse effect could be considered “confusing” if we agreed on the organic origin of auto-fluorescence, as there is no explanation for the increase of the fluorescence intensity in demineralised dentine in which the amount of the proposed fluorescent compound- that is the organic component- did not change. This could support the role of the inorganic component of dental tissues in its auto-fluorescence. In fact, Benerjee & Boyde (1998) and Banerjee *et al.* (1999) indicated that the distribution of auto-fluorescence was not absolutely correlated with the mineral content and microhardness in these lesions respectively, where auto-fluorescence signals terminated within zones of unsound dentine. However this could be explained by the fact that the authors were detecting fluorescence above 515 nm, below which dentine auto-fluorescence is also detectable and its signal is affected by caries, but probably resulting from demineralisation per se, and not by infection.

In addition to the change in the intensity of emission spectra of carious enamel and dentine, caries caused a red shift in these spectra (Armstrong 1963a, Spitzer & ten Bosch 1976, Alfano & Yao 1981, Thomas *et al.* 2011), accompanied by the appearance of new emission peaks in the red and infra-red region (König *et al.* 1993, Hibst *et al.* 2001, Koseki *et al.* 2004, Thomas *et al.* 2010) which were attributed to porphyrin metabolic products produced by bacteria (König *et al.* 1993, Hibst *et al.* 2001) or from blood or food remnants introduced into the carious lesion (Banerjee *et al.* 1999). Armstrong (1963b) examined the changes in the light absorption associated with dental caries and found an increased absorption of light in the U.V region. Therefore, in terms of fluorescence, dental caries is considered a combination of fluorescent and absorbent or "quenching" components that determine the characteristic excitation and emission spectra of this structure. The fluorescence lifetime of carious dental tissues was also studied and characterised (Alfano & Yao 1981, König *et al.* 1993, Matsumoto *et al.* 1998, McConnell *et al.* 2007, Lin *et al.* 2011). Results of these studies were partially consistent; however discrepancy existed especially in the effect of the dental caries process on the fluorescence lifetime. König *et al.*(1993) reported that the overall fluorescence lifetime of carious dentine is longer than that of sound tissues, in contrary to McConnell *et al.*(2007) who detected an inverse effect.

1.4.3 Second harmonic generation microscopy

Second harmonic generation microscopy was first used to study the normal structure of dental tissues by Altshuler *et al.* (1984) who detected the SHG signal in sound dentine mainly, and to a much lower extent in sound enamel. This led to the speculation of the origin of the SHG signal in dental tissues to be from the collagen fibrils and not from hydroxyapatite crystallites. Later studies by Kim *et al.* (1999), Kao (2004), Chen *et al.(* 2007), and Elbaum *et al .*(2007) confirmed the role of collagen as the source of SHG in dentine. No SHG signal was detected in sound enamel (Kao *et al.* 2004, Chen *et al.* 2008), however it was detected in enamel cracks and white spot lesions (Chen *et al.* 2008), this was attributed to the stress induced breakage of hydroxyapatite crystallites in these defects. Third harmonic generation (THG), on the contrary, was detected

in both sound enamel and dentine, which was showing the inter-prismatic spaces in the enamel (Kao *et al.* 2004, Chen *et al.* 2008). In dentine, the THG signal was attributed to the interface between the tubular lumen and peritubular dentine Elbaum *et al.* (2007). Second harmonic generation microscopy was suggested for the study of carious dentine structure (Altshuler *et al.* 1984, Panayotov *et al.* 2011).

1.4.4 Backscattered electron-Scanning electron microscopy

Backscattered electron imaging of mineralized tissues with scanning electron microscopy was first introduced by Boyde and Jones in 1983. This technique is based on the detection of backscattered electrons after the scanning beam collides with the surface of the sample. Electron scattering is correlated to the atomic number of the scattering substrate, therefore when this signal is converted into a greyscale digital image, the greylevel or intensity of each pixel is related to the average atomic number of the corresponding area (Bloebaum *et al.* 1997, Boskey 2006). Backscattered electron- SEM has been successfully applied in quantitative (Reid & Boyde 1987, Boyde *et al.* 1993, Roschger *et al.* 1995) as well as qualitative (Boyde & James 1983, Fratzl *et al.* 1996) studies of the mineralised tissues such as bone (Boyde & Jones 1983, Boyde *et al.* 1993) and dentine (Boyde & Jones 1983, Banerjee *et al.* 1998). In comparison with other mineral imaging techniques such as X-ray microradiography or X-ray microtomography, backscattered electron imaging has better resolution (Davis & Wong 1996), around 0.07- 137 μm^3 volumetric resolution (Bloebaum *et al.* 1997), which reveals highly detailed images with atomic number contrast.

1.4.5 Raman spectroscopy

Raman spectroscopy has been widely used to characterise the chemical composition of different Portland and calcium silicate cements, and to monitor the changes associated with the hydration and ageing of these cements (Ibáñez*et al.* 2007, Martinez-Ramirez *et al.* 2006). In the dental literature, this technique has been found invaluable in studying the molecular and microstructural features of sound and carious dental tissues (Tsuda*et al.*1996, Tramini *et al.* 2000, LeRoy *et al.* 2002, Sakoolnamarka *et al.* 2005, Ko *et al.*

2006, Gilchrist *et al.* 2007), as well as the mechanical properties of dental materials (Kawano *et al.* 1998, Sato *et al.* 2007), and most importantly the interfacial characteristics between adhesive materials and dental tissues (Suzuki *et al.* 1991, Van Meerbeek *et al.*1993, Xu *et al.*1997, Spencer *et al.* 2000). These studies have benefitted from the ability of the Raman spectroscope in characterising materials accurately and observing the changes affecting their molecular structure, and therefore their unique optical properties.

1.5 Aims & Objectives:

1- To characterise the composition and constituents of the un-hydrated powder of Biodentine, as well as its hydration products using Raman spectroscopy. This will be the first step in understanding the cement's behaviour when in contact with dentine.

2- To evaluate and quantify the carbonation process on the surface of hydrated calcium silicate based dental cements using Raman spectroscopy. This process will be evaluated in water and carbonate rich media in order to examine the effect of the latter on the carbonation process.

3- To evaluate the morphological, microstructural, as well as chemical changes affecting the dentine underneath calcium silicate based dental cements in comparison with GIC. This will enable the understanding of the nature of the interface between these substrates using confocal & scanning electron microscopy, as well as Raman spectroscopy.

4- To evaluate the bioactivity and remineralising potential of calcium-silicate based dental cement (Biodentine) using tetracycline labelling with two-photon fluorescence microscopy for the observation of remineralisation inside demineralised dentine. And to use this technique to compare its mineralising potential with glass ionomer cement.

Chapter 2 Raman spectroscopic characterisation of the Biodentine, and its surface carbonation rate.

2.1 Introduction:

Biodentine is a calcium silicate based dental cement which was developed with a short-setting time to suit its use as a direct filling material. The cement's formulation exhibits a relatively short initial setting time, around 12 minutes (Biodentine Data sheet), unlike the slower setting mineral trioxide aggregate (MTA), which has an initial setting time of 3 to 4 hours (Torabinejad *et al.* 1995). Such differences between Biodentine and MTA are strongly related to their formulation, which despite sharing the same basic composition of Ordinary Portland Cement (Taylor 1997, Camilleri 2008), they vary in the percentage, purity, and the presence or absence of certain constituents. In these cements, the tri- and di-calcium silicates form the main components of their un-hydrated powders, which comprise around 70% of their weight (Song *et al.* 2006). However, in comparison with MTA, Biodentine does not contain calcium sulphate, aluminate, aluminoferrite, or bismuth oxide. Instead, it contains calcium carbonate and zirconium dioxide that act as a filler and radiopaquer respectively.

For the Biodentine, as a new material, it is important to understand the changes associated with the cement after setting and during ageing in conditions mimicking the clinical situation. This is essential in order to explain the nature of the relation between the cement and dental tissues, whether sound or carious, and the possible interactions between the two substrates and the surrounding environment. Several studies have been conducted on the characterisation and analysis of MTA (Torabinejad *et al.* 1995, Camilleri *et al.* 2004, Asgary *et al.* 2004, Dammasche *et al.* 2005, Islam *et al.* 2006, Song *et al.* 2006, Camilleri 2007), which could be used as a guide to understand Biodentine. However due to the core difference between these cements in their formulation and setting time, an individual characterisation of Biodentine is required.

One important feature that is strongly related to Portland cements, but yet not well studied in relation to calcium silicate based dental cements is the carbonation process. This process, which affects cements over time due to their

exposure to atmospheric carbon dioxide, leads to a gradual conversion of calcium hydroxide resulting from the hydration reaction into calcium carbonate (Matsushita *et al.* 2000). The importance of studying this process in dental cements originates from the fact that applying such cements intra-orally would expose them to a different environment and conditions compared with the atmospheric conditions to which Ordinary Portland Cement is exposed when used for building construction. The higher temperature and saliva are both factors that are expected to encourage the carbonation process of calcium silicate inside the oral cavity (Roy *et al.* 1999). Saliva could act as a reservoir for carbonate and bicarbonate ions, as well as a wetting source that provides continuous hydration.

In this study, we aim to characterise the composition of Biodentine's powder and hydrated cement using Raman spectroscopy. In addition we aim to observe the carbonation process associated with the ageing of this cement under conditions simulating the oral environment.

2.2 Materials and Methods:

2.2.1 Sample preparation

Three samples of un-hydrated Biodentine powder were obtained from three different capsules (Table 1). The powder was packed gently into three polyvinyl square moulds fixed to a glass slide. Twelve samples hydrated Biodentine cement were prepared after mixing the cement following manufacturer's instructions. Hydrated Biodentine was packed in split cylindrical shaped acetyl copolymer moulds, Samples were kept at a temperature of 37˚C while wrapped inside a wet towel for 1 hour. Then they were de-moulded and placed separately in 10ml glass vials containing deionised water. Depending on the ageing time, samples were divided into 4 equal groups; 1 day (D1), 4 days (D4), 7 days (D7), and 14 days (D14). Samples were stored in deionised water and kept at a fixed room temperature of 25˚C while exposed to atmospheric conditions (CO_2 level: 0.039%) for the designated duration of time. Before obtaining the Raman readings, samples were collected from the solutions, left to dry in air for 2 minutes then crushed and ground using a pestle and a mortar.

Eight standardised samples of hydrated Biodentine (8 x 8 x 2 mm) were prepared using plastic square shaped frames. Each 4 frames were attached together. Biodentine was triturated following manufacturer's instructions for 30 seconds and packed into the frames. The cement was packed and moulded into the plastic frames using a mixing spatula, then compressed gently with two parallel and wetted glass slides to flatten the surfaces of the cement, then wrapped with wet paper tissues and left to set in an incubator at 37ºC temperature. After one hour, samples were placed into two separate plastic plates; the samples in the four attached frames were aged together. In one group, samples were stored in deionised water, and in the other group samples were stored in a 5.0 M carbonate/ bicarbonate buffering solution (Segma-Aldrich C3041-50CAP. Gillingham- UK). This solution was prepared with a concentration to mimic the carbonate levels in saliva (Bardow *et al.* 2000). All samples were kept at a fixed room temperature of 25ºC while exposed to atmospheric air (CO_2 level: 0.039%). Framed cement samples were mounted at the bottom of a small Petri dish using moulding clay (Harbutts Plasticine Ltd, Bath, UK) before adding the storing solutions. Solutions were replaced every two days.

Sample	Number	Ageing conditions
Biodentine Powder	n=3	none
Hydrated Biodentine in cylindrical moulds	n=3	1 day in water
	n=3	4 days in water
	n=3	7 day in water
	n=3	14 day in water
Hydrated Biodentine in square frames	n=4	0-14 days in water
	n=4	0-14 days in Carbonate-Bicarbonate buffering solution

Table 1: Numbers and ageing conditions for the samples prepared.

2.2.2 Raman spectroscopy

For each of the crushed Biodentine samples, as well as the unhydrated powder, three Raman extended scans, from 100 cm^{-1} to 2000 cm^{-1}, were obtained using

the Renishaw inVia Raman microscope (Renishaw plc, Wotton-under-Edge, UK). Raman spectra were displayed using Renishaw's Wire 3.2 software (Renishaw plc, Wotton-under-Edge, UK). A 50x/0.75 NA (numerical aperture) objective lens was used with 785 nm laser beam of 25 mW power, and a diffraction grating of 1200 grooves/mm and 10 seconds exposure time. All spectra were copied in a text format into a Microsoft Excel sheet, and the average spectrum for each group was calculated and plotted.

For the aged Biodentine samples, Raman readings of the surface of each sample were taken after 1 and 6 Hours of mixing and after 1, 2, 4, 7, 10, 14 days. Before imaging, the ageing solution in the Petri dish was removed and samples were gently rinsed with deionised water. Samples were leveled parallel to the focal plane, and placed on the microscope's motorised stage using a glass slide glued to the lower surface of the Petri dish. The dish was marked at one side to indicate its direction relative to the stage and ensure the same positioning of samples before each reading. Three reflected light images were then obtained for the surface of each sample through a 5x/0.12 NA objective lens using the charge-coupled device (CCD) supplied with the system. The area showing in each image was selected for a StreamLineTM map acquisition that was composed of 4900 points. The points were distributed in vertical lines 200 µm apart, where the distance between each point at the same line was 0.9 µm. The acquisition time was 3 seconds, and the centre of the spectrum was 710 cm^{-1}. A water immersion x60/1.2 NA Plan Apo VC objective lens was used with a 785nm laser source (25 mW line illumination) and a 600 lines/mm diffraction grating.

Using in-house curve fitting software, the intensity of the carbonate's Raman characteristic peak (1088 cm^{-1}) was measured in each map relative to the intensity of the zirconium dioxide peak (470 cm^{-1}) which was used as an internal standard. Following the uploading of the Raman maps, the estimated energy of each characteristic peak, as well as the minimum and maximum energy values, and the full width half maximum (FWHM) were all defined. These values were estimated as 1090 cm^{-1}, 1066 cm^{-1}, and 1099 cm^{-1} respectively for the carbonate's peak with FWHM of 13cm^{-1}, while estimated as 470 cm^{-1}, 420 cm^{-1},

480 cm^{-1}, and FWHM of 12 $cm^{-1}$for the zirconium dioxide's characteristic peak. These values were estimated through examining the Raman spectra obtained on the first day. The curve fitting software converted each Raman chemical map into 32 bit Tagged Image File Format (TIFF) images. These images displayed the distribution of both carbonate and zirconium dioxide in two separate images. In each image, the 32 bits value of each pixel corresponds to the intensity of the Raman peak at that point.

For each reading, the two images representing the carbonate and zirconium dioxide were opened using image processing software ImageJ (NIH, Bethesda, MD, USA). The average intensity of each peak was measured from the corresponding image, and the ratio of the 1088 cm^{-1} to the 470 cm^{-1} Raman peaks was then calculated.

2.3 Results:

The graph in Figure 4 represents the averaged Raman spectra obtained from both un-hydrated Biodentine powder (Black) and the hydrated cement after 7 days of maturation in water (Red).The designated vibrational modes and chemical bonds of each peak are listed in Table 2. The powder's spectrum indicates the presence of four major constituents; tri-calcium silicate (C_3S), di-calcium-silicate (C_2S), Zirconium dioxide (ZrO_2), and calcium carbonate ($CaCO_3$). In addition, several peaks located at 241, 1019, 1365, 1526, 1579, 1679 cm^{-1} were detected in both spectra (except for the 241 cm^{-1} peak which disappeared after hydration). These peaks were not exactly identified, taking into consideration the proprietary nature of the cement's formulation which restricted the identification of these constituents; however it is believed that they represent a polymer, which might include amides (Ignatova *et al.* 2009).

Hydration of the Biodentine's powder was associated with some changes on the Raman peaks. Peaks located at 240 and 517 cm^{-1} both disappeared, while peaks located at 535 and 800-1050 cm^{-1} all decreased in intensity compared with the reference peak at 470 cm^{-1}. On the other hand, peaks located at 155,

284, 712 and 1088 cm^{-1} all increased, while new peaks located at 354 cm^{-1} and 856 cm^{-1} appeared after the hydration.

The graph in Figure 5 demonstrates the change in the intensity of the carbonate's Raman peak at 1088 cm^{-1}. This peak represents a symmetrical stretching mode of the C-O bond (Table 2) in the carbonate group. The spectra were obtained from ground hydrated Biodentine samples that were aged in water for 1, 4, 7, and 14 days. The change in the intensity of this peak corresponds to the change in the amount of calcium carbonate in these samples. In the un-hydrated powder of the cement, the peak intensity represents calcium carbonate that exists originally in the cement's formulation. The amount of calcium carbonate almost doubled after one day of hydration. Calcium carbonate formation kept increasing over time, but with a reduced rate.

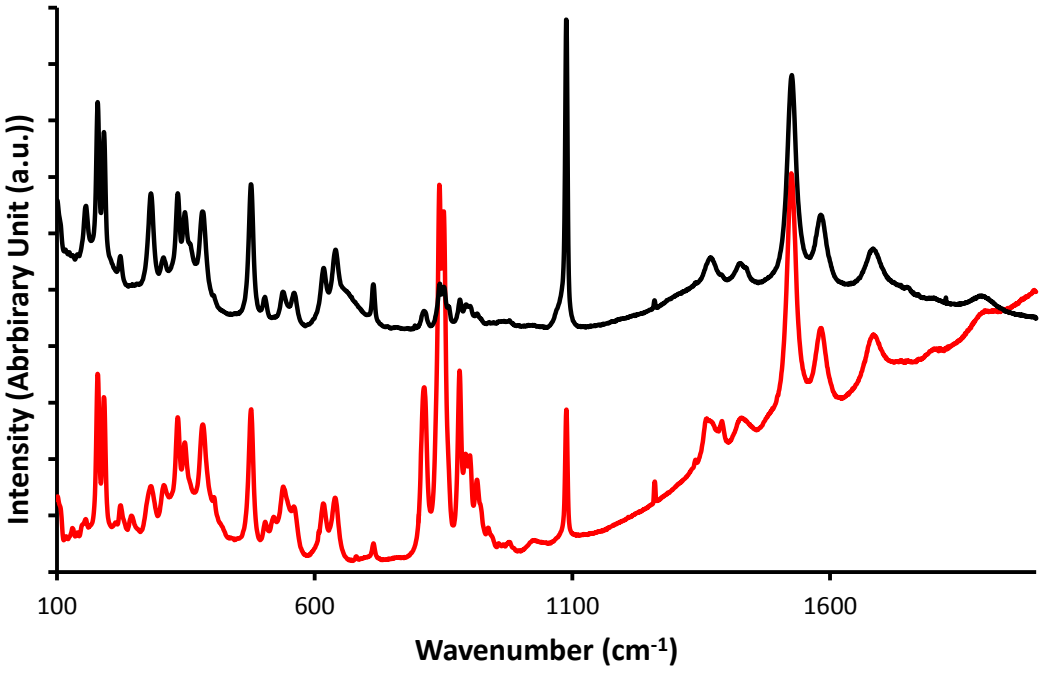

Figure 4: Averaged Raman spectra for the un-hydrated Biodentine powder (Red) and hydrated Biodentine cement (black) after 7 days.

Peak position (cm^{-1})		Attribution	Constituent	References								
Un-hydrated	Hydrated 7 days			Kumari *et al* 2008	Barberis *et al* 1997	Kirkpatrick *et al* 1997	Ibáñez *et al*. 2007	Tarrida *et al* 1995	Wehrmeister *et al* 2010	Conjeaud & Boyer 1980	Ramirez *et al* 2006	Ramirez & Fernández 2011
150	155	C-O lattice mode	CO_3			>280			154			
178	180	Zr-Zr	ZrO2	178	177							
190	191	Zr-Zr	ZrO2	187	189							
220	221.9	Zr-Zr	ZrO2	217	221							
250	252	Eg(T)	Ca(OH)2			<250	250	253				
284	281	lattice mode	CO3			280						
308	304.9	Zr-O	ZrO2	307	306							
336	335	Zr-Zr	ZrO2	333	332.5							
350	349.3	Zr-O	ZrO2	341	346.6							
	354.7	Ca-O A1g	Ca(OH)2			300-350	355	356				
383	382.6	O-O	ZrO2	380	381.1							
477	476	O-O	ZrO2	477	474.6							
503	503.3	O-O	ZrO2	500	500.2							
517			C_2S									517
541	538.9	O-O	ZrO2	537	537.1							
560	558.6	O-O	ZrO2	555	557.9							
616	616.5	O-O	ZrO2	611	615.2							
640	640	O-O	ZrO2	625	637.6							
	658.4	Si-O-Si (v2)(v1)	C-S-H			600-700	665	662		670v1		
711	713.2	O-C-O (v4)	CO_3				711		711			
	751	C-O-C (v2)	CO_3	754		740						
	793.4		C_3S									
812			C_2S							813		813
	842.9	Si-O (v1)	C_3S					840 C3S		845-C3S		
846	848.8	Si-O (v1)	C_3S, βC_2S					850 C3S		848-SiO4 v1-βC2S		
	856.7	Si-O (v1)	C_3S, βC_2S							860 SiO4 v1-βC2S	Si-O (v1)	
883	882.2		C_3S					880 C3S		885-C3S		
894	893	Si-O (v1)	CSH/C_3S			870-900						
	895.9		C_2S							895-C3S		
915	912.5		C_3S							917-C3S		
976	969.6	Si-O (v1)	CSH/C3S			950-1010						
	1018.5	Si-O-Si (v3)	C_2S								1010 βC2S v3	
1088	1088.7	C-O (v1)	CO_3			1077			1085-v1			
1429	1421	C-O (v3)	CO_3			1080						

Table 2: Raman Peaks of calcium silicate cements in the hydrated and un-hydrated forms with the designated vibrational modes and chemical bond of each peak

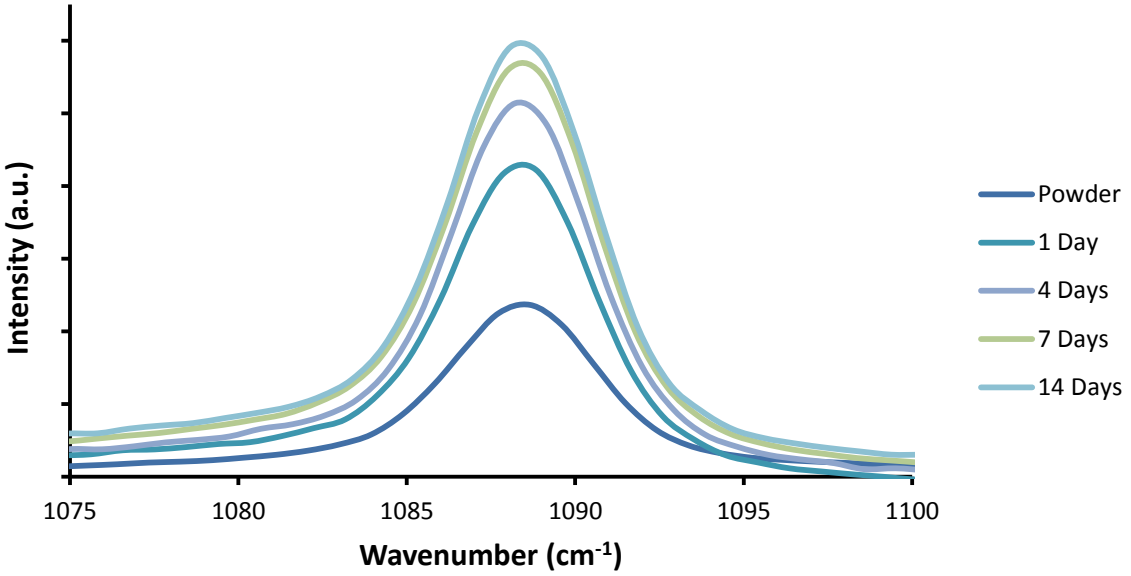

Figure 5: Normalised Raman spectra of hydrated Biodentine cement showing the 1088 cm^{-1} peak, which represents the carbonate. The intensity of this peak increased overtime as the cement was stored in deionised water while exposed to atmospheric conditions. This allowed the carbonation of the cement's hydration products, which explains this increase.

The change in the intensity of the carbonate's Raman peak (1088 cm^{-1}) relative to the internal standard- ZrO_2 (470 cm^{-1}) is demonstrated in the graph in Figure 6. It represents the carbonation rate on the surface of hydrated Biodentine samples that were aged in water (Blue) or carbonate/ bicarbonate buffer solution (Red). The chart exhibits a gradual increase in the carbonate formed on the surface of the samples in both groups. This increase eventually reached a maximum that was followed by a gradual declination back to a level equal to the initial point. In both groups, the maximum carbonate formation was almost equal, however the carbonation rate was faster in the samples aged in carbonate/bicarbonate buffer, and the drop was faster too.

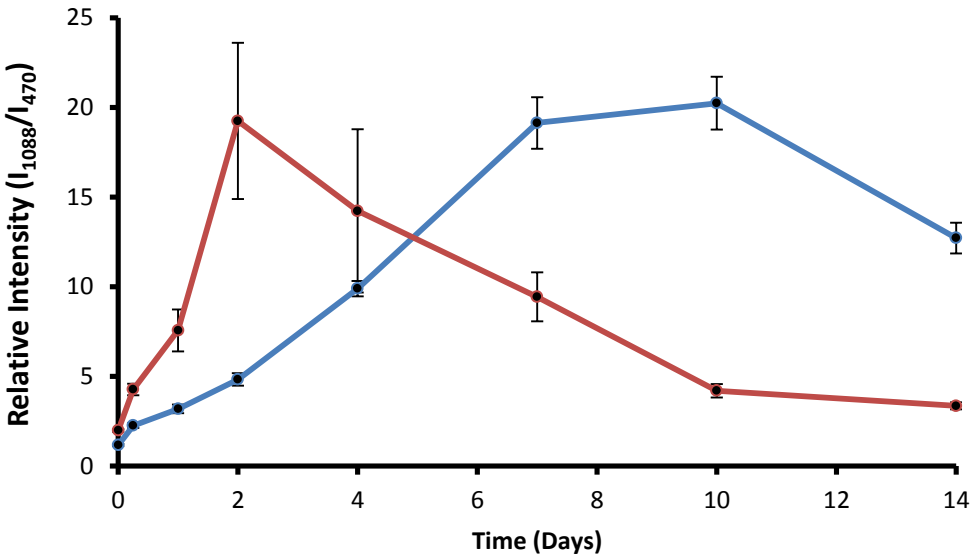

Figure 6: The change in the intensity of calcium carbonate forming on the surface of Biodentine cement blocks is demonstrated by the change in the intensity of the carbonate Raman peak at 1088 cm^{-1} relative to 470 cm^{-1} Raman peak, which represents ZrO_2 that was considered as the internal standard. This change was much faster in the samples that were stored in carbonate /bicarbonate buffer (red) in comparison with the samples stored in water (blue).

2.4 Discussion:

For the characterisation of cementitious materials, Raman spectroscopy proved to be a very useful and efficient tool in comparison with other techniques such as X-ray diffraction (XRD) and Energy-dispersive X-ray spectroscopy (EDAX) (Ibáñez *et al.* 2007). XRD is usually useful for the characterisation of crystalline structures; hence it could be inadequate for the characterisation of amorphous or poorly crystalline substances such as the hydration products of calcium silicate cements (Kirkpatrick *et al.* 1997). EDAX on the other hand provides information about the elemental composition of the examined substance; which could be easily misinterpreted when considering constituents at the molecular level (Camilleri 2007). Unlike the EDAX, no sample preparation is required for the Raman spectroscopy. Using acetone dehydration and epoxy resin inclusion for the samples in order to obtain representative sections are not needed with the streamline scanning, which can be used to obtain maps for representative areas without the need to search for one specific point (Camilleri 2007, 2011).

Furthermore, reduced impurities in the synthetic constituents of Biodentine reduced the background noise, which provided a better quality Raman imaging (Martinez-Ramirez *et al.* 2006, Martinez-Ramirez & Fernandez 2011).

On comparing the Raman spectra of the hydrated and un-hydrated cement (Figure 4), the intensity of the Raman peaks representing the un-hydrated calcium silicate phases (C_3S and C_2S), which are located between 800 and 1050 cm^{-1}, decreased after the hydration. However, the un-hydrated phases did not totally disappear, which confirms their existence during and after the setting reaction. This complies with the hydration chemistry of Ordinary Portland Cement (Taylor 1997). On mixing the liquid and powder, the hydration reaction takes place by the dissolution of the tri- and di-calcium silicate phases to produce a gel-like and poorly crystalline layer of calcium silicate hydrate (CSH), which precipitates on the surface of un-hydrated granules. Due to its poor crystallinity, the CSH is usually weakly detectable, however it can be recognised by the appearance of the new peak at 658 cm^{-1} which represents a symmetrical Si-O-Si stretching mode in the CSH (Conjeaud & Boyer 1980, Kirkpatrick *et al.* 1997, Ibáñez *et al.* 2007).

In addition to the formation of poorly crystalline calcium silicate hydrate matrix gel, the hydration reaction also produces calcium hydroxide, which distributes throughout the water filled spaces and pores within the cement structure (Camilleri 2007, 2008). The continuous production of calcium hydroxide, as well as calcium carbonate that results from its carbonation, may have led to the increase in the Raman peaks designated for both compounds at 157, 284, 712, 1088 cm^{-1}. In addition, the appearance of a new peak at 353 cm^{-1} strongly indicates the formation of calcium hydroxide (Bensted 1976). The designation of these Raman peaks located below 300 cm^{-1} has been usually agreed by investigators to represent calcium hydroxide (Kirkpatrick *et al.* 1997, Potgieter-Vermaak *et al.* 2006). However, in the current study, a peak located at 240 cm^{-1} disappeared after hydration. Therefore this peak is believed to represent constituents other than calcium hydroxide. No specific bond was designated for this peak.

The change in the intensity of the carbonate's v1 peak at 1088 cm^{-1} (Figure 5) indicates that the amount of calcium carbonate has increased over time. This could happen as a result of the carbonation of the calcium hydroxide that is continuously released from the cement. Carbonation results from the interaction between atmospheric carbon dioxide, or carbonate ions (Taylor 1997), with the hydration products of the cement; calcium silicate hydrate and calcium hydroxide (Matsushita *et al.* 2000). It occurs after the dissolution of the gaseous CO_2 into the pore solutions within the hydrated paste and produces carbonic acid, which reacts with Ca^{2+} and OH^- ions released during the setting reaction (Ibáñez *et al.* 2007).

Carbonation has beneficial effects on the cement's mechanical properties. It enhances both compressive and tensile strengths of the cement (Chi *et al.* 2002, da Silvaa *et al.* 2002, Chang *et al.* 2003), and improves its elastic modulus and hardness (Chang *et al.* 2003). These changes are due to the replacement of weaker calcium hydroxide crystals by the stronger calcium carbonate, and the reduction of the cement's pore size, where calcium carbonate crystals occupy a larger volume than calcium hydroxide. Surface porosity of the cement can be reduced by 5-12% after carbonation over 3 months (da Silvaa *et al.* 2002). These changes could be also beneficial for the Biodentine when applied intra-orally as a filling material, which could enhance its mechanical properties, and modify the chemistry and structure of its interface with dentine.

On measuring the formation of calcium carbonate on the surface of hydrated Biodentine samples, it was found to be faster when samples were aged in a carbonate/bicarbonate buffer solution (Figure 6). This difference confirms the influence of the carbonate and bicarbonate ions on the carbonation rate of calcium silicate based cements. The presence of both ions encouraged more calcium carbonate precipitation on the surface of the cement (Brodersen 2003). This could be reflected on the clinical situation, where the Biodentine is flooded by saliva, which is rich with carbonate and bicarbonate ions, when placed intra-orally. In addition, the cement will be constantly wetted under higher

temperatures; which are additional factors that will favour the carbonation process (Roy *et al.* 1999).

Unexpectedly, calcium carbonate formation on the surface of samples stored in the carbonate rich solution dropped back to its initial level after reaching a maximum level (Figure 6). The drop that was measured represents the reduction in the ratio between the carbonate and zirconium dioxide Raman signals. Since the latter is inert, and is not involved with the changes affecting the cement (Camilleri *et al.* 2011), the change in this ratio is genuinely due to the drop in the calcium carbonate formed on the surface. This drop could be explained by the loss of calcium carbonate from the surface after its precipitation. As a result of the continuous precipitation and growth of calcium carbonate crystals, they might have reached a maximum after which they started to dissociate. This could be supported by the fact that the maximum level of carbonate formation in the other group (W) was almost equal, however it occurred later at day 7, which means that the calcium carbonate crystals behaved the same in both solutions, and after they reached a certain level dissociation occurred. Another explanation could be the transformation of calcium carbonate into a different salt.

The drop in the carbonate level that was detected on imaging the surface of Biodentine blocks was not detected when aged samples were crushed into powder (Figure 5). This difference would suggest two different forms of calcium carbonate formation in calcium silicate cements when aged in water. The former is described as efflorescence, which leads to the precipitation of calcium carbonate crystals on the surface of the cement, and results from the carbonation of calcium hydroxide that diffuses out of the hydrated cement into the water (Daw & Glasser 2003). The other form of carbonation, which affects the structure of the hydrated cement, occurs principally due to the carbonation of calcium hydroxide distributed within the fluid filled pores of the cement. It affects the outer surface of the cement, which has the highest exposure to atmospheric CO_2 that is responsible for the carbonation (Ibáñez *et al.* 2007). Therefore, in addition to the formation of calcium carbonate within the matrix and pore structure of hydrated cement, calcium carbonate could form or

precipitate over the surface of the cement, this could occur much faster in the presence of carbonate or bicarbonate ions (Figure 6). Clinically, this could mediate the formation of a carbonate rich layer on the interfacial and oral surfaces of the filling, in which the cement is exposed to carbonate rich fluids; pulpal fluid and saliva respectively.

2.5 Conclusions:

For the study and characterisation of Biodentine, Raman spectroscopy was useful to identify the constituents of the cement's powder and hydration products which demonstrated the production of hydrated calcium silicate phases and calcium hydroxide. Carbonation affected calcium silicate based dental cements similar to the ordinary Portland cement. The process started shortly after mixing of the cement, which was demonstrated by the prompt and continuous deposition of calcium carbonate on the surface of the hydrated cement just after mixing. The presence of a carbonate/bicarbonate buffering system, as found in the saliva, had a prominent effect on calcium carbonate production, which caused rapid deposition but for a shorter time. Such effects could have clinical implications such as affecting the mechanical properties of the filling material, which could be enhanced with carbonation.

Chapter 3 Chemo-morphological characterization of the dentine Biodentine interface in comparison with glass ionomer cement.

3.1 Introduction:

Gray mineral trioxide aggregate (MTA), was the first Portland cement derived dental material that was formulated by Torabinejad in 1993 as a root canal repair material (Lee *et al.* 1993). Since that time, improved formulas of the MTA have been produced and developed, but with the main application of these materials limited to endodontic applications such as repairing perforated roots, apexification, and pulp capping (Torabinejad & Chivian 1999, Asgary *et al.* 2005, Dammaschke *et al.* 2005). Biodentine, on the contrary, is produced as a dentine replacement material, which in addition to its conventional endodontic applications, is proposed to be used as a coronal restorative material, where the material is applied directly over coronal dentine under definitive restorations, to benefit from its properties on an injured pulp or caries-affected dentine.

Biodentine is principally composed of a highly purified tricalcium silicate powder that contains small proportions of dicalcium silicate, calcium carbonate and a radiopaquer (Biodentine scientific file). It is dispensed in a fixed powder:liquid proportion, providing the cement with a shorter setting time of 12 minutes (Biodentine scientific file), compared with the 3-4 hours of MTA (Torabinejad *et al.* 1995). The cement sets through a hydration reaction, which involves a gradual dissolution of calcium silicate granules to produce calcium silicate hydrate and calcium hydroxide. The former provides the matrix that holds unhydrated granules and includes water filled micro-spaces where the calcium hydroxide distributes providing the high alkalinity (Taylor 1997, Kjellsen & Justnes 2004).

Glass ionomer cements (GIC) are another group of water-based restorative materials. GIC setting, however, is an acid-base reaction that involves the formation of polyalkenoate salts as a result of the polyalkenoic acid's attack on fluoroaluminosilicate glass fillers. Being of an acidic nature, GICs are considered self-etching cements, and when applied on wet dentine, they trigger

an ionic exchange with the interface accompanied by water movement between the two substrates (Watson 1999).

In this chapter, we investigate the structure and chemical nature of the interface between human dentine and Biodentine in comparison with dentine's interface with GIC. Both cements could be considered partially equivalent in their clinical applications, and close in their nature being both water-based restorative materials. For this purpose a variety of microscopic techniques will be used: confocal reflection and fluorescence microscopy (Watson *et al.* 2008), micro-Raman spectroscopy (Martinez-Ramirez *et al.* 2006, Ibáñez *et al.* 2007), scanning electron microscopy (SEM), and two photon auto-fluorescence and second-harmonic generation (SHG) imaging (Chen *et al.* 2007). A summary of these techniques is listed below (Table 3).

3.2 Material and Methods:

3.2.1 Sample preparation

3.2.1.1 Micropermeabilty tests:

Eighteen extracted human teeth were collected after the patients' informed consent was obtained under a protocol approved by East Central London Research Ethics Committee-1 (ethical approval number 10/H0721/55). Occlusal cavities with standardized dimensions of 7mm x 4mm wide and 4 mm deep with a cavo-surface angle of 90^{o} were prepared using a high-speed handpiece and type 012 diamond bur. Teeth were kept refrigerated after their extraction, and cavities were prepared large enough to obtain the widest area for the dentine-cement interface just below the cavity. In 13 teeth, Biodentine was applied into the cavities after it was mixed as per manufacturer's instructions for 30 seconds using the Linea TAC 400 M amalgamator (Linea Tac S.r.L, Montegresso D'Asti, Italy). The manufacturer recommends the application of the cement directly over the dentine without any acid etching; however eight cavities were etched using a 36% phosphoric acid gel that was applied for 15 seconds, while five cavities were left without etching. In the remaining 5 teeth, a Fuji IV glass ionomer

cement (GC Corporation. Tokyo, Japan) was applied after mixing it following manufacturer's instructions, and after conditioning of the dentine beneath it.

Table 3: List of the imaging techniques used in the study of the dentin-cement interfaces

<table>
<tr><th>Technique</th><th>Number of samples</th><th>Description</th><th>Purpose</th></tr>
<tr><td rowspan="5">Confocal Microscopy</td><td>Micropermeability
Page 59
GIC n = 5
B + etch n=8
B (no etch) n=5
Total n=18</td><td>Rhodamine-B dye solution was applied into the pulp chamber to permeate through the dentinal tubules into the interface.(Figure 7)</td><td>Evaluation of the water dynamics and permeability of the interface to fluids from the pulp.</td></tr>
<tr><td>Cement labelling
Page 63
GIC n=1
B + etch n=2
B (no etch) n=1</td><td>Fluorescein is mixed with the cement before its application on the dentine.</td><td>To evaluate the distribution of the labelled cement within the dentine.</td></tr>
<tr><td>Double labeling
Page 63</td><td rowspan="3">The combination of micropermeability & cement labelling in the same sample.</td><td rowspan="3"></td></tr>
<tr><td><table><tr><td>Mp</td><td>CL</td></tr><tr><td>RB +
LY +
RB +</td><td>LY n=1
RB n=1
Fl n=12</td></tr></table></td></tr>
<tr><td>GIC n=5
B n=7
Total n=17</td></tr>
<tr><td>Two-photon Fluorescence Microscopy & Second</td><td>Page 66
GIC n=5
B n=5
Total n=10</td><td>Samples did not require any staining or labelling. The stain-free imaging relies on the</td><td>To detect any changes in the structure of interfacial dentine</td></tr>
</table>

Harmonic Generation Imaging (SHG)		intrinsic fluorescence of samples without the need to use any labelling fluorophores.	that could affect the auto-fluorescence or second harmonic signal normally exhibited by the sound dentine.
Scanning Electron Microscopy (SEM)	GIC n=5 B n=5 Total n=10 **Page 64**	Dentine discs (1.5mm) were cut, and cement was applied on one surface. Discs were fractured before imaging.	To detect any micro-structural changes in the interfacial dentine using high magnifications.
Raman Spectroscopy	**Fractured discs** (n=4) **Page 64**	Dentine discs (1.5mm) were cut, and cement was applied on one surface. Discs were fractured before imaging.	For chemical mapping of the dentine-cement interface.
Raman Spectroscopy	**Fractured crowns** (n=4) **Page 65**	Occlusal filled teeth were fractured in bucco-lingual direction to expose the interface for imaging.	
Raman Spectroscopy	**Sequence grinding** (n=10) **Page 65**	Occlusal filled teeth were sectioned and ground frequently before imaging.	

Table 3 (Cont'd): list of the imaging techniques used in the study of the dentin-cement interfaces. B: Biodentine™, Mp: micropermeability, CL : Cement Labelling.

The acid etching was performed to widen the dentinal tubules and remove the smear layer and therefore to enhance the observation of the interface and any formation of intra-tubular tags. The cement was very well compacted using an amalgam condenser, and all the samples were then moved and kept inside an

incubator at a temperature of 37^{o}C with continuous wetting. The samples were kept in deionised water inside the incubator for variable durations that ranged between 1 hour and 3 weeks.

Before imaging, teeth were sectioned horizontally 1mm below the cement-enamel junction to expose the pulp chamber, and then pulpal tissues were removed carefully with tweezers. Tooth sectioning was performed using a water cooled slow speed diamond wafering blade XL 12205 (Benetec Limited, London, UK). The crowns of sectioned teeth were mounted up-side down in a small water filled container (Sidhu & Watson 1998); the water was added to keep the dentine wet and its level was kept lower than the upper sectioned surface of the roots (Figure 7). A fluorescent dye solution, 0.25% Rhodamine-B (R6626-Sigma-Aldrich, Dorset, UK), was added to the pulp chamber. Samples were left for three hours to allow the permeation of the dye to reach the interface, and the dye was topped up every hour. In one sample, a 0.25% Fluorescein sodium solution (F6377 Sigma-Aldrich, Dorset, UK) was applied in the pulp chamber to evaluate its use for the micropermeability test as a pilot.

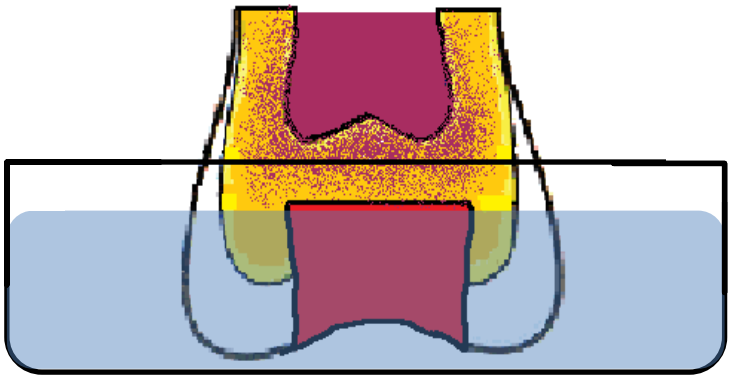

Figure 7: Micropermeability test. After sectioning their roots, filled teeth were mounted up-side down in a small water filled container. A fluorescent dye solution (Rhodamine-B) was added to the pulp chamber and maintained for 3 hours before it was washed away and crowns were sectioned and polished for imaging.

After three hours, samples were collected, rinsed with deionised water, and then sectioned vertically through the middle. Each half was then polished using

a series of silicon carbide discs with reducing roughness; 500, 1000, 1200 grit respectively. After each grade, samples were cleaned for 3 minutes in a Biosonic ultrasonic bath (Cotlène/Whaledent Inc, Cuyahoga Falls, Ohi, USA), and after the final polishing samples were cleaned for further 5 minutes. The ultrasonic bath was used to reduce any surface contamination caused by smearing of the dentine, the cement, or the fluorescent dyes during the cutting or polishing processes, which results in a better imaging quality.

3.2.1.2 Cement labelling:

Fluorescein sodium salt dye powder-1.0 mg (F6377 Sigma-Aldrich, Dorset, UK) was added to the Biodentine's and GIC's powders just before adding their liquids (Watson *et al.* 1991). Cements were then mixed following manufacturer's instructions. The Fluorescein labelled cements were then applied and compacted into 4 prepared occlusal cavities; one was filled with GIC and three were filled with Biodentine, two of which were acid etched with 36% phosphoric acid gel for 15 seconds. Two other samples were filled with Biodentine labelled with Rhodamine-B dye, and both cavities were acid etched. Samples were placed in an up-side-down position to reduce the leaching of the dye into the dentine, and were wrapped with wet tissues. After one hour samples were moved into glass vials containing deionised water and kept in an incubator with a maintained temperature of 37^{o}C for 2 weeks. The Rhodamine labelled samples were kept for 4 hours under the same conditions. All the samples were then sectioned, prepared and examined the same way as in the micropermeability test.

3.2.1.3 Double labeling:

This study was a combination of the previous two tests, where the cements were labelled with one fluorescent dye, and a different fluorescent dye solution was applied inside the pulp chamber of the sectioned teeth for micropermeability. Three combinations of fluorescent dyes were used during the pilot studies:

1- A 0.25% Rhodamine-B dye solution for the micropermeability test and a 0.1% Lucifer yellow dye solution (L0259, Sigma-Aldrich, Dorset,UK) for Biodentine labelling (1 sample)
2- A 0.1% Lucifer yellow dye solution for the micropermeability test and a 0.25% Rhodamine-B dye solution for Biodentine labelling (1 sample)

3- A 0.25% Rhodamine-B dye solution for the micropermeability test and Fluorescein powder for Biodentine labelling (7 samples).

However, the fluorescent dyes combination in the third group was found to give the best imaging quality under the experimental conditions of this study, and therefore used for the preparation of the rest of the Biodentine samples. Additionally, five GIC samples were prepared using the same methodology. All the cavities were not acid etched. And samples were kept in the same conditions as in the previous tests for 1 day.

3.2.1.4 Fractured discs:

Fourteen dentine discs, 1.5 mm thick were cut from freshly extracted human third molars. All discs were then cleaned for 5 minutes in an ultrasonic bath and kept in deionised water. Freshly mixed Biodentine cement was applied on nine discs, and mixed GIC was applied on five discs using a plastic instrument with gentle compaction forces to distribute the cement evenly. Samples were kept in an incubator at 37°C for 1 hour under 100% humidity until the initial setting of the cements, then samples were moved and stored separately in 10 ml glass vials containing deionised water. Four Biodentine samples were used for Raman mapping of the interface after total storage duration of 10 days. Raman spectra readings were taken at days 1, 2, 5, and 10 using an Renishaw inVia micro-Raman microscope (Renishaw plc, Wotton-under-Edge, UK) after the discs were fractured vertically and mounted on a glass slide, where the fractured surface was facing the objective lens. The remaining samples (Biodentiene (n=5) and GIC (n=5)) were stored under the same conditions for 4 days. Then they were taken out of water and left air-exposed at room temperature for one day for drying before they were fractured vertically. One

half of each sample was mounted on a metal SEM stub using electro-conductive putty (Leit C, Agar Scientific, Stansted, UK) before coating the samples with gold.

3.2.1.5 Fractured crowns:

Occlusal cavities were prepared in 4 extracted sound premolars (as described above). A vertical slot was created through the cavity using the water cooled cutting blade. This slot was created bucco-lingually to ease the fracturing of the tooth after setting of the cement. The idea was to attempt to image the interface of a fractured tooth rather than a fractured dentine disc. Teeth were than cleaned in an ultrasonic bath for 5 minutes before applying freshly mixed Biodentine. The cement was packed very well into the cavity. Samples were stored in an incubator at 37°C and 100% humidity for 1 hour until the initial setting of the cement, and then they were moved and stored separately in 10 ml glass vials containing deionised water. Samples were stored for 4 days, and one sample was fractured before each reading and mounted on a glass slide.

3.2.1.6 Sequence grinding:

This study was performed in two stages; the first stage was a pilot study in which standardised occlusal cavities (8 mm x 4 mm wide and 4 mm deep) were prepared in three freshly extracted human third molars using a high-speed handpiece and a type-835 diamond bur with a cavosurface angle of 90° (Figure 8-a). A customised stage was used to mount the handpiece while cutting to ensure a flat cavity floor. All the teeth were then cleaned in an ultrasonic bath for 5 minutes before applying the mixed Biodentine cement into the cavities with good condensation. Samples were kept inside an incubator at 37^{o}C temperature and 100% humidity. After 24 hours, a flat sectioned surface was created using a water cooled slow speed diamond wafering blade across the mesial/distal side of the restoration to expose the interface. Samples were then ground using a series of silicon carbide discs with reducing roughness; 500, 1000, 1200, 2400 grit respectively. Grinding was performed in one direction from the dentine towards the cement. After each grade, samples were cleaned for 3 minutes in the ultrasonic bath and for a further 5 minutes after the final grade. In the second stage of this study 6 samples were prepared using the

same technique; however samples were included within light cured methacrylate blocks-Magilight (Davis Schottlander & Davis Ltd. Herts, UK) before sectioning, to avoid any loss of flatness with the sequence grinding. Three further cavities, which were prepared as described above, were filled with Fuji IX GIC.

Samples were stored separately in closed glass vials containing 10mL of deionised water inside an incubator at 37^{o}C for a total duration of 16 days. Raman readings were taken after 1, 2, 4, 8, and 16 days. Before each reading samples were washed with deionised water and the sectioned surface was ground using the same polishing technique that was used for the first reading to remove any surface mineral precipitation. Samples were then mounted on a glass slide and leveled horizontally; they were positioned so that the surface was parallel to the lower edge of the glass slide.

3.2.1.7 Second Harmonic Generation Imaging:

Occlusal cavities were prepared in 10 teeth following the same steps used in cavity preparation in the previous experiments. Five of these teeth were filled with Biodentine cement after mixing, and the other 5 were filled with GIC. Cavities were only cleaned in an ultrasonic bath for 5 minutes after their preparation, with no acid etching or conditioning performed for any of the samples. Samples were kept in a wet towel for an hour in an incubator at 37°C temperature to allow enough time for the cements to set before placing them in glass vials containing deionised water for a further 23 hours at the same temperature. Samples were then collected and sectioned vertically using a water cooled diamond wafering blade, then polished as described previously

3.2.2 Imaging & data analysis

All samples for the micropermeability test were examined using the tandem scanning confocal microscope (TSM) (Noran Instruments, Middleton, WI, USA). Samples were mounted on glass slides using molding clay (Harbutts Plasticine Ltd, Bath, UK) and were leveled horizontally. They were all examined with oil immersion objective lenses of x60 and x100 original magnifications in

conjunction with x10 eyepiece, and 546 nm excitation and 600 nm long-pass emission filters. The confocal images were shown on a computer screen through an electron multiplying charge-coupled device iXon 885 EM-CCD (Andor Technology, Northern Ireland, UK); images were viewed using capture and analysis software Andor iQ 1.6 (Andor Technology, Northern Ireland, UK).

Samples with Fluorescein-labelled cement and double-labelled samples were all examined using a confocal laser scanning microscope Leica TCS SP2 (Leica Microsystems Heidelberg GmbH, Milton Keynes, UK) with 63x and 100x Oil immersion objective lenses and 488nm excitation wavelength at 25% laser power and a 530 nm emission filter for Fluorescein dye. For Rhodamine-B imaging, a 568 nm excitation laser source at 63% laser power and a 640 nm emission filter were used. For the measurement of the width of the richly dye infiltrated layer formed in the interface, five representative interfacial images, 512x 512 pixels each, were chosen from each double labelled sample. The contrast of images was optimised using image processing software- ImageJ (National Institute of Health-USA) and rotated until the interface was positioned exactly horizontal with the cement located above. The 512 pixel-wide images were then reduced into 1-pixel width, where the intensity of each pixel represented the average intensity of all the pixels located on the same line. An intensity line profile was then plotted against distance, and the width of the fluorescent band was measured as the area confined to 85% under the line profile curve.

Raman readings were obtained for the fractured or sectioned dentine-cement surfaces using the StreamLine^{TM} technology provided in the Renishaw inVia Raman microscope (Renishaw plc, Wotton-under-Edge, UK). Before each use of the device, the motorized stage of the microscope was set at a specific point of origin (the most upper left point that the stage can reach) and a Raman spectrum for a reference silicone sample was obtained to calibrate the spectra before every use. The Raman Streamline maps were obtained using a water emersion 60x/1.2 NA objective lens Plan Apo VC (NIKON Instruments Europe BV. Surrey, UK) a 785 nm laser source of 25mW power and a 600 grooves/mm diffraction grating.

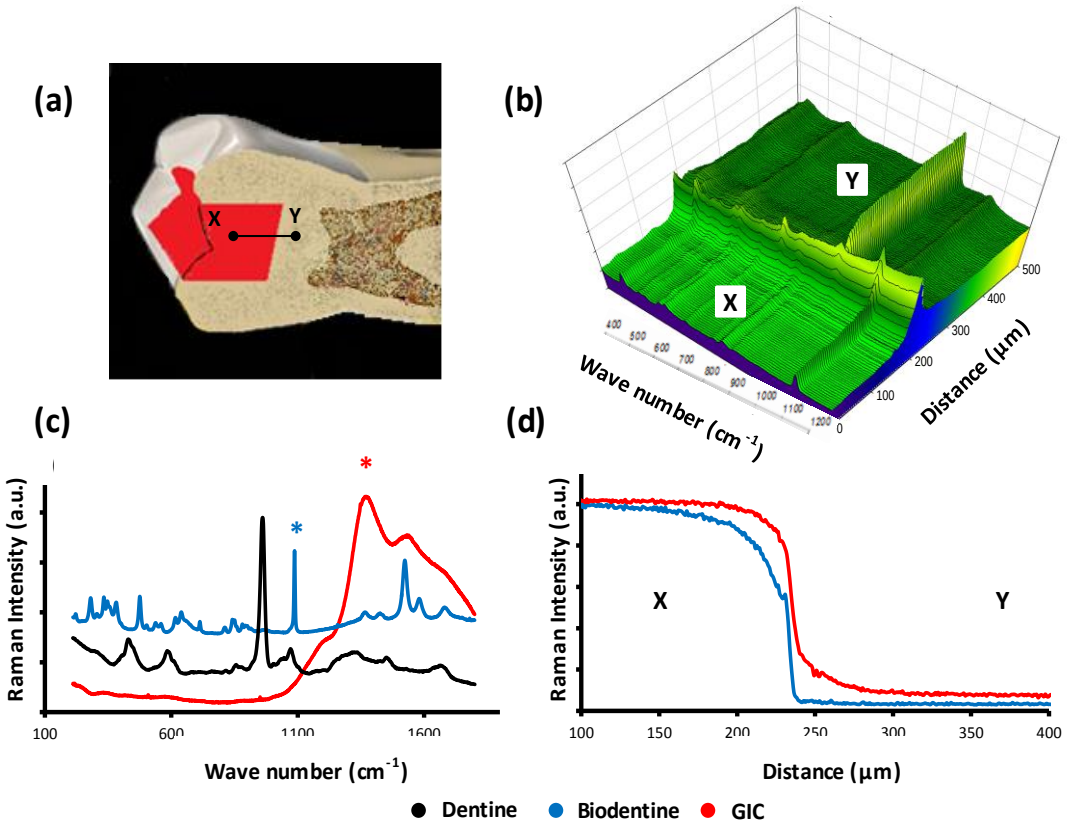

Figure 8:(a) Raman area maps were obtained for the dentine-cement interface in GIC and Biodentine filled teeth using the StreamLine™ scanning from point X to Y. Raman spectral maps were analysed with a curve fitting software which averaged each area map into a single line, where each point on that line was represented by an averaged Raman spectrum **(b)**. From the cements' Raman spectra **(c)**, representative characteristic peaks; 1082 cm^{-1} and 1262 cm^{-1} (marked with asterisks) were designated for Biodentine and GI cements respectively. **(d)** Intensity line profiles were generated for each of these Raman peak, intensity of these peaks were plotted against distance from the interface and the average penetration depth was measured.

Prior to Raman measurements, samples were positioned in focus, placing the interface exactly parallel to the horizontal line of the crosshairs pointer. Using the charge-coupled device (CCD) supplied with the system a high-resolution mosaicked large scale white light reflection image was created from each sample before every reading. The mosaicked image was composed of 2 x 15 images in the horizontal and vertical directions respectively and started 200 µm above the interface within the restorative material (Figure 8-a). The whole area on the montage image (200 µm x 1200 µm) was then selected for the acquisition of a StreamLine Raman map with a 10 µm distance between each line and a 0.9 µm resolution across the interface (Figure 8-b).

All the Raman images were uploaded together into in-house curve fitting software. For each Raman map reading, an intensity line profile for each characteristic Raman peak was generated by plotting the photon intensity of the fitted peak over the distance across the interface (Figure 8-d). The penetration depth was measured by calculating the length across the interface corresponding to 85% of the step function curve area.

For the stain-free second harmonic generation and auto-fluorescence imaging, an in-house multi-photon microscope was used. Each sample was placed on a thin glass cover slip with the polished surface facing the glass. An oil immersion x40/1.3 NA objective lens was used with 950 nm excitation wavelength and 475 nm emission filter for the collagen SHG imaging, and 830 nm excitation wavelength and 500 nm emission filter for the tissue auto-fluorescence imaging.

For the scanning electron microscopy, samples were examined using a Hitachi S3500N scanning electron microscope (Hitachi High Technologies, Maidenhead, UK). The opposite “clean” surface, where no cement was applied, was used as a negative control.

3.3 Results:

3.3.1 Tag like structures

Tag-like microstructures were detected within the dentinal tubules just beneath the dentine: Biodentine interface when imaged using the confocal and scanning electron microscopes. In the reflection mode TSM confocal images taken for the interface, tag-like microstructures were extending from the cement into the underlying opened dentinal tubules in acid etched samples (Figure 9-a). In the samples with Fluorescein labelled Biodentine, these cement tags were also detectable (Figure 9-b), despite leaching of the Fluorescein dye out of the cement, which slightly obscured their appearance. In the un-etched samples, these tags were showing on the bottom surface of the Biodentine cement after it detached from underlying dentine on desiccation.

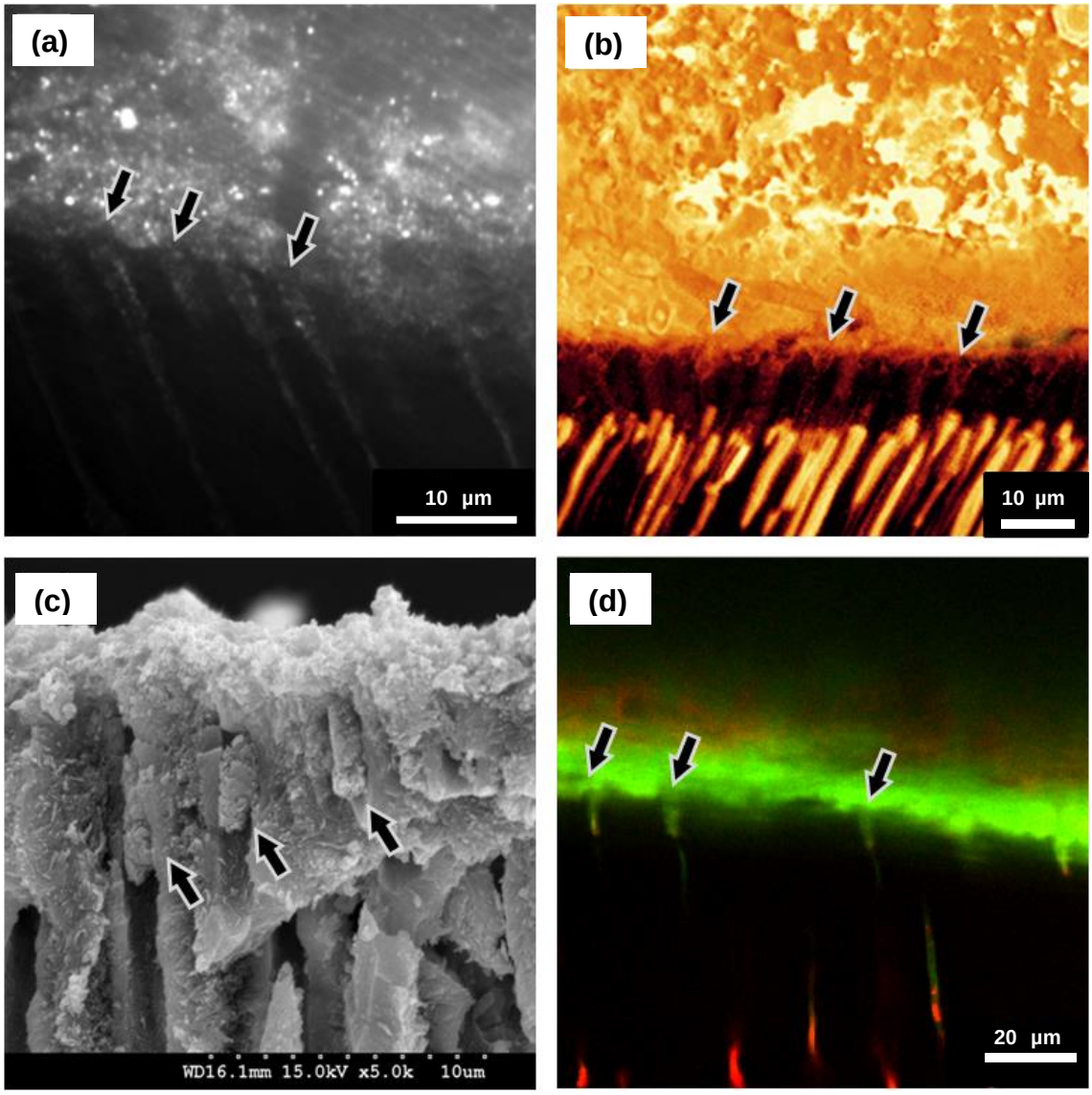

Figure 9: (a) Reflection mode TSM image for the dentine-Biodentine interface showing the tag-like structures (arrows) X100/ 1.4 NA OI TSM **(b)** Fluorescence mode CLSM image showing the cement tags, which appear on the interfacial surface of the Fluorescein labelled Biodentine (above) after it was pulled away from dentine due to desiccation. 63x/1.4NA OI. **(c)** SEM micrograph of fractured dentine beneath a Biodentine restoration. Tag-like structures were detected forming within the dentinal tubules (arrows). **(d)** A fluorescence mode confocal image for a double labelled sample showing the formation of cement-tags (arrows) by Fluorescein labelled Biodentine (green) in the dentine. Composite image of fields taken at 488/530 and 546/600 nm x63/ 1.4 NA OI.CLSM.

In the SEM images, cement tags were clearly detectable within the lumen of fractured dentinal tubules (Figure 9-c). Figure 9-d represents a CLSM image for double labelled un-etched Biodentine sample, the cement tags can be detected with a clear separation between the Fluorescein labelled tags and the

Rhodamine-B permeating from the pulp. There was little evidence of tag-like structures beneath the GIC restorations.

3.3.2 Dye-infiltrated zone

In typical reflection mode TSM confocal images obtained for the dentine-Biodentine interface, a bright band was noticed within the structure of the dentine directly below the interface (Figure 10-a). This band extended along the interface, where its width ranged between 5 and 15 micrometres. A fluorescence mode confocal image for the Rhodamine-B dye (Figure 10-b) taken for the same area, showed the permeability of the dye solution within this layer.

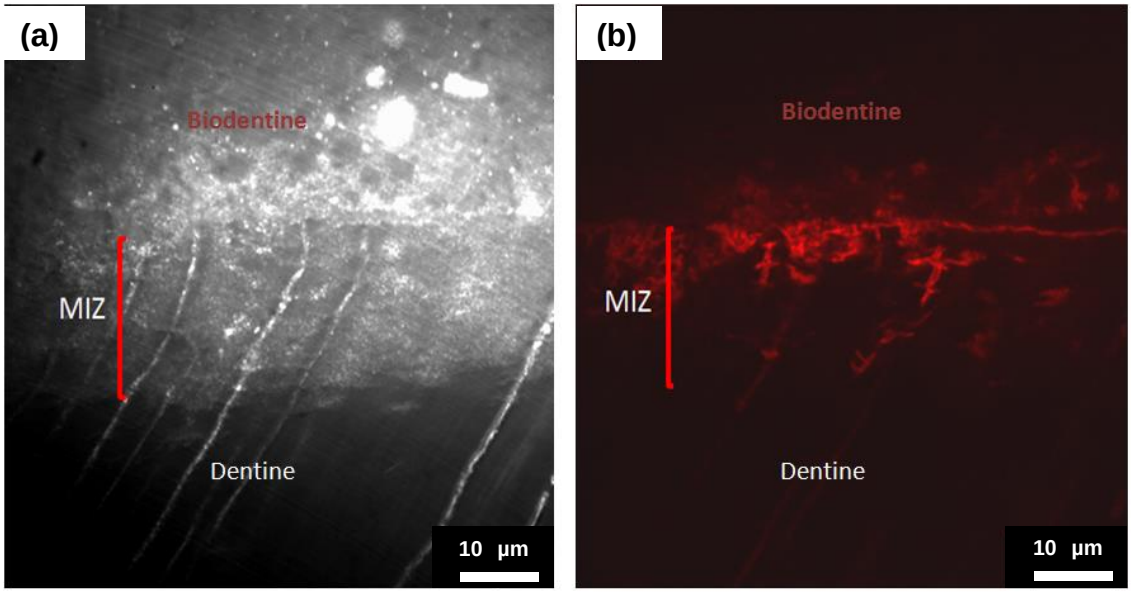

Figure 10: (a) Reflection mode TSM image for the dentine-Biodentine interface, the mineral infiltration zone (MIZ) appears as a band of highly reflective dentine beneath the interface, indicating a change in the dentine's mineral content within this zone. The fluorescence mode image of the same area **(b)** shows the distribution of Rhodamine-B dye, which permeated from the pulp chamber into the interface and cement. X100/ 1.4 NA OI TSM. 546/600 nm.

In the CLSM fluorescence images obtained for the double labelled samples, a dye-infiltrated zone was detectable within the dentine and just beneath the cement in both Biodentine and GIC samples, they measured 6.5 µm ± 0.6 µm and 14.5 µm ± 1.9 µm in width respectively (Figures 11-c1,c2). However, the distribution of the two fluorescent dyes (Rhodamine-B and Fluorescein) was

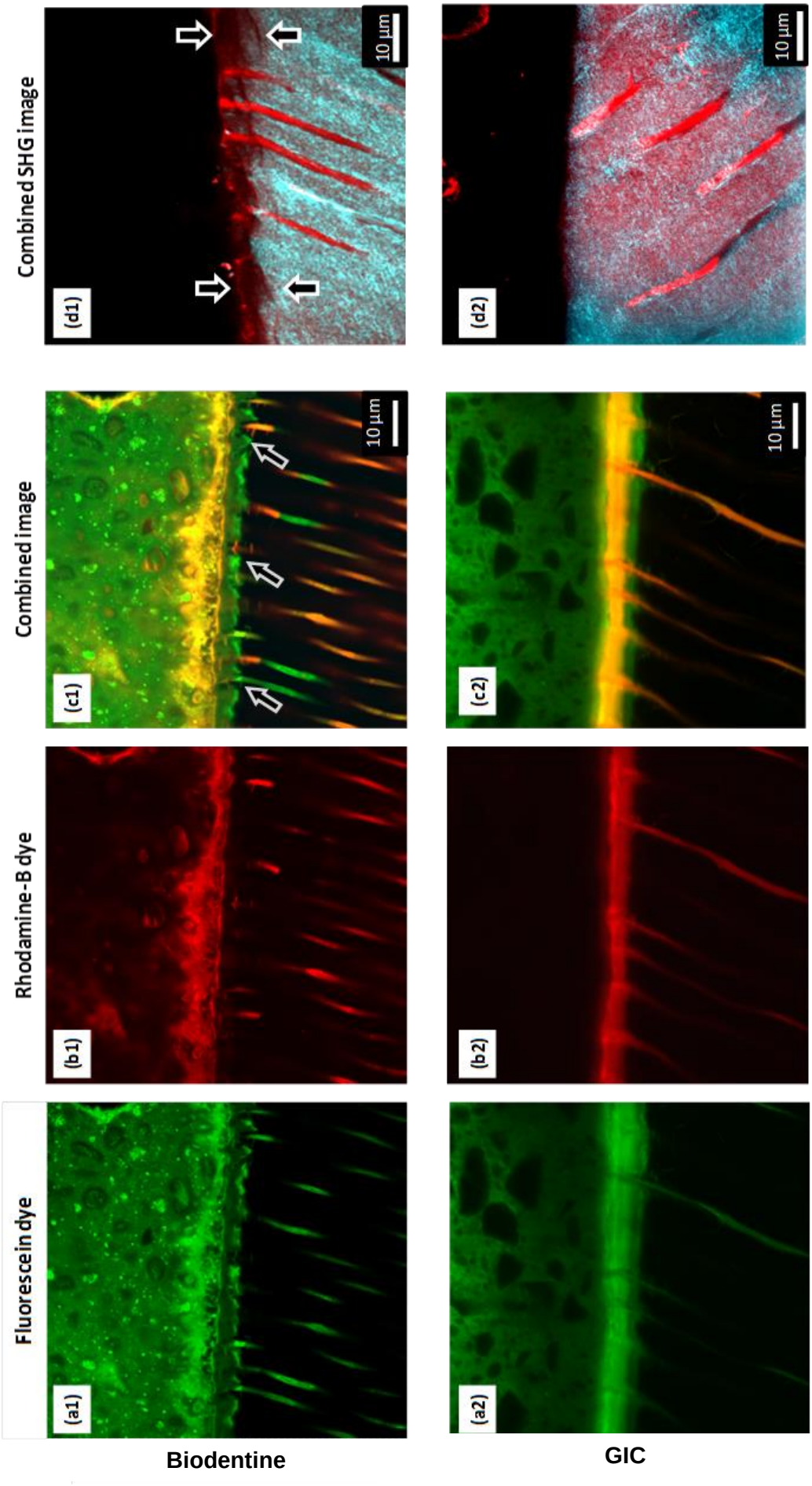

Figure 11: **(a-c)**. Fluorescence mode CLSM images for the Biodentine and GIC interfaces with dentine. (a1) Distribution of the Fluorescein dye labelling the Biodentine cement shows a band of dye-infiltrated dentine just beneath the interface, this band cannot be seen with Rhodamine-B micropermeability (b1).. Caption is continued next page.

Figure 11-cont'd… where the dye permeated through this band and diffused into the cement above the interface without any mixing with Fluorescein. This band is believed to be formed as a result of the strong alkaline effect of calcium hydroxide leaching out of the cement, and it corresponds to the MIZ. (c1) Dye-deficient areas can be seen within this zone (arrows) which represent the un-affected peri-tubular dentine. (a2) Fluorescein distribution in GIC samples showed a richly dye-infiltrated dentine band too, but this band was formed due to the acidic effect of GIC, which affected both inter-tubular and peri-tubular dentine. (b2) Rhodamine-B permeating from the pulp has also infiltrated this band, which diffused laterally through the affected tubular walls and mixed with Fluorescein as shown in (c2). (d1) Second harmonic generation (SHG) signal, originating from the inter-tubular collagen (red), is weak and almost absent in the interfacial dentine beneath the Biodentine (arrows) when superimposed over the dentine's auto-fluorescence signal (cyan), which reflects its actual margin. Unlike the images for GIC samples (d2) where the SHG signal has the same distribution as the dentine's auto-fluorescence signal.

different between the Biodentine and GIC samples. In the Biodentine filled teeth, this zone was richly infiltrated by the Fluorescein alone (Figure 11-a1), with traces of Rhodamine-B (Figure 11-c1), unlike the case in GIC samples where both of the dyes were infiltrating this zone and mixing together (Figure 11-a2 ,c2).

In higher magnification CLSM images taken for the dentine cement interfaces (Figure 12), the tubular structure of dentine was still detectable, where few dentinal tubules were noticeable crossing the dye-infiltrated dentine. In the Biodentine samples (Figure 12-a), peri-tubular dark spaces were noticeable surrounding the tubules along their pathway within this area. These spaces represent areas that were not infiltrated by the fluorescent dyes. On the contrary, no peri-tubular dark spaces were noticed in the GIC samples (Figure 12-b). In these samples the fluorescent dye has infiltrated the tubular walls much deeper than in the adjacent inter-tubular dentine, creating a scalloped border.

The combined two-photon auto-fluorescence and SHG images of the Biodentine samples showed a band of low SHG signal intensity within the dentine near the interface (Figure 11-d1). The tubular structure of dentine is still detectable within this area. No such alteration in the SHG signal was detectable

near the dentine: GIC interface, indicating no structural changes have affected the collagen fibrils (Figure 11-d2).

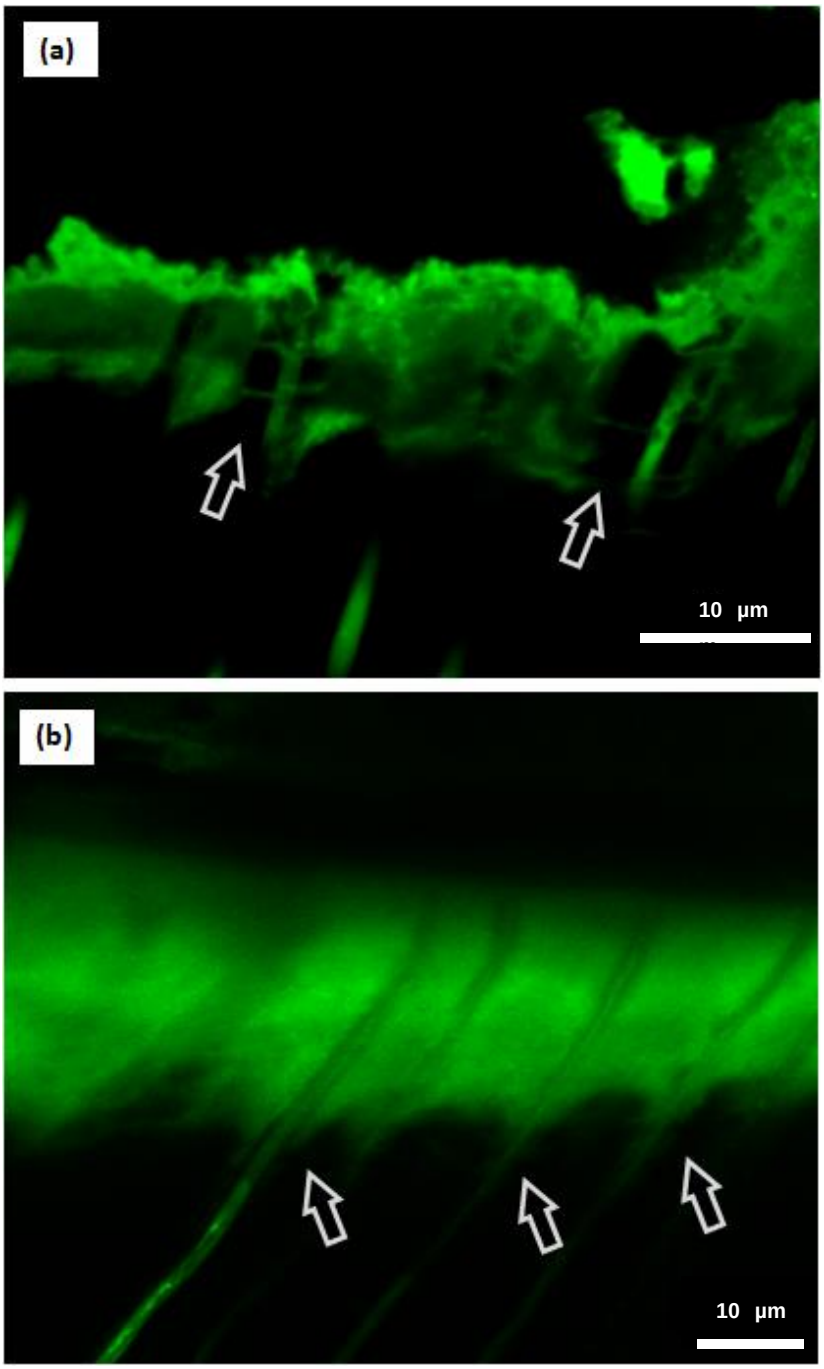

Figure 12: (a) Interfacial dentine under Fluorescein labelled GIC. The scalloped appearance of the interfacial layer, which shows the deeper infiltration of the fluorescent dye towards the pulp in areas adjacent to the tubular lumina (arrows), this is caused by the acidic effect of the GIC, which affects the highly mineralised peri-tubular dentine to a greater extent compared with the inter-tubular dentine. **(b)** The interfacial dentine under Fluorescein labelled Biodentine, exhibited the inverse effect, where peri-tubular dark spaces appeared in the interfacial layer, due to the selective caustic etching effect of the alkaline cement, which spared the peri-tubular dentine, and affected the inter-tubular dentine that has much higher protein content.

In the SEM images, a band of structurally altered dentine was visible just below the interface in the Biodentine samples (Figure 13-a) but not in the GIC samples (Figure 13-b). Within this 10- 20 µm wide band, micro-structural alterations were noticeable but absent on the opposite surfaces of the discs where no cement was applied (Figure 13-c,d). In the surface exposed to the Biodentine, the dentinal tubules appeared blocked and did not open to the surface unlike the tubules in the clean, unexposed surface. There was little evidence of micro-structural changes on the dentine beneath the GIC restorations.

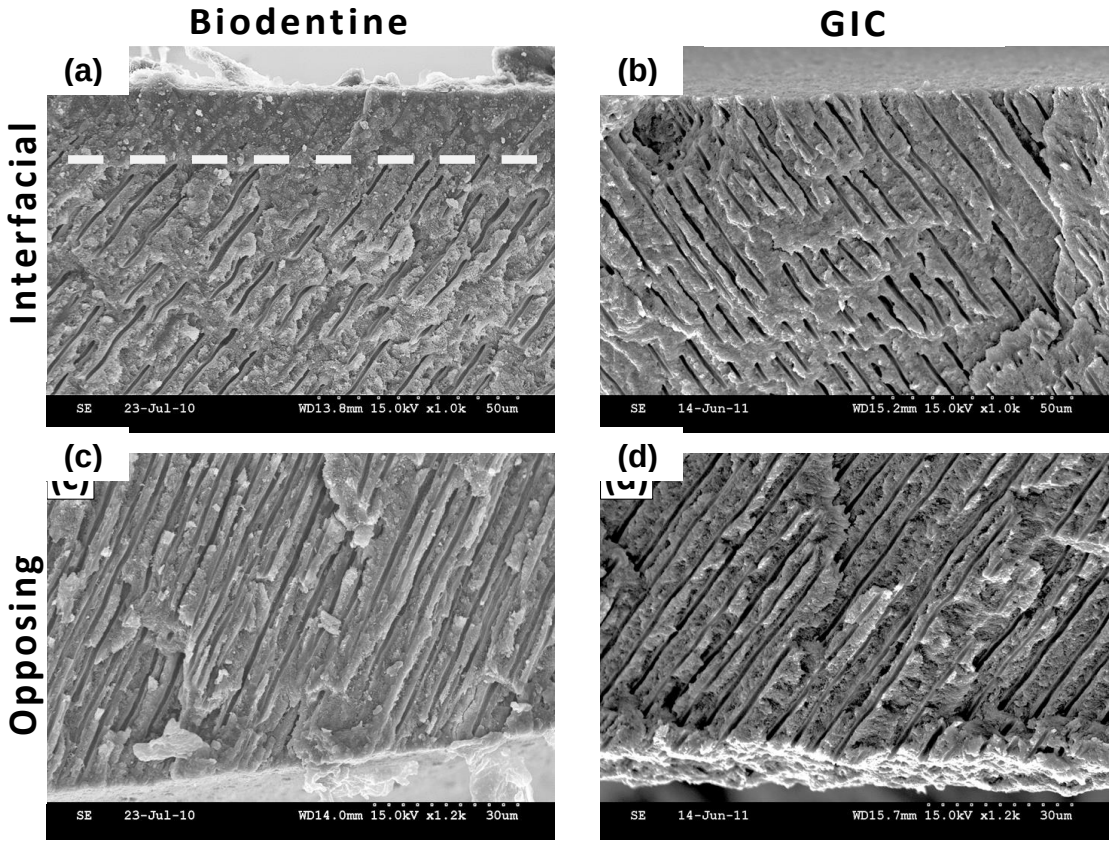

Figure 13: SEM micrographs for fractured dentine discs that were exposed to Biodentine **(a)** or GIC **(b)**. A band of structurally altered dentine is extending along the interface, as can be seen by the obliterated dentine tubules above the dotted line in **(a),** when compared with dentine of the opposing surface where no cement was applied **(c). (b)**no structural changes can be detected in the dentine beneath GIC when compared with dentine of the opposing surface (**d**).

3.3.3 Chemical mapping

The 1082 cm^{-1} carbonate Raman peak (Figure 8-c), representing the stretching mode of the C-O bond in the carbonate group (Martinez-Ramirez *et al.* 2006), was associated with the presence of calcium carbonate from the Biodentine, originating either from calcium hydroxide carbonation or present originally in Biodentine. The GIC's broad peak (Figure 8-c) located at 1262 cm^{-1} corresponds to the overlapping of smaller peaks that represent the polyacrylic (PAA) and tartaric acids and their salts (Young *et al.*, 2000). The intensity of both cements' peaks declined at points located beneath the interface, but in different patterns. This declination was gradual throughout the whole depth for the GIC samples but was followed by a sudden drop in the Biodentine samples. The penetration depth of Biodentine and GIC measured 48±10 µm and 51±6 µm respectively.

3.3.4 Horizontal lines

In both TSM (Figures 14-a, b) and CLSM (Figures 14-c, d) fluorescence mode images, groups of short horizontal lines appeared crossing the dentinal tubules perpendicular to their long axis. These lines appeared beneath the interfaces of both Biodentine (Figures 14-a, b, c) and GIC (Figure 14-d) within a distance of 20 µm. They were parallel to the interfaces and to each other, and equally separated by a distance of an average 2.6 µm. Additionally, they were extending bilaterally beyond the walls of the dentinal tubules. These lines were also detectable in coronal dentine (without restoration) after soaking it in a 0.25% Fluorescein dye solution for three hours (Figure 15).

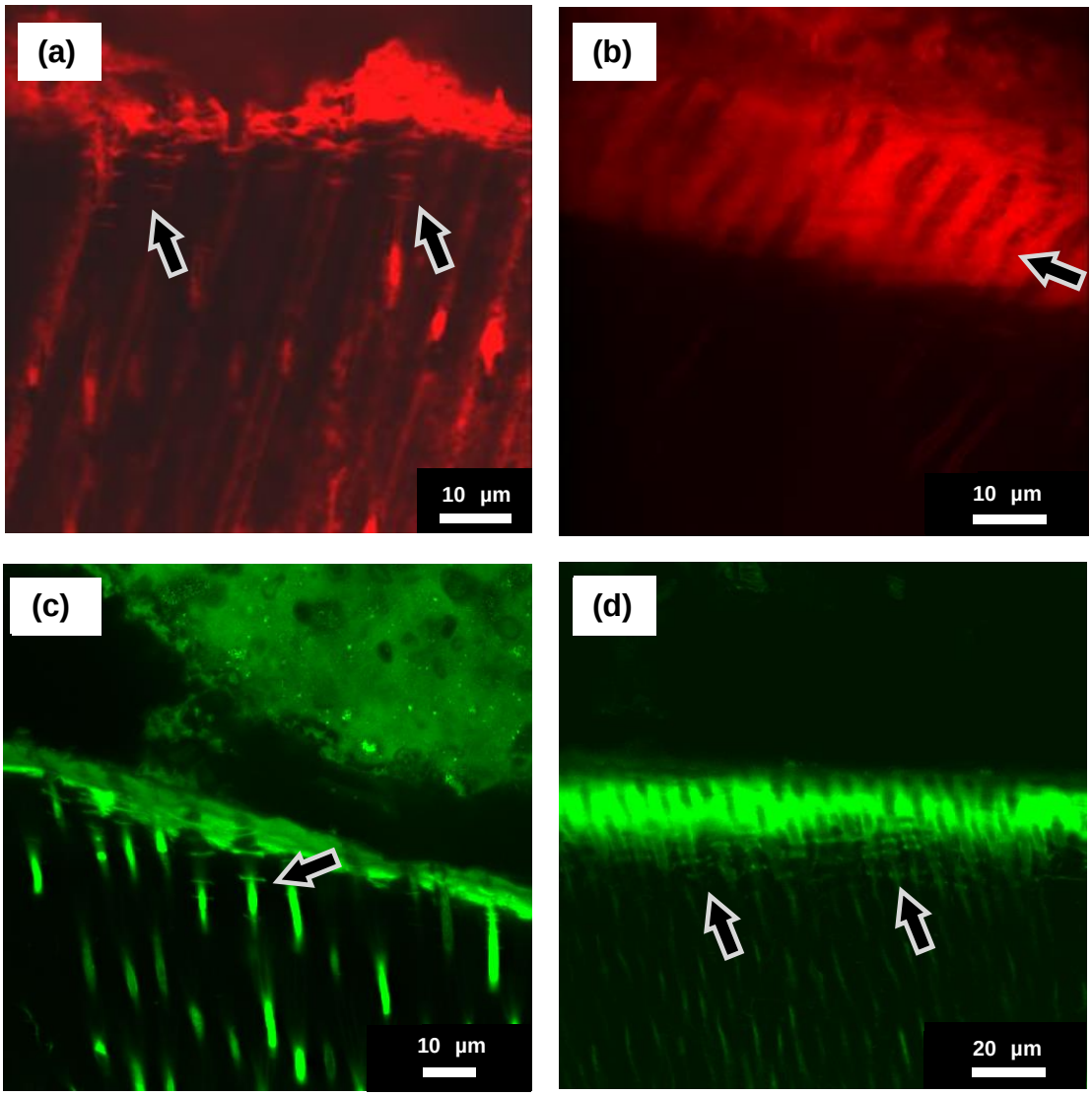

Figure 14: In confocal images obtained for Biodentine **(a, b, c)** and GIC (**d)** samples, it was observed that there were a. **(a)** and**(b)** fluorescence mode confocal images for dentine-Biodentine interface x100/1.4 NA OI TSM. Fig (b) shows clearly the presence of trans-tubular microstructures that cross the tubules (arrows). **(c)** A fluorescence mode image for a dentine-Biodentine interface showing the same horizontal lines (arrows) x63/1.4 NA OI CLSM. **(d)** A fluorescence mode confocal image for dentine -glass ionomer interface under Fluorescein labelled cement (x63/1.4 NA OI CLSM).

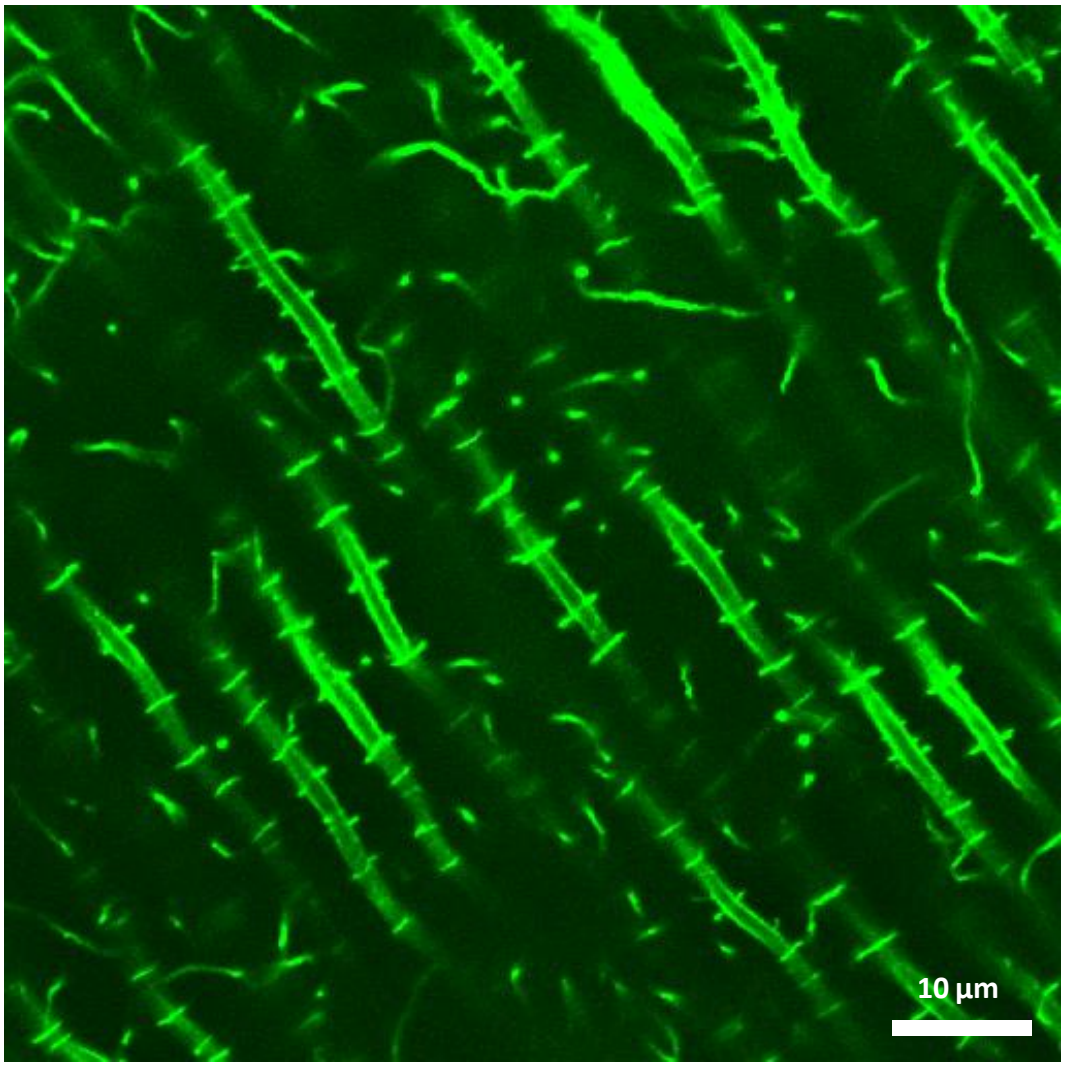

Figure 15: Reconstructed z-stack image that was taken of mid-coronal dentine after it was soaked in a 0.25% Fluorescein solution for 3 hours, showing the horizontal lines crossing the dentinal tubules.

3.4 Discussion:

Studying the interfacial properties of the dentine underneath a calcium silicate based coronal restoration such as the Biodentine was essential for the understanding of the nature and dynamics of this interface, and the mechanism of potential mineralising effects of these cements. However this study was associated with some challenges related to the novelty of the material and the sensitivity of the techniques we were using, which required the development of a variety of pilot studies to determine the most suitable protocols that could enable us to efficiently use these techniques in studying this new interface.

In the confocal imaging studies, different imaging techniques, as well as combinations of fluorescent dyes where tested. However the best results were obtained when Fluorescein powder was mixed with the cement's powder in combination with a 0.25% Rhodamine-B solution for micropermeability (Figure 11). Using this combination of fluorophores provided enough separation between the excitation and emission wavelengths of these two dyes that minimised the overlapping of signals (cross-talk) between these two labels (Watson 1989, D'Alpino *et al.* 2006).

The combination of high spatial resolution (1 µm), rapid map acquisition (around 70 points/min) along with an efficient curve fitting and data analysis software provided a unique technique for the characterisation of the kinetics and chemical changes of the dentine: cement interfaces (Figure 8). Bearing in mind the sensitivity of this technique, different methods have been used to prepare the samples before their investigation, the main concern was the possibility of the cement being smeared over the dentine surface if cutting was used. Fractured dentine-Biodentine discs and fractured whole crowns filled with Biodentine were both used trying to obtain "clean" un-sectioned surfaces. However, because of the unevenness of these surfaces, the obtained Raman spectra were of poor quality, because of the diffused scattering nature of the fractured surface, which affected the curve fitting analysis. On the other hand, no effect of smearing was noticed upon examining sectioned surfaces, which was not expected. Cement smearing into the dentine was minimized by

performing the sectioning and polishing in one direction beginning from the dentine towards the cement.

Tag-like microstructures were clearly detectable in both confocal (Figures 9-a, b, d) and SEM (Figure 9-c) images. Fractured rather than sectioned dentine surfaces were examined with the SEM to avoid any intrusion of the cement into the tubules during sectioning. In addition, deep sections for the interface were obtained using the optical sectioning ability of both of the TSM and CLSM to exclude any alterations caused by the cutting process. These tags have previously been reported in MTA (Reyes-Carmona *et al.* 2009) and Biodentine (Han & Okiji 2011). Following cement hydration, the flowable consistency of the cement might have aided in its penetration through the opened orifices of dentinal tubules and transformed overtime into crystalline clusters within these tubules, as suggested by Weller *et al.* (2008).

However, the confocal images of the Biodentine samples also showed an interfacial layer within the structure of dentine, just beneath the cement. This layer appeared both as a highly reflective band (Figure 10) and a richly dye infiltrated band flooded by fluorophores leaching from the cement (Figures 11-a1, c1). This layer, which we call the “mineral infiltration zone” (MIZ), may be associated with an altered inter-tubular microstructure leading to a change in the optical properties of the interfacial dentine. This layer is confirmed by the SEM micrographs that showed the same band of structurally altered dentine immediately beneath the Biodentine (Figure 13-a). The GIC samples (Figure 13-b) and the dentine of the opposite surface of the discs (Figure 13-c, d), however, did not show such changes.

The MIZ conceptually resembles the inter-diffusion zone in the interface between dentine and adhesives (Ferrari & Davidson 1996), or the ion exchange layer that appears interfacially between dentine and GIC (Wilson 1983) shown in (Figure 11-c2). However, the mechanism for the formation of the MIZ might be different, bearing in mind the alkaline nature of unset calcium-silicate cements compared with acidic GICs. The MIZ could be attributed to a dual effect of the calcium hydroxide released by the cement (Figure 16); firstly an

alkaline caustic etching, followed by mineral diffusion. This makes the calcium hydroxide leaching out of the cement act as an active product (Holland *et al.*1999), while the hydrated silicate phases act as a matrix that holds the structure of the cement (Camilleri *et al.* 2005).

Calcium hydroxide is a highly alkaline material (pH = 13) and could induce a caustic degradation effect on exposed collagen. The extent of this caustic effect on dentine is unclear. The high pH can induce structural changes in the collagen due to the breakdown of intermolecular bonds in the collagen fibrils, which leads to the increase in their water absorption and therefore swelling (Bowes 1950, Kemp & Tristram 1971). A stronger caustic effect, similar to the effect of a heated solution on dentine as described by Allred (1968), could be also suggested. Allred noticed that collagen fibrils on the surface of dentine treated with boiling 0.02% acetic acid were absent, unlike dentine surfaces that have been acid etched without heat, this made it evident that heat has mediated the removal of collagen fibres in a more rapid pattern than acid mediated removal of the inorganic phase, and created a porous structure of the affected dentine. The high alkalinity of hydrated Biodentine might have the same effect, which induces the denaturation of the inter-tubular dentinal collagen fibrils when exposed to the cement and produces a porous structure, with a lesser effect on the peri-tubular dentine which appeared as dye deficient areas in the mineral interaction zone (Figure 12-a).

Andersen *et al.* (1992) referred to the alkaline caustic effect of calcium hydroxide in explaining the decrease in the weight of pulpal tissues when exposed to calcium hydroxide. They attributed this change to the breakdown of ionic bonds in proteins and destruction of their tertiary structures. The denaturing effect of calcium hydroxide was also suggested by Andreasen *et al.* (2002) and White *et al.* (2002) who noticed a negative effect of this paste on root mechanical properties. This was confirmed by the reduced, or even absent SHG signal originating from dentine within the MIZ (Figure 11-d1), indicating changes in the collagen conformation (Sun *et al.*, 2006) unlike in GIC samples (Figure 11-d2) where the SHG signal was not affected. The high alkalinity of hydrated Biodentine could therefore induce a caustic denaturing effect on the

organic collagen component of interfacial dentine, which explains the concentration of fluorophores within the altered dentine. This alkaline caustic effect or “caustic etching” has virtually no effect on the highly mineralised peri-tubular dentine due to its lower collagen content, and is therefore represented by a dye deficient area in the MIZ (Figure 12-a).

In the GIC samples, the dye-infiltrated layer formed beneath the interface was a result of the demineralising effect of the PAA and tartaric acids on the inorganic dentine component (Sennou *et al.* 1999). This inverse effect showed deeper infiltration of the cement-labelling fluorophore into the higher mineralised peri-tubular dentine (Figure 12-b), associated with lateral diffusion of the dye permeating from the pulp space through the demineralized peri-tubular dentine in that zone, leading to mixing of both dyes (Figure 11-c2). This mixing did not appear in the Biodentine samples (Figure 11-c1), where the dye permeating from the pulp failed to diffuse laterally in the MIZ, indicating an intact peri-tubular dentine.

Formation of an interfacial layer between the dentine and calcium silicate cements was previously reported by Sarkar *et al.* (2005), Reyes-Carmona *et al.* (2009), and Han & Okiji (2011). However, they suggested that this layer forms in between the two substrates due to hydroxyapatite formation, unlike our findings, where the mineral infiltration zone formed within the structure of the dentine. Our study shows that this layer is rich with carbonate ions. However, no direct comparison should be made as the samples in our study were kept in distilled water to delineate the effect of the cement alone, unlike the aforementioned studies which used phosphate buffered saline solutions.

Infiltration of calcium hydroxide/carbonate into interfacial dentine is associated additionally with mineral transfer, shown by the Raman maps (Figure 8). The drop in Biodentine’s Raman peak towards the pulp was gradual near the interface, corresponding to diffusion but dropped suddenly at greater depth, suggesting the presence of a diffusion barrier: calcium carbonate crystallisation could be limiting further penetration. Dentine buffering may also explain this sudden drop. In GIC samples the characteristic Raman peak dropped gradually

throughout the whole penetration depth, which is consistent with diffusion products not being hindered by crystallisation. This type of cements' diffusion into the inter-tubular dentine should be differentiated from "tubular diffusion" through the fluid filled dentinal tubules, and therefore we suggest the term "inter-tubular diffusion" to describe it (Figure 16).

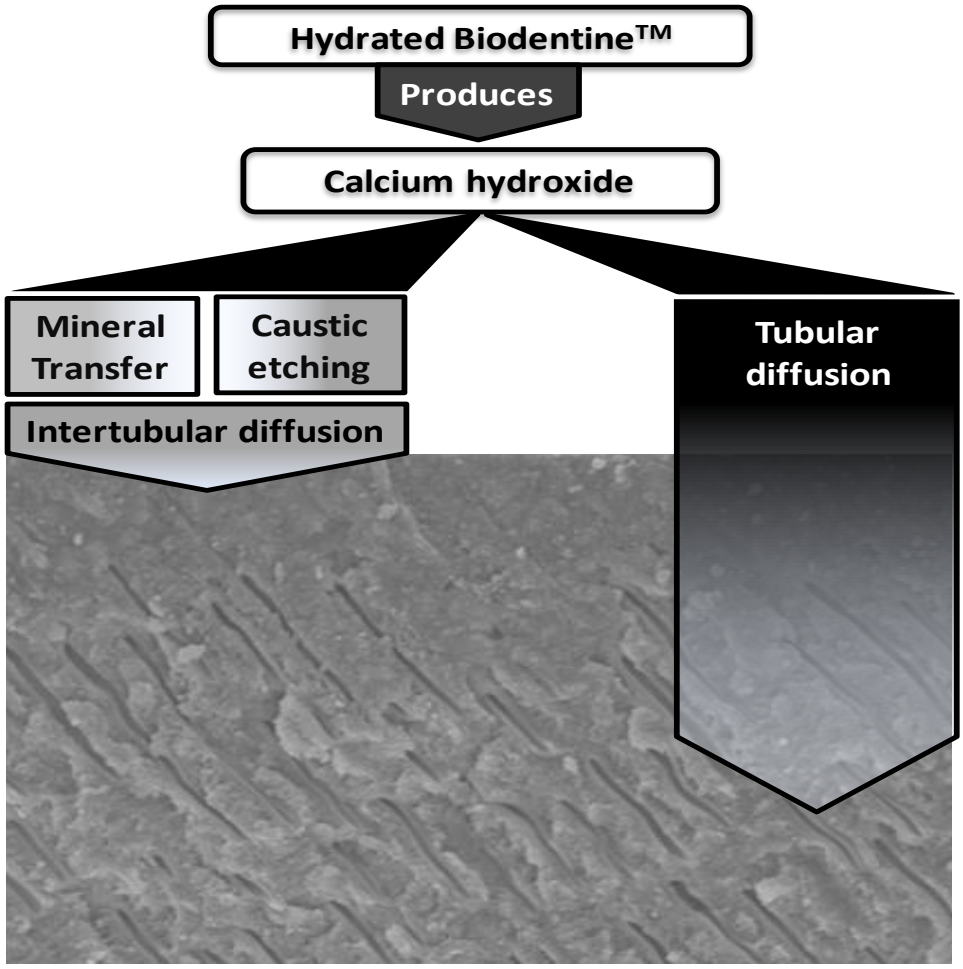

Figure 16: The dual effect of Biodentine on the interfacial dentine is mediated by the diffusion of calcium hydroxide into the intertubular dentine, which induces an alkaline caustic effect on the organic component of dentine, associated with mineral transfer. This diffusion is different than the tubular diffusion of hydration products that occur through the dentinal tubules towards the pulp chamber.

3.5 Suggested model for the horizontal lines:

By referring to the literature, only one paper (Kagayama *et al.* 1999) reported the appearance of similar structures in confocal images of human dentine (Figure 15). These images were obtained for dentine samples stained with Alizarin Red fluorescent dye using a confocal laser scanning microscope. They

described these structures as “nodules”, which were extending across the tubules to the interface between peri-tubular and inter-tubular dentine giving the tubules a bamboo like appearance. This resembles the appearance of the structures that we noticed (Figure 15). Kagayama *et al.* 1999 classified the dentinal tubules into type I and type II depending on the absence or presence of these nodules respectively. In older studies, trans-tubular structures were reported in SEM micrographs of fixed human dentine samples. Tsatsas & Frank (1972) noticed the presence of annular organic substance that was surrounding a central space within the boundaries of dentinal tubules in cross sections. In a later study, Thomas & Carella (1983) confirmed the presence of a lining sheath to the tubular lumen that extended throughout their length from the predentine-dentine junction into the dentine-enamel junction; they suggested this lining to be called the “lamina limitans”, they also reported fibrillar structures that extended from the inter-tubular dentinal matrix through the peri-tubular dentine that were reaching the lamina limitans. Two years later, Szabo *et al.*(1985) described the lamina limitans as a two layered sheath that lines the dentinal tubules in the whole thickness of the dentine in most of the tubules; in addition they described a group of transverse constricting septa in the middle and outer dentine that divided the tubules into a system of chambers. These findings were also reported later by Yoshiyama *et al.* (1989) in dentine of hypersensitive teeth, and mentioned by Holland in 1994.

Our findings (Figure 14-b & Figure 15) indicate the presence of narrow spaces that are sandwiched and confined within the peri-tubular dentine matrix (Figure 17-a). These ring-shaped spaces (Figure 14-d), which we suggest calling the “peri-tubular rings”, are strongly related to the peri-tubular dentine and might have been created as a result of frequent interruption in the deposition of this matrix, and therefore, allowed the fluorescent dyes to permeate through its thickness (Figure 17-a,b). The regular frequency of the peri-tubular rings might suggest that their formation follows a chronological pattern that could coincide with the dentine incremental lines. This chronological pattern could be a result of interference of other concomitantly occurring processes; such as lateral branching of dentinal tubules or trans-tubular septa formation, or could be a self-induced controlled inhibition of the peri-tubular dentine formation.

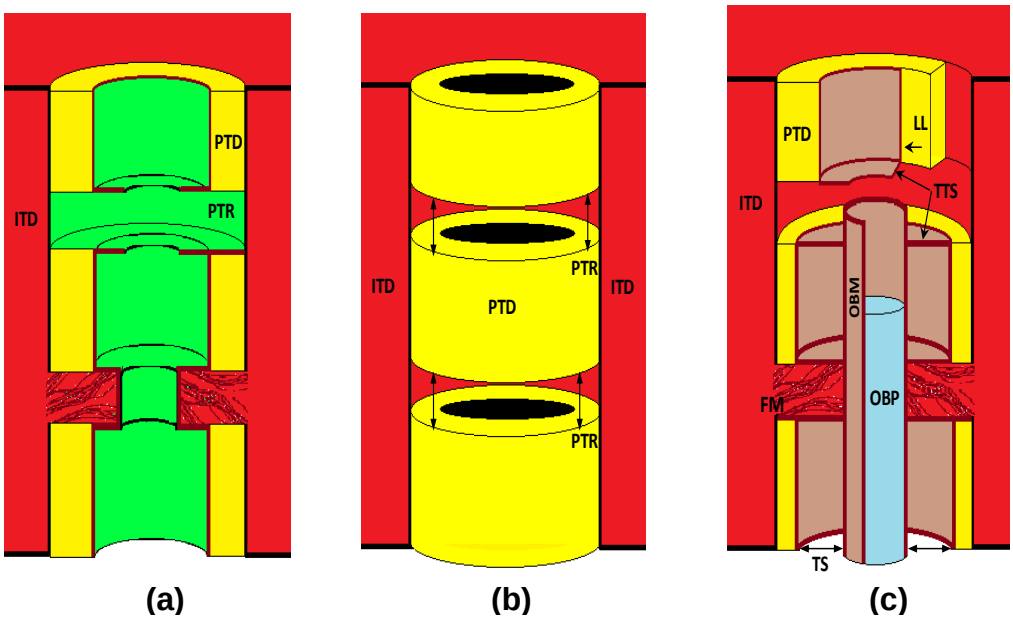

Figure 17: When applying the fluorescent dye (green) inside the dentinal tubules, it infiltrates into these spaces to give the appearance of peri-tubular rings (PTR). In un-erupted or newly erupted teeth (lower ring), these rings do not appear due to the difference in the nature of the substance occupying these spaces, where the dye cannot infiltrate. **(b)** a schematic demonstration for the peri-tubular spaces that are confined within the peri-tubular matrix (yellow). These spaces extend between the tubular lumen (black) and the inter-tubular matrix (red) disturbing the continuity of the peri-tubular dentine. **(c):** Trans-tubular septa (TS), which are formed by central extensions of the lamina limitans (LL), extend towards the tubular space (TS) and attach the odontoblastic process membrane (OPM). These septa enclose the fibrous material (F) that is believed to extend from the inter-tubular matrix through the peri-tubular rings and the lumen of dentinal tubules. in un-erupted or newly erupted teeth. OBP: Odontoblastic process.

3.5.1 Dentinal tubule micro-branches:

The peri-tubular rings could be related to the micro-branches of dentinal tubules, which is one type of tubules' lateral branching that Mjör & Nordahl (1996) described as extending almost perpendicularly to the main tubules with a diameter of 0.05 to 0.1 µm. Their description is in accordance with our observations (Figure 14-a & Figure 15) in terms of location and diameter. In addition, they mentioned that these branches extend through the peri-tubular dentine into the inter-tubular matrix to anastomose with corresponding micro-branches, a description that agrees with our observations in Figure 15, which shows how branch-like structures are extending from the peri-tubular rings and anastomosing with branches of adjacent tubules. Holland (1982) also described

lines that run in a right angle to dentinal tubules in cats' dentine and related these structures to side branching to these tubules.

The relation between micro-branches of dentinal tubules and the peri-tubular rings could be explained by the former's relation with the peri-tubular dentine formation; where it would be sensible to assume that micro-branching of dentinal tubules, or odontoblastic processes, could interfere with deposition and continuity of the peri-tubular dentine. This would create a series of circular defects in the cylindrical peri-tubular matrix, which corresponds to the frequency of the micro-branches where no deposition of dentine matrix could have occurred. These defects could be occupied by a substance of different nature or mineral content.

The frequent and regular appearance of the peri-tubular rings and their relation to the micro-branches of dentinal tubules could suggest that these lateral branches follow a chronological pattern, which might coincide with the incremental pattern of inter-tubular matrix deposition. This was expressed before by Mjör & Nordahl 1996, who suggested that this process should be considered as part of the changes that affect dentine over time, and take place alongside the continuous vital activities within the peri-odontoblastic space and the deposition of peri-tubular dentine.

3.5.2 Trans-tubular septa

On comparing our findings with those of the previous SEM studies (Tsatsas & Frank 1972, Thomas & Carella 1983, Szabo *et al.* 1985, Yoshiyama *et al.* 1989) we tend to assume that all of the aforementioned observations refer to the same structure, and therefore assume the presence of trans-tubular septa that originate from the inter-tubular dentine matrix and cross the peri-tubular dentine and tubular space to reach the centrally located odontoblastic process (Figure 17-c), where they could interfere with the deposition process of the peri-tubular dentine matrix.

It is clear that the peri-tubular rings have a much higher permeability for the fluorescent dyes compared with the surrounding impermeable peri-tubular dentine, which confined the dye solution in ring shaped spaces (Figure 17-a). The higher permeability indicates that the substance occupying these spaces could be of a different mineral content compared with the peri-tubular dentine, or hypo-mineralised as suggested by Kagayama *et al.* 1999.

The nature of the peri-tubular rings' contents is unclear; however, it seems to be related to the functional stage of teeth as well as the extent of the odontoblastic process, which was indicated by the different appearances of these structures in the SEM images for teeth of different functional stages. Thomas & Carella 1983 described a fibrillar material that connected the inter-tubular dentine matrix with the lamina limitans when they examined un-erupted third molars. Unlike Tsatsas & Frank 1972, who examined extracted molars and premolars from subjects aged between 11 and 75 years and described a hyaline organic material surrounding what appeared as a central space in cross sections of dentine (Figure 17-a).

The fibrillar material described by Thomas & Carella 1983 in the dentine of un-erupted teeth supports the theory that peri-tubular rings in un-erupted teeth might contain fibrous tissues that cross the peri-odontoblastic space to connect with the odontoblastic process while enclosed within extensions of the lamina limitans, as suggested by Szabo *et al.* 1985, forming the trans-tubular septa (Figure 17-c). These fibres might remain shortly after tooth eruption, which could also explain the absence of peri-tubular rings in the dentine of newly erupted premolars (Kagayama *et al.* 1999), where the fibrous nature of these tissues could have prevented permeation of the fluorescent dye and therefore the rings did not appear (Figure 17-a). However, with progressive deposition of secondary dentine and retraction of the odontoblastic process, these fibres disappear and are replaced with a more permeable organic substance, which explains the appearance of peri-tubular rings in outer and middle dentine of older teeth (Kagayama *et al.* 1999).

Whether due to the presence of trans-tubular septa, tubular micro-branches or any other process, the presence of the peri-tubular rings is strongly related to the peri-tubular matrix, as it was also suggested by Kagayama *et al.* 1999, who referred to this relation in explaining the absence of the rings, or “nodules” in inner dentine, where the peri-tubular dentine formation is very minimal compared with outer and middle dentine. This difference might be due to the absence of these structures, or due to a difference in their content. Therefore, absence of peri-tubular rings in the young teeth could be related to the different nature of the substance filling these spaces, or due to minimal peri-tubular matrix deposition in these teeth similar to un-erupted teeth.

Absence of the peri-tubular rings in young teeth could be also related to the minimal deposition of peri-tubular dentine at early functional stages. Mendis & Darling (1979) found that dentinal tubules of erupted teeth without any attrition have the same amount of peri-tubular dentine as in un-erupted teeth, leading to the suggestion that attrition is the main influencing factor on peri-tubular dentine deposition. And since attrition in its mildest form is a physiological process related to the tooth functionality, we can conclude that the peri-tubular dentine deposition is related to the tooth functionality. Hence, the peri-tubular rings, which are related to the peri-tubular dentine, appear in fully erupted and functional teeth rather than un-erupted or newly erupted teeth, where no much deposition of peri-tubular dentine. This relation could not be confirmed in this study, and therefore further investigations are still needed.

Relating the trans-tubular septa to the odontoblastic process remains speculative, however the presence of such a relation suggests that these structures might act as lateral sinews that could keep the odontoblastic process centrally pulled from the tubular walls during the process of dentineogenesis, and prevent it from crawling pulpally inside the tubules; especially that the tubules at early stages have wide diameters due to the incomplete formation of the peri-tubular dentine (Figure 17-c). This could explain the absence of the trans-tubular septa in inner dentine, as reported by Szabo *et al.*(1985) and Kagayama *et al.*(1999), where the odontoblastic process might have enough

support provided by its width and proximity to the pulpally located odontoblast cell body.

3.6 Conclusions:

In conclusion, the application of calcium silicate based dental cements, such as the Biodentine, on wet dentine is associated with changes in its micro-structure and mineral content. A band of altered dentine, described as the mineral infiltration zone, could appear as a result of the action of calcium hydroxide released during the setting and maturation of the cement. This highly alkaline hydration product affects the organic component of the dentine, and allows mineral transfer in the form of calcium carbonate. On the contrary, the effect of the glass ionomer cement on dentine is mediated by the acidic nature of the material, which targets the inorganic component of the dentine. This was demonstrated in the selective effect of the acidic cement on the highly mineralised peritubular dentine. The use of stain-free SHG imaging technology also indicates the modification of the dentine collagen beneath the calcium silicate cement. Additionally, the alkaline and acidic effects of the calcium silicate and GI cements, respectively, could explain the appearance of short horizontal lines just beneath the interface. The alkaline or acidic effect might have increased the water permeability into these structures, either by increasing water absorbance by their organic content or by increasing their porosity respectively.

Chapter 4 Calcium silicate cement -induced remineralisation of totally demineralised dentine in comparison with glass ionomer cement: Tetracycline labelling and two-photon fluorescence microscopy.

4.1 Introduction:

Studying the restorative materials mediated remineralisation of dentine has been gaining more attention in the last few years with a growing body of research on this subject. This, on one hand, is strongly related to the growing interest in minimally invasive approaches for the management of dental caries (Onishi *et al.* 2008, Carneiso *et al.* 2009, Petersson & Kambara 2010). While on the other hand it is encouraged by the growing interest in the protective role of remineralisation on acid etched dentine underneath resin-based restorations (Tay & Pashley 2008), which has triggered attempts to develop remineralising protocols to restore the structure and function of calcium depleted collagen fibrils as a protective measure against their hydrolysis.

For the in-vitro study of dentine remineralisation, different techniques have been applied to detect the change in the mineral content of mineralising substrates. These techniques included scanning and transmission electron microscopy (SEM) & (TEM) (Eisenmann & Yaeger 1972, Tay & Pashley 2008), Fourier transform infrared spectroscopy (FTIR) (Li & Chang 2008), Raman spectroscopy (Vollenweider *et al.* 2007), X-ray diffraction (XRD) (Saito *et al.* 2003), energy dispersive X-ray spectroscopy (EDX) (Zhang *et al.* 2012), microradiography (Arends *et al.* 1990, Kawasaki *et al.* 1998), Micro-CT scanning (Liu *et al.* 2011b), and nanoindentation (Bertassoni *et al.* 2011). Despite the significance of these techniques, their ability to detect mineralisation is limited to surface characterisation, whether morphological, chemical, or mechanical that requires careful sample preparation, some may also suffer of relatively low resolution such as Micro-CT scanning. These techniques do not enable the high resolution observation of the mineralisation process and associated morphological features deep within the structure of the remineralised organic matrix, which may be more informative and representative.

Two-photon fluorescence microscopy is an advanced deep imaging technique that enables the observation of deep tissues with a high resolution. A high intensity illumination laser source with twice the wavelength required for the fluorophore excitation is used to deliver a high flux of excitation photons with half of the fluorophore excitation energy (Boyd & Masters 2008). Therefore, for the fluorophore excitation and subsequent fluorescence the energy of two photons should be transferred. This confines sample excitation into a small volume and reduces unwanted scattering. The use of a long wavelength laser source allows deeper penetration into the sample, and insures wider wavelength separation from the emission spectrum. Two-photon microscopy has the ability to image deep into tissues up to 500 µm, compared with conventional confocal microscopes that can seldom be used in the UV range and have limited depth penetration of 100 µm (Helmchen & Denk 2005).

Combining the deep tissue imaging capability of the two-photon fluorescence microscopy with an appropriate mineralisation labelling technique could provide a useful imaging technique for the study of mineralisation. Tetracycline is one of the labelling agents that has been commonly used for the study of mineralisation in osseous (McLure 1982, Tapp *et al.* 1965), as well as dental tissues (Kabasawa *et al.* 1995, Moseley *et al.* 2003). Tetracycline is composed of four carboxylic rings, which enables it to chelate calcium ions within the mineralised tissues. It can fit calcium ions in the C10, C12, and C2 carbons without major distortions to their crystalline structures (Skinner & Nalbandian 1975). Upon this chelation, Tetracycline exhibits enhanced yellow green fluorescence under ultra-violet (UV) excitation (Aaron *et al.* 1984, Schneider *et al.* 2003).

In an in-vitro mineralisation model, calcium-silicate based cements could induce the formation of apatites when placed in phosphate rich media, such as phosphate buffered saline (PBS) solution (Tay & Pashley 2008). Calcium-silicate based cements release calcium during their setting reaction in the form of calcium hydroxide (Camilleri *et al.* 2011), which in the presence of high phosphate concentrations will form calcium phosphate and precipitate on the exposed collagen fibrils to re-mineralise the organic matrix (Tay *et al.* 2007, Tay

& Pashley 2008, Kim *et al.* 2009). By adding the Tetracycline to the mineralisation medium, this fluorophore is expected to be incorporated within the calcium containing minerals; therefore it could be a useful probe to observe the remineralisation of an organic matrix using the two-photon microscopy. In addition to the role of Tetracycline as a labelling agent, Tetracycline is well known for its antimicrobial and anti-matrix metalloprotease (MMP) (Osorio *et al.* 2011) properties, which could be beneficial in preventing bacterial growth in the mineralisation media and inhibiting the hydrolysis of exposed collagen in demineralised dentine, respectively.

Glass ionomer cements have been extensively studied for their potential remineralising effects on carious dental tissues (Miyauchi *et al.* 1978, ten Cate & Van Duinen 1995). This has encouraged their use as part of minimal invasive procedures to induce the remineralisation of caries affected dentine (Yip *et al.* 2001). These effects were principally attributed to the rich fluoride release by the GIC (Frosten 1998, Murai *et al.* 1998), which induces the formation of highly acid resistant fluoroapatites (Tsanidis & Koulourides 1992). Ion exchange with dentine, including calcium and strontium, was reported (Sennou *et al.* 1999), and therefore indicated the dentine remineralisation (Ngo *et al.* 2006). However, the role of GIC in dentine remineralisation remains controversial in the absence of conclusive results about this role (Randall & Wilson 1999). Furthermore, studies could not demonstrate the remineralising potential of GIC in totally demineralised dentine. On the contrary, GIC failed to induce remineralisation of totally demineralised dentine (Kim *et al.* 2010).

This study aims to: 1- Evaluate the mineralising potential of calcium silicate based dental cement (Biodentine) to induce remineralisation of totally demineralised dentine in comparison with glass ionomer cement. 2- Evaluate the use of tetracycline labelling in conjugation with two-photon fluorescence microscopy for the study and detection of mineralisation, and compare it with back-scattered electron-scanning electron microscopy. 3- Characterise the chemical composition of the mineralisation using Raman spectroscopy.

4.2 Materials and Methods:

4.2.1 Sample preparation

Forty dentine discs of 1.5 mm thickness (Figure 18-a) were prepared from extracted human third molars using a water cooled slow speed diamond wafering blade XL 12205 (Benetec Limited, London, UK). Ethical approval and consent were obtained (East Central London Research Ethics Committee-1 (10/H0721/55)). Dentine demineralisation was conducted using 17% Ethylenediaminetetraacetic acid solution (EDTA) (Calasept®, Nordiska Dental, Ängelholm- Sweden), in which the dentine discs were stored for 5 days with continuous stirring (Figure 18-b). After demineralisation, all the dentine discs were rinsed with deionised water, and cleaned in an ultrasonic bath for 3 minutes. Calcium silicate based dental cement Biodentine™ (Septodont, Saint Maur des Fosses- France) was mixed as per the manufacturer's instructions, the liquid was added to the powder and triturated for 30 seconds, then packed into rectangular moulds (8 x 8 x 2 mm) using a plastic instrument. The cement blocks were left to set for 30 minutes at 37°C temperature under continuous wetting (Figure 18-c).

Twenty-two demineralised dentine discs were placed on top of the set Biodentine blocks after they were taken out of the moulds (Figure 18-d). Both the dentine and cement were held together using a cotton thread. Samples were stored separately in glass vials containing 7.0 ml of the storage solution and were divided into 3 groups based on the storage medium as follows (Figure 19-a);

- BTP group (n=10): 0.015% Tetracycline (87128 Sigma-Aldrich, Dorset, UK) in a phosphate buffered saline (PBS) solution (Oxoid Limited, Hampshire, UK)
- BTW group (n=4): 0.015% aqueous Tetracycline solution without PBS
- BP group (n=8): PBS solution alone.

Additionally, 4 dentine discs were stored separately in a 0.015% Tetracycline and PBS solution without the cement (Group DTP). Further 11 samples were prepared as described above but the cement blocks were prepared from glass

ionomer cement (GIC) Fuji IX (GC Corporation. Tokyo, Japan), samples were distributed into 3 groups as follow:

- GTP group (n=5): 0.015% Tetracycline and PBS solution
- GTW group (n=3): 0.015% aqueous Tetracycline solution without PBS
- GP group (n=3): PBS solution alone.

All the samples were stored for 8 weeks in an incubator at 37°C, and the solutions were replaced every two days.

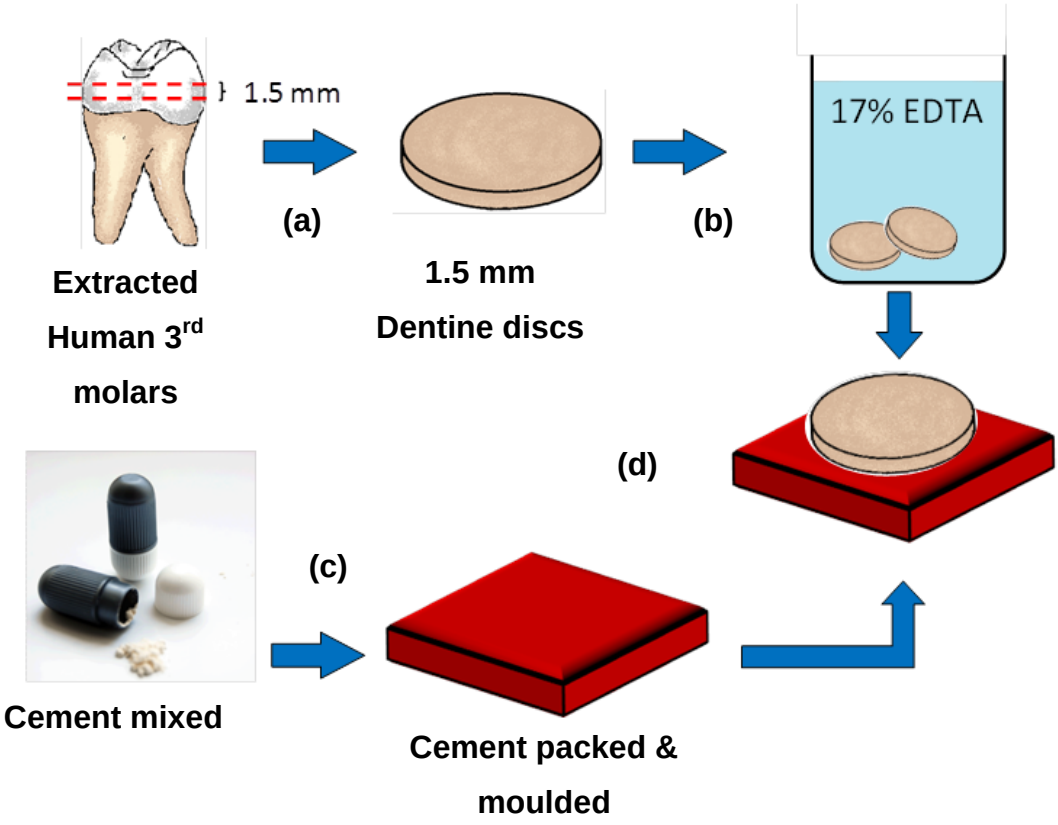

Figure 18: Sample preparation. Dentine discs (1.5 mm) cut from extracted third molars **(a)** and demineralised using EDTA **(b)**. Cement blocks of Biodentine (or GIC) were placed under the dentine discs **(d)** after the cement was mixed and packed in square shaped moulds for 30 min **(c).**

4.2.2 Imaging:

After storage, samples were retrieved and rinsed with deionised water to remove any surface precipitates, and then they were cleaned in an ultrasonic bath for 10 minutes. The dentine discs were sectioned vertically after they were included in light-cured methacrylate (Magilight, Davis Schottlander & Davis Ltd. Herts, UK) (Figure 20). Sectioned surfaces were then polished using a 1200-grit

carborundum paper and cleaned in an ultrasonic bath for a further 3 minutes. One half of each sample was examined using an in-house manufactured two-photon fluorescence microscope using a x40/1.3 NA oil immersion objective lens with 800 nm excitation wavelength and 550 ±20nm emission filter (Schmitt & Schneider 2000).

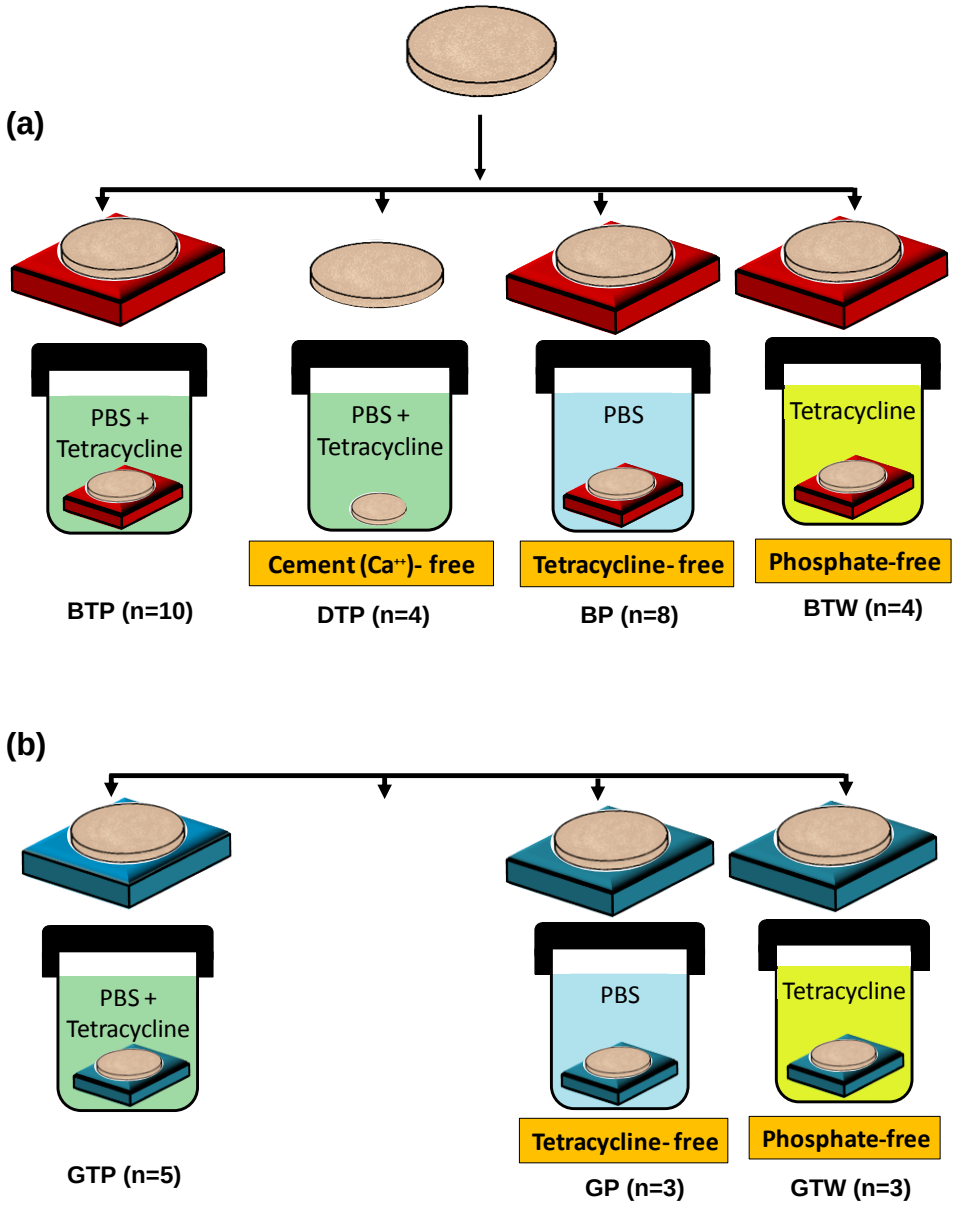

Figure 19: Sample storage. Samples with Biodentine **(a)** or GIC **(b)** cements were stored for eight weeks in designated storage media. B: Biodentine™, G: GIC, T: Tetracycline, P: PBS, W: Water

Six fluorescence intensity images, 512 x 512 pixels each, were obtained from the sectioned dentine, and the fluorescence intensity of each image was calculated using Image J analysis software (ImageJ, Wayne Rasband, NIH, USA). The fluorescence intensity values were averaged for each sample and the average fluorescence intensity of each group was then calculated and plotted. Using the fluorescence lifetime imaging (FLIM) option of the same microscope, five FLIM images, 256 x 256 pixels each, were obtained for each sample. Additional FLIM images were obtained for freshly demineralised dentine discs (n=3), sound dentine discs (n=3), Tetracycline powder, and Tetracycline-calcium complex, which acted as controls to compare the fluorescence lifetime calculated for the dentine in each group. Using TRI2 FLIM analysis software, the fluorescence decay curves were fitted using a tri-exponential model and the average lifetime was calculated for each image, and averaged for each group. One-way ANOVA test was performed on the fluorescence intensity and FLIM results using IBM SPSS Statics Viewer 21software (IBM United Kingdom limited, UK)

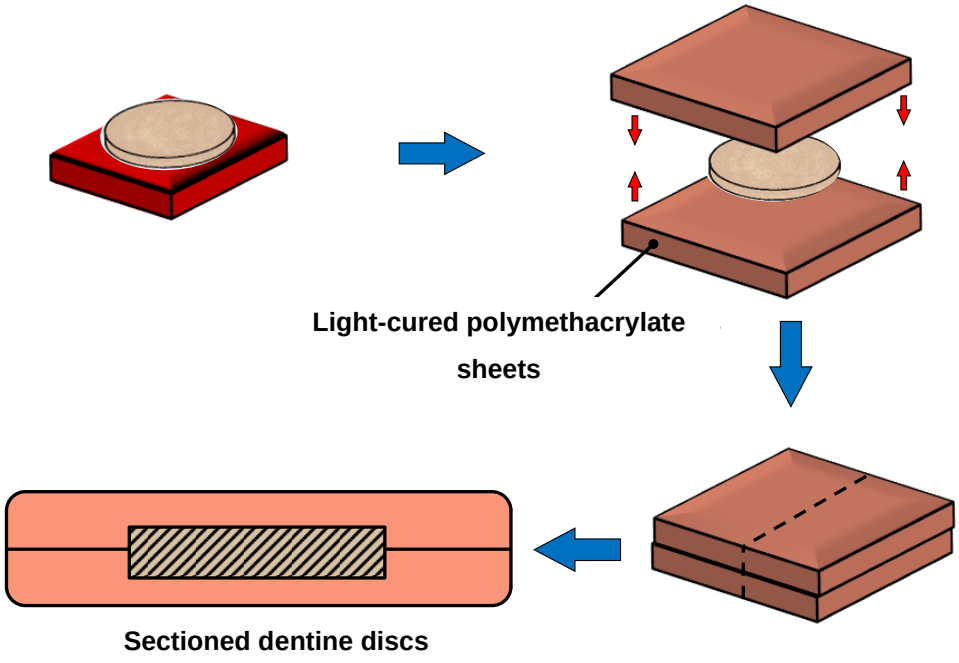

Figure 20: Samples sectioning. Before imaging, dentine discs were collected from the storage media and cleaned before they were included in light-cured polymethyl-metharcylate sheets in order to section the discs and image the sectioned surface.

For the chemical analysis, a Renishaw inVia Raman spectroscope (Renishaw plc, Wotton-under-Edge, UK) was used to examine samples of demineralised dentine stored alone in PBS (DP), with Biodentine (BP), or with GIC (GP), in addition to Raman spectra obtained for sound dentine (SD). Raman spectra were obtained using a x50/0.75 NA objective lens and 785 nm excitation laser source and 1200 grooves/mm diffraction grating. Three extended Raman scans (100-2000 cm^{-1}) were obtained for each sample with 10 seconds acquisition time. Obtained spectra were then normalised to the laser power and averaged for each group before they were plotted together. Four samples of the dentine discs stored with Biodentine and PBS (BTP & BP groups) were further examined using backscattered electron- scanning electron microscopy BSE-SEM. For this type of imaging, samples were gradually dehydrated using methanol then imbedded in polymethyl-methacrylate (PMMA), sectioned, and polished on successive abrasives papers.

4.3 Results:

4.3.1 Dentine degradation:

On retrieving the dentine discs after storage, it was unexpectedly noticed that the bulk of the aged dentine discs, which were exclusively stored with Biodentine in phosphate rich media (BTP and BP), were partially degraded; leaving a shell-like structure of 300 µm thickness on the outer and side surfaces (Figure 21). While the dentine discs in the other storage media (DTP, BTW) or that were stored with the GIC (GTP, GTW, GP) were totally intact after storage, with no detectable degradation macroscopically.

4.3.2 Two-photon fluorescence imaging

Representative fluorescence intensity images of the demineralised dentine from each of the Biodentine groups as well as the cement-free group are shown in Figure 22. Image intensity was standardised in all of the images to demonstrate the actual difference in the fluorescence intensity, while the inset represents the same image after enhancing the intensity.

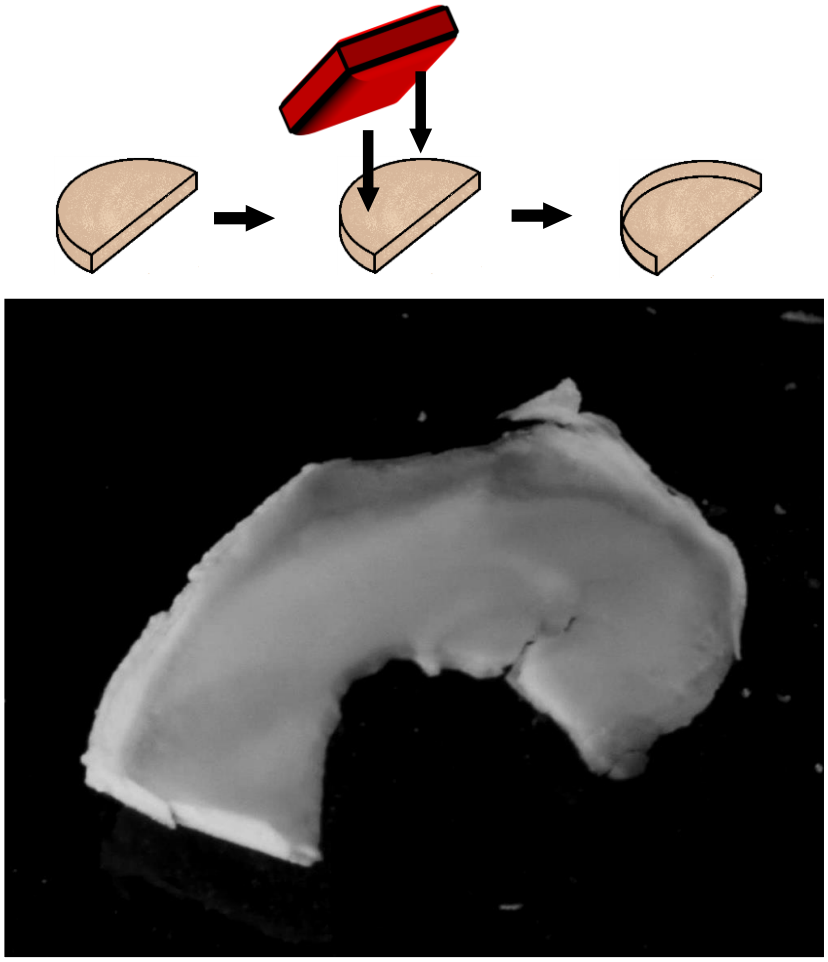

Figure 21: A photograph taken of the inner surface of the shell-like structure of the remineralised dentine after ageing in a phosphate rich medium with calcium silicate cement Biodentine. The inset shows the location of this remaining structure.

The graph in Figure 23 represents the average fluorescence intensity of the demineralised dentine in each of these groups. The strongest fluorescence was detected in the BTP group (Figure 22-a). Samples that were stored with the Biodentine in a phosphate-free solution of Tetracycline (BTW) exhibited weaker fluorescence (Figure 22-b), approximately 40% of the fluorescence measured in the BTP group. Statistical analysis revealed no significant difference between the BTW, DTP, and BP groups; however the difference was only significant between each one of these groups and the BTP group (Table 4). Measuring the ratio of the fluorescence intensity of the BTP group to BTW could be considered as an indicator for the formation of Tetracycline incorporated calcium-phosphate minerals over Tetracycline complexes with free calcium or non-phosphate containing minerals, which measured 2.63 (Figure 24). Fluorescence intensities

of the dentine samples stored in the cement-free solution (DTP) (Figure 22-c) or Tetracycline-free solution (BP) (Figure 22-d) were almost equal, exhibiting around 17% and 16% of the fluorescence detected in the first group, respectively.

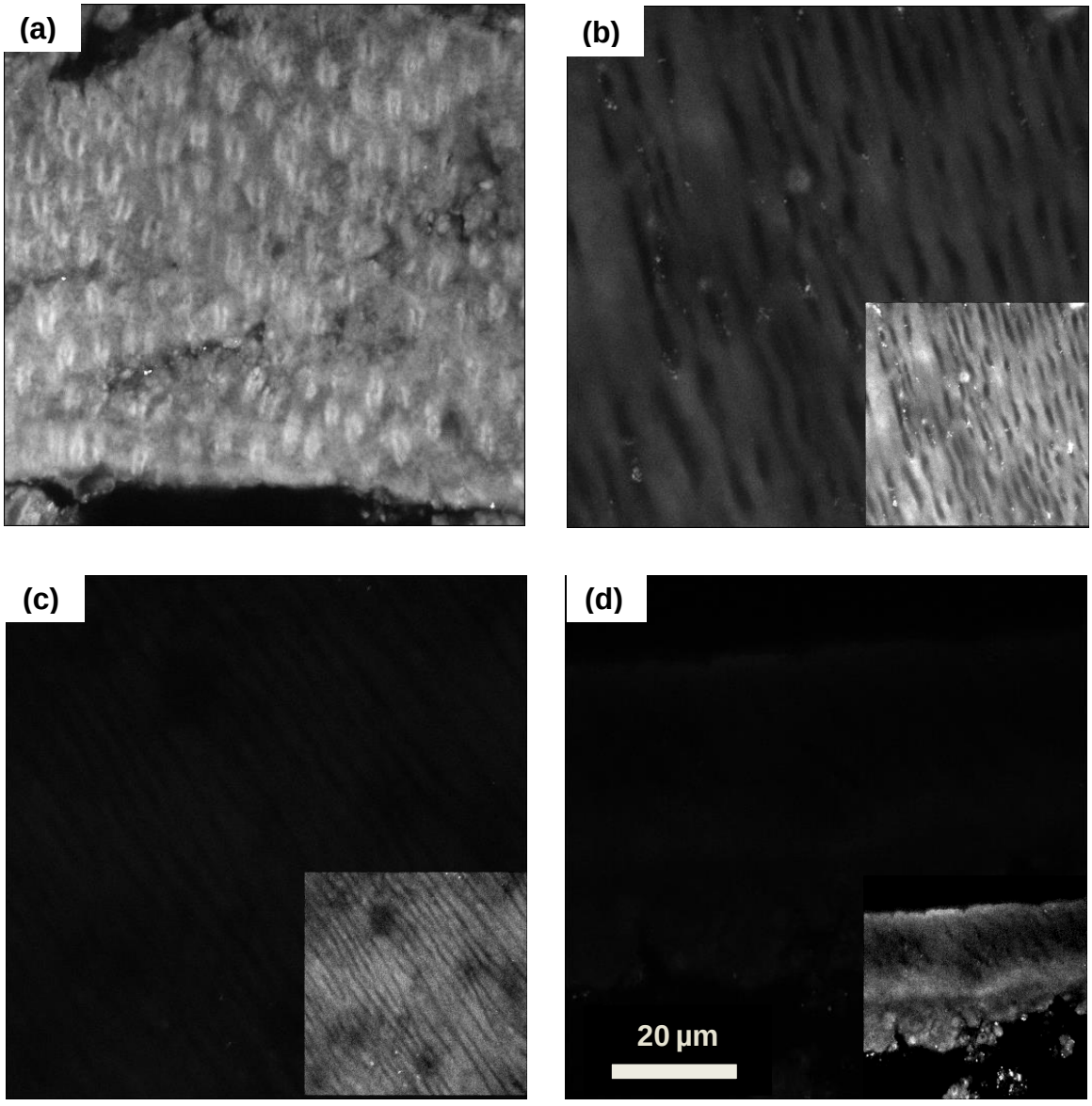

Figure 22: Comparing the fluorescence intensity of the demineralised dentine discs after storage with the Biodentine cement in: **(a)** Tetracycline and PBS solution (BTP). **(b)** Tetracycline and water (BTW). **(c)** Tetracycline and PBS without the cement (DTP)**. (d)** PBS alone (BP)**.** The fluorescence intensity of these images have been standardised to exhibit the real difference among the different groups. The insets show the same images after enhancing the fluorescence intensity.

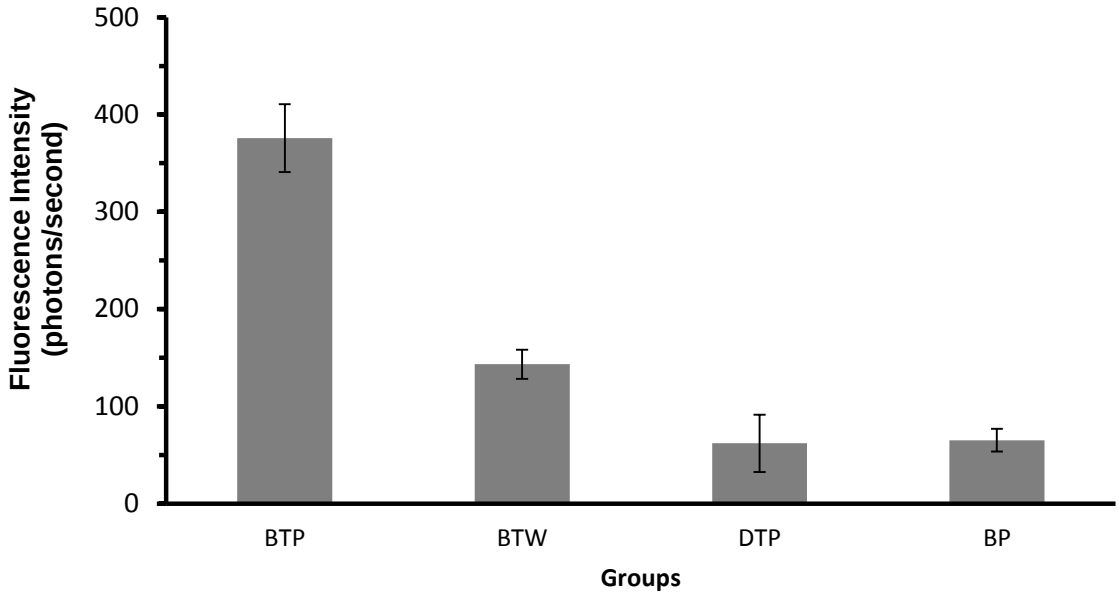

Figure 23: The average fluorescence intensity of each dentine group after 8-week storage in different media with the Biodentine cement (BTP, BTW, BP), or without the cement (DTP).

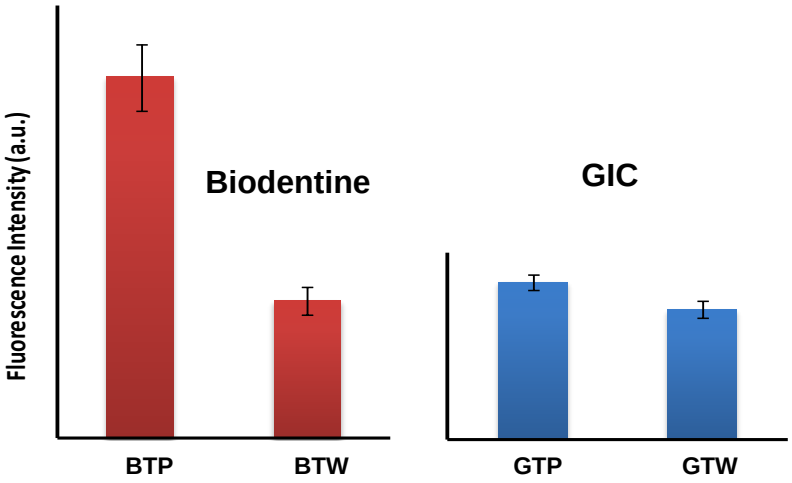

Figure 24: Fluorescence intensity ratio between ageing of totally demineralised dentine in phosphate rich media and phosphate –free media with the Biodentine cement or GIC.

The fluorescence lifetime measurements obtained for the dentine samples with or without the Biodentine are demonstrated in the chart in Figure 25. The fluorescence lifetime of the demineralised dentine samples stored in

Tetracycline-containing solutions (BTP, BTW, and DTP) were close to each other, measuring 0.72, 0.52, and 0.63 ns respectively, and were close to the fluorescence lifetime of the tetracycline powder (0.43 ns) and Tetracycline-calcium complex (0.56 ns) controls, with no statistically significant difference between these groups (Table 5). Whereas the dentine samples stored in the Tetracycline-free solution (BP) exhibited longer fluorescence lifetime, around 2.18 ns, which was close to the auto-fluorescence lifetime measured in sound (2.17 ns) and demineralised (2.61 ns) dentine, and there was no statistically significant difference between these values. However, the difference in the FLIM results obtained from samples stored in Tetracycline containing solution (BTP. BTW, DTP) was significantly different in comparison with samples stored in Tetracycline-free solution (BP, demineralised dentine, sound dentine) (Table 5).

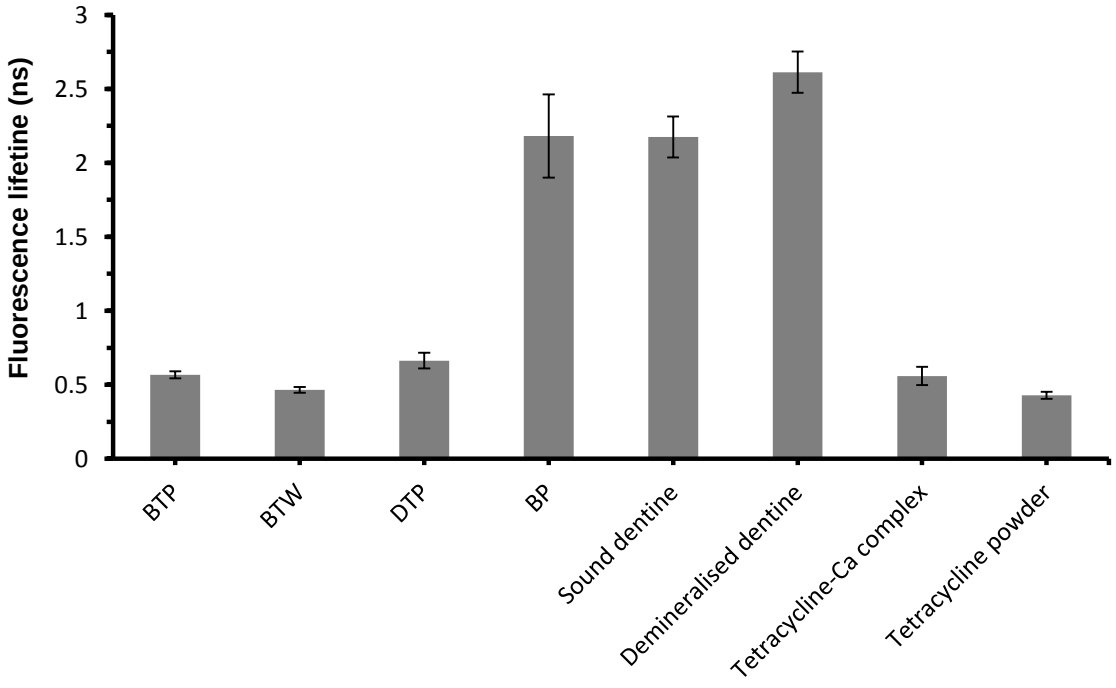

Figure 25: The average fluorescence lifetime of each dentine group after 8-week storage in different media with the Biodentine cement (BTP, BTW, BP), or without the cement (DTP). Fluorescence lifetime was also measured for sound and totally demineralised dentine, as well as for Tetracycline in its free or Ca^{2+} forms.

Fluorescence Intensity

Group	(J) Group	Mean Difference (I-J)	Std. Error	Sig.	95% Confidence Interval	
					Lower Bound	Upper Bound
BTP	**BTW**	232.31664*	40.58524	.000	123.1962	341.4371
	DTP	313.68090*	41.90618	.000	201.0089	426.3529
	BP	310.48183*	38.94102	.000	205.7822	415.1815
BTW	**BTP**	-232.31664*	40.58524	.000	-341.4371	-123.1962
	DTP	81.36427	47.83606	.551	-47.2513	209.9798
	BP	78.16520	45.26105	.522	-43.5270	199.8574
DTP	**BTP**	-313.68090*	41.90618	.000	-426.3529	-201.0089
	BTW	-81.36427	47.83606	.551	-209.9798	47.2513
	BP	-3.19907	46.44921	1.000	-128.0858	121.6877
BP	**BTP**	-310.48183*	38.94102	.000	-415.1815	-205.7822
	BTW	-78.16520	45.26105	.522	-199.8574	43.5270
	DTP	3.19907	46.44921	1.000	-121.6877	128.0858

Table 4: One-way ANOVA statistical analysis to compare the means of the fluorescence intensity among the different groups. (*) The mean difference is significant at the 0.05 level.

In addition to the high fluorescence intensity detected in the dentine of the BTP group, micro-structural features were exclusively detectable in the dentine samples of this group. Lines separating between areas of high fluorescence and areas of low fluorescence indicated what could be considered as mineralisation fronts that reflects the progression of mineral deposition within the matrix (Figure 26). Furthermore, highly fluorescent cylindrical shaped structures were detectable inside the widened dentinal tubules indicating intra-tubular

mineralisation (Figure 27). Intra-tubular mineralisation was also detected in cross sectioned tubules (Figure 28) which appeared obliterated with highly fluorescent structures. Mineralisation features were also detectable in the inter-tubular dentine matrix, which appeared in the form of microspherules that ranged in size between 0.5 and 1 µm (Figures 27 & 28), or fine granules (Figure 29). Acicular shaped structures were also detectable in some areas of the intertubular dentine matrix (Figure 30). The back scattered electron SEM imaging of the BTP and BP samples revealed the same mineralisation features detected by the two-photon fluorescence microscopy, including the mineralisation fronts, intra- and inter-tubular mineralisation (Figure 31).

Fluorescence Lifetime

(I) Group	(J) Group	Mean Difference (I-J)	Std. Error	Sig.	95% Confidence Interval	
					Lower Bound	Upper Bound
BTP	BTW	.10265	.17080	1.000	-.4454	.6507
	DTP	-.09555	.24652	1.000	-.8866	.6955
	BP	-1.61336*	.18183	.000	-2.1968	-1.0299
	Demin D	-2.04460*	.17862	.000	-2.6178	-1.4714
	Sound D	-1.60681*	.17315	.000	-2.1625	-1.0512
	Tc-Ca	.13800	.24652	1.000	-.6531	.9291
	Tc	.00828	.20567	1.000	-.6517	.6683
BTW	BTP	-.10265	.17080	1.000	-.6507	.4454
	DTP	-.19820	.24652	1.000	-.9893	.5929
	BP	-1.71601*	.18183	.000	-2.2995	-1.1325
	Demin D	-2.14725*	.17862	.000	-2.7205	-1.5741
	Sound D	-1.70946*	.17315	.000	-2.2651	-1.1538
	Tc-Ca	.03535	.24652	1.000	-.7557	.8264
	Tc	-.09437	.20567	1.000	-.7544	.5656
DTP	BTP	.09555	.24652	1.000	-.6955	.8866
	BTW	.19820	.24652	1.000	-.5929	.9893
	BP	-1.51781*	.25429	.000	-2.3338	-.7018
	Demin D	-1.94905*	.25201	.000	-2.7577	-1.1404
	Sound D	-1.51126*	.24816	.000	-2.3076	-.7149
	Tc-Ca	.23355	.30394	1.000	-.7418	1.2089
	Tc	.10383	.27185	1.000	-.7685	.9762

BP	**BTP**	1.61336*	.18183	.000	1.0299	2.1968
	BTW	1.71601*	.18183	.000	1.1325	2.2995
	DTP	1.51781*	.25429	.000	.7018	2.3338
	Demin D	-.43124	.18920	.693	-1.0384	.1759
	Sound D	.00655	.18404	1.000	-.5840	.5971
	Tc-Ca	1.75136*	.25429	.000	.9353	2.5674
	Tc	1.62164*	.21492	.000	.9320	2.3113
Demin D	**BTP**	2.04460*	.17862	.000	1.4714	2.6178
	BTW	2.14725*	.17862	.000	1.5741	2.7205
	DTP	1.94905*	.25201	.000	1.1404	2.7577
	BP	.43124	.18920	.693	-.1759	1.0384
	Sound D	.43779	.18088	.484	-.1426	1.0182
	Tc-Ca	2.18260*	.25201	.000	1.3739	2.9913
	Tc	2.05288*	.21221	.000	1.3719	2.7339
Sound D	**BTP**	1.60681*	.17315	.000	1.0512	2.1625
	BTW	1.70946*	.17315	.000	1.1538	2.2651
	DTP	1.51126*	.24816	.000	.7149	2.3076
	BP	-.00655	.18404	1.000	-.5971	.5840
	Demin D	-.43779	.18088	.484	-1.0182	.1426
	Tc-Ca	1.74481*	.24816	.000	.9485	2.5412
	Tc	1.61509*	.20763	.000	.9488	2.2814
Tc-Ca Complex	**BTP**	-.13800	.24652	1.000	-.9291	.6531
	BTW	-.03535	.24652	1.000	-.8264	.7557
	DTP	-.23355	.30394	1.000	-1.2089	.7418
	BP	-1.75136*	.25429	.000	-2.5674	-.9353
	Demin D	-2.18260*	.25201	.000	-2.9913	-1.3739
	Sound D	-1.74481*	.24816	.000	-2.5412	-.9485
	Tc	-.12972	.27185	1.000	-1.0021	.7426
Tc powder	**BTP**	-.00828	.20567	1.000	-.6683	.6517
	BTW	.09437	.20567	1.000	-.5656	.7544
	DTP	-.10383	.27185	1.000	-.9762	.7685
	BP	-1.62164*	.21492	.000	-2.3113	-.9320
	Demin D	-2.05288*	.21221	.000	-2.7339	-1.3719
	Sound D	-1.61509*	.20763	.000	-2.2814	-.9488
	Tc-Ca	.12972	.27185	1.000	-.7426	1.0021

Table 5: One-way ANOVA statistical analysis to compare the means of the fluorescence lifetime (FLIM) among the different groups. TC: Tetracycline. (*) The mean difference is significant at the 0.05 level.

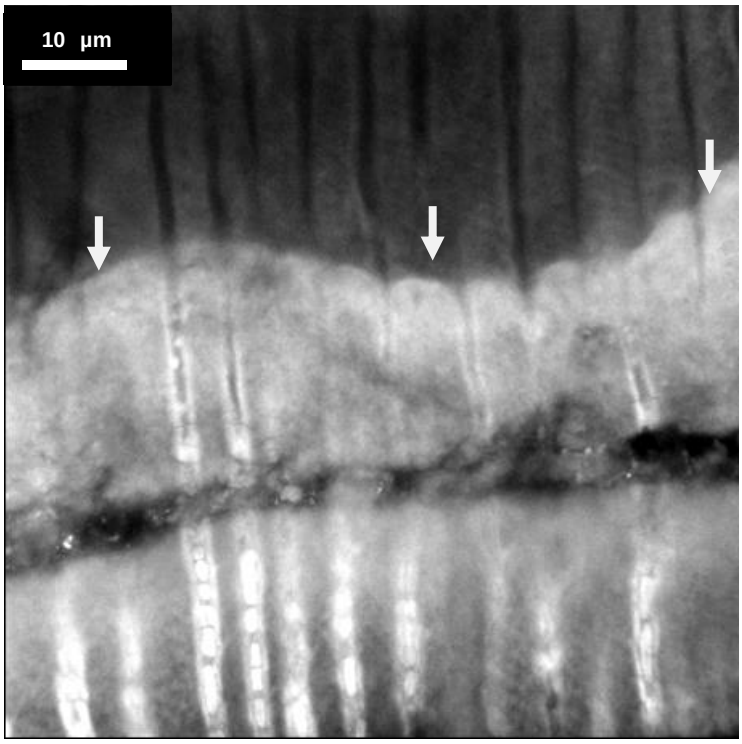

Figure 26: Two-photon fluorescence mode image for a demineralised dentine sample stored with Biodentine in PBS solution and Tetracycline. The mineralisation front (arrows) appears to separate between the highly fluorescent mineralising areas below, and the less fluorescent dentine matrix above.

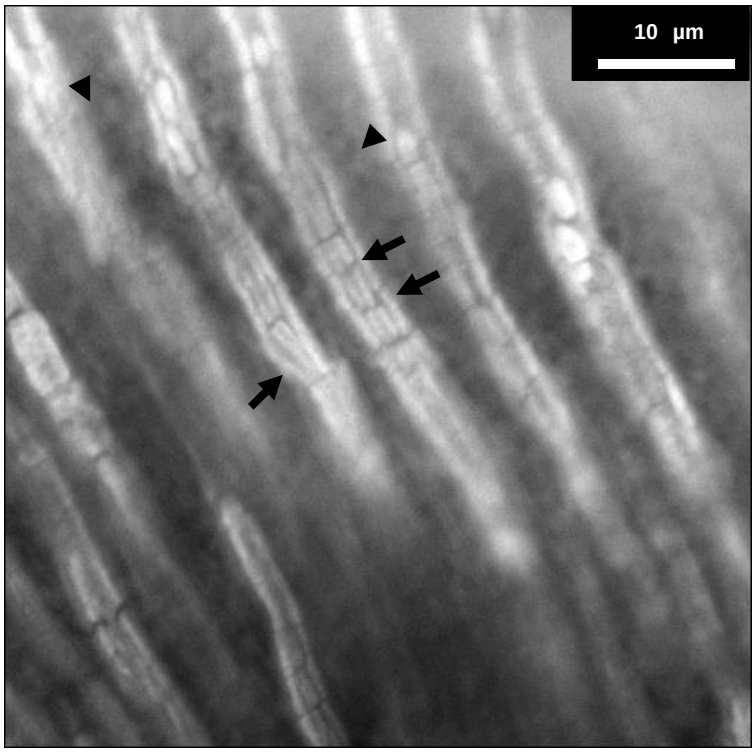

Figure 27:Intra-tubular mineralisation: Highly fluorescent structures (black arrows) are aligned within the widely opened dentinal tubules indicating intra-tubular mineralisation. Micron sized spherules (Black arrow heads) can be detected between the tubules in the inter-tubular matrix.

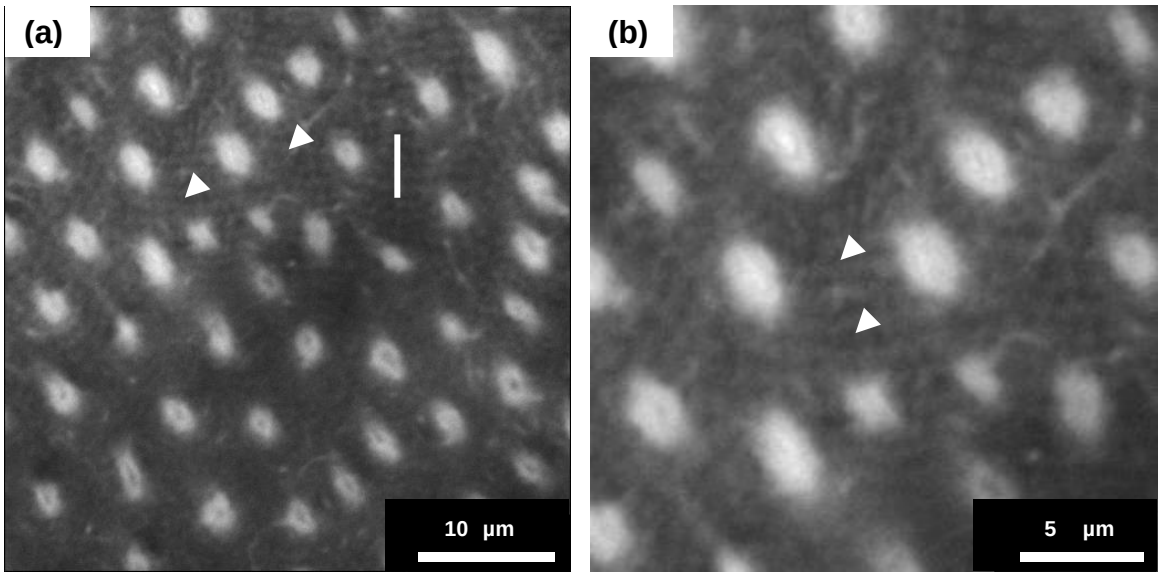

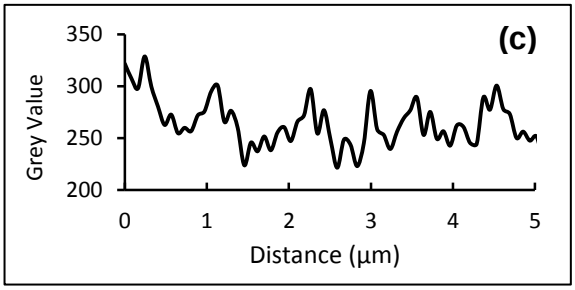

Figure 28: Intertubular mineralisation**. (a)** Two-photon fluorescence mode image showing fluorescent spherules (arrow heads) within the intertubular dentine matrix of demineralised dentine samples that were stored with the Biodentine cement in tetracycline and PBS (BTP group). **(b)** Higher magnification image shows the arrangement of these spherules in organized architecture. The dentinal tubules are totally obliterated with minerals. **(c)** A plot profile for the white line drawn in Figure-a showing the size of these spherules to be around 1 µm.

In the dentine samples that were stored with the GIC (GTP & GTW), the dentine discs remained intact after the ageing period with no signs of macroscopic degradation. The ratio of the average fluorescence intensity in the GTP samples to GTW was around 1.2, which is much lower than that of the Biodentine samples, therefore indicating a very minimal formation of phosphate containing minerals. However, no features of intra- or inter-tubular mineralisation were detectable in both groups (Figure 32-a). Dentine in these samples exhibited similar linear and annular patterns or banding noticed in the inter-tubular dentine of BTP group (Figure 32-b), however they appeared as continuous bands, with no microspheres detected.

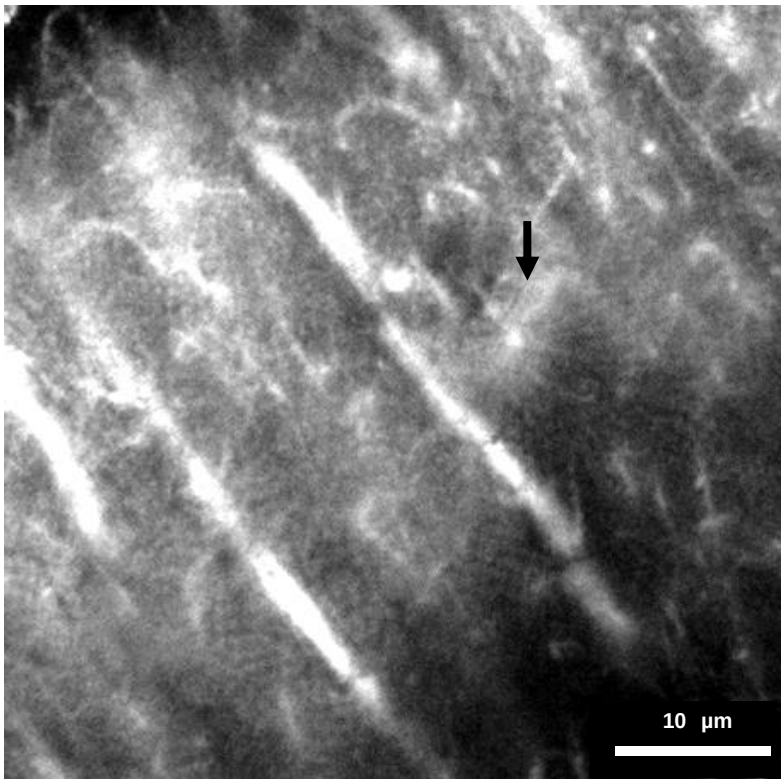

Figure 29: Inter-tubular mineralisation. Two-photon fluorescence intensity image showing highly fluorescent granular structures arranged in patterns along with acicular structures (arrow) in the inter-tubular matrix of dentine samples stored with the Biodentine cement in tetracycline and PBS.

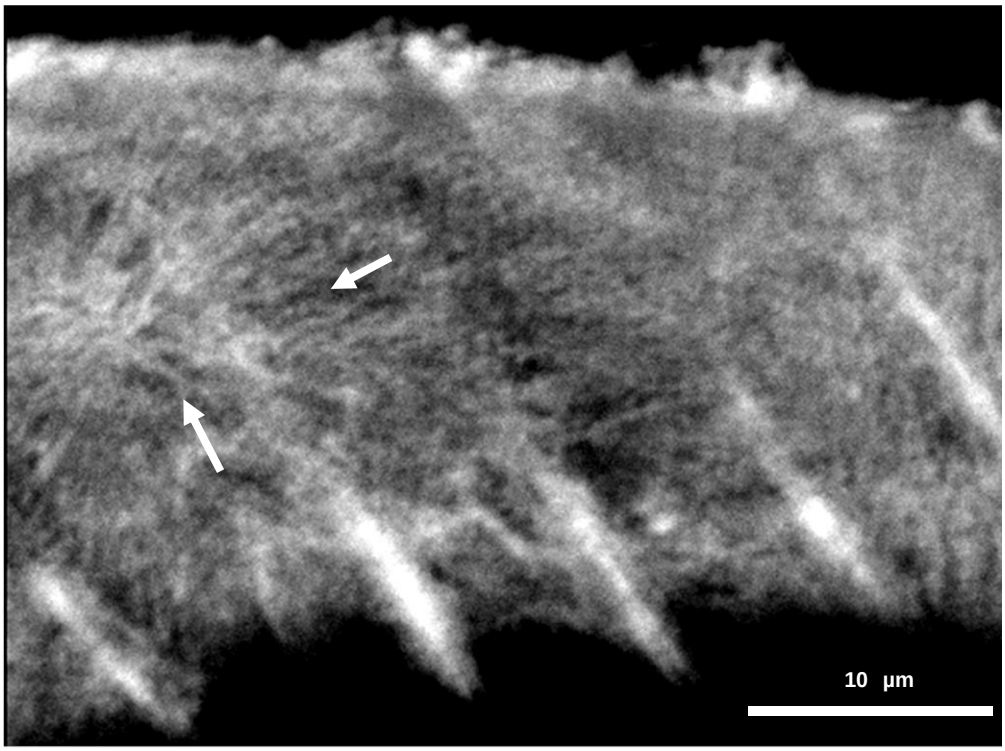

Figure 30: Two-photon fluorescence mode image showing acicular microstructures (arrows) forming within the inter-tubular matrix of demineralised dentine after storage with Biodentine in a PBS solution and Tetracycline.

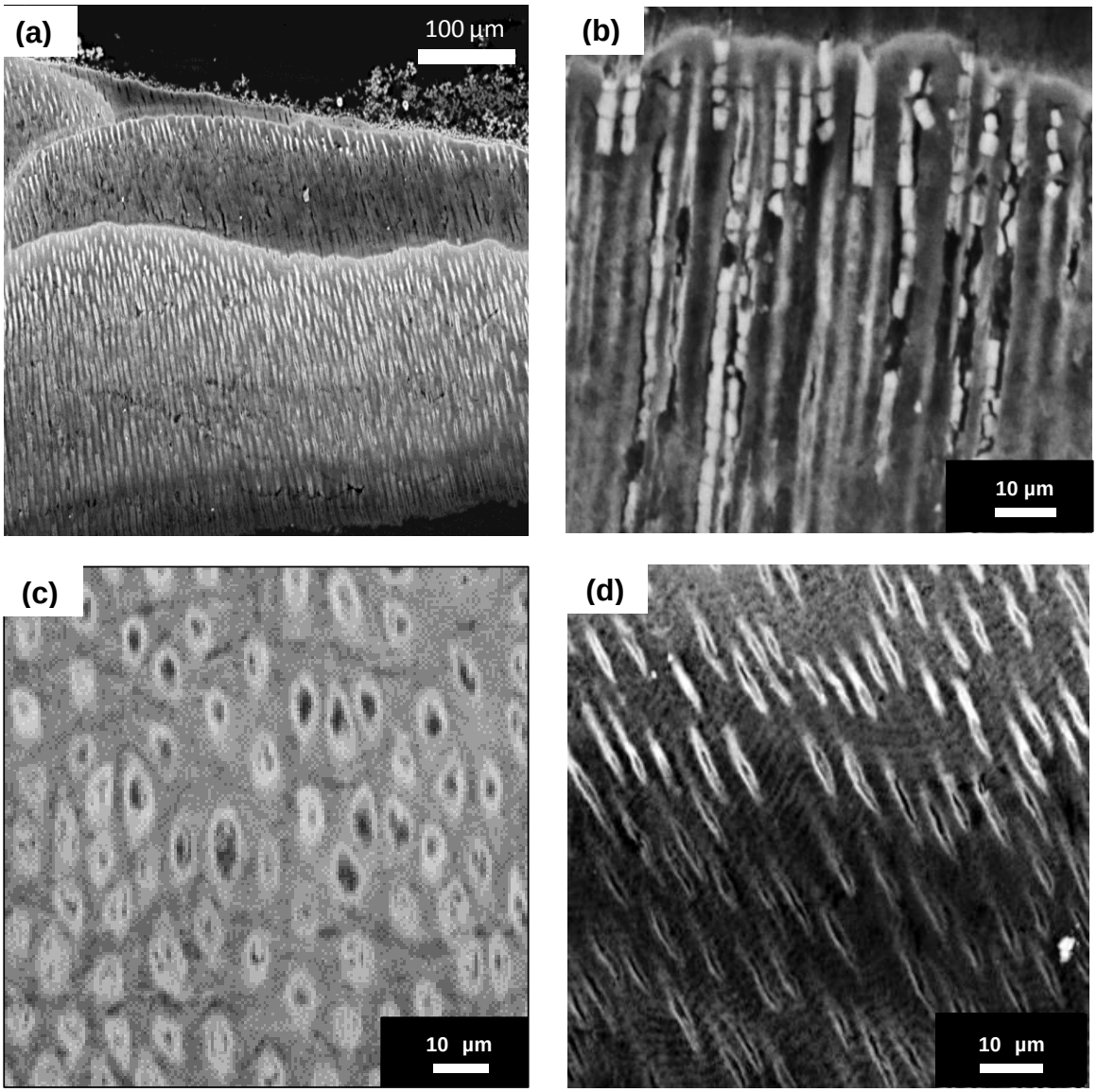

Figure 31: Back scattered electron SEM images for remineralised dentine discs after storage in phosphate rich media with Biodentine (BTP and BP). Micro-structural features of mineralisation; mineralisation lines (**a**), intra-tubular mineralisation (**b**), and intertubular mineralisation (**c**) were detectable with this imaging technique. The arrangement of intertubular mineralisation in regular patterns (**d**) might reflect the influence of the organic matrix in the deposition and arrangement of the forming minerals. Accelerating voltage=20 kV, current=626 pA.

4.3.3 Raman spectroscopy

The Raman spectra obtained from each group were normalised for the laser power, and plotted all together (Figure 33). By comparing the spectra of demineralised (DP) and sound dentine (SD), the missing peaks in the former can be clearly noticed at 432 cm^{-1}, 448 cm^{-1} & 570- 625 cm^{-1}, 961 cm^{-1}, and 1020-1095 cm^{-1}. These peaks represent respectively the v_2, v_4, v_1, and v_3 vibrational modes of the phosphate group (PO_4^{3-}) in the hydroxyapatite. These

peaks were only detectable in the re-mineralised dentine samples of the BP group. In the glass ionomer samples (GP), these peaks were not detectable.

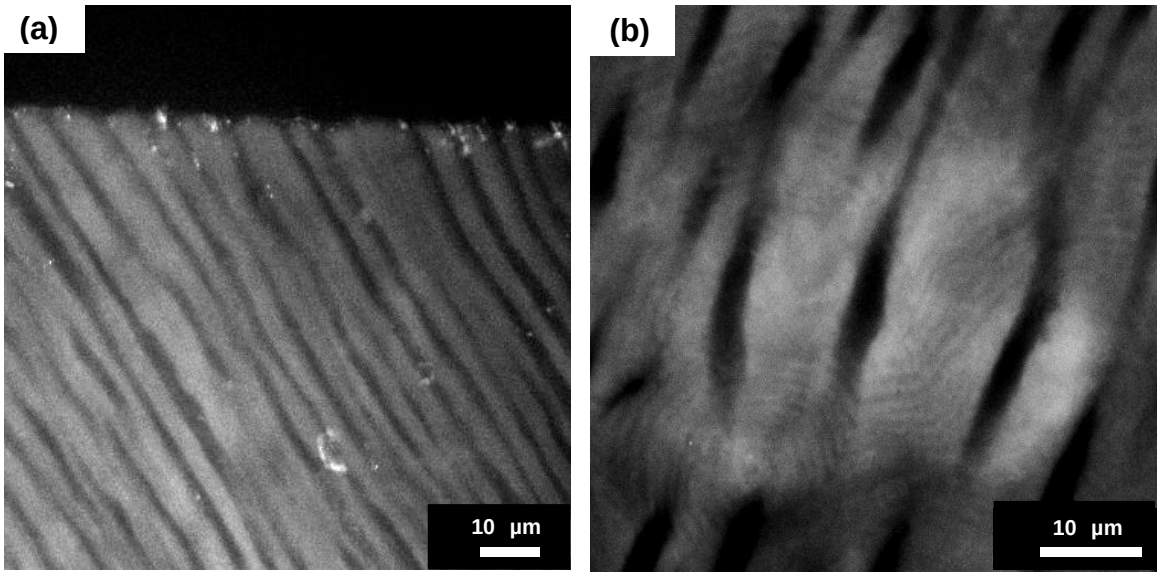

Figure 32: Two-photon fluorescence mode images of demineralised dentine after storage with glass ionomer cement in a PBS solution and tetracycline (GTP), showing no signs of intra- or inter-tubular mineralisation, with no structural changes in the matrix except for the increased fluorescence induced by adsorbed Tetracycline **(a).** Adsorption of the tetracycline stain might be responsible for the appearance of annular patterns in these samples **(b),** as well as in the GTW, BTP and BTW.

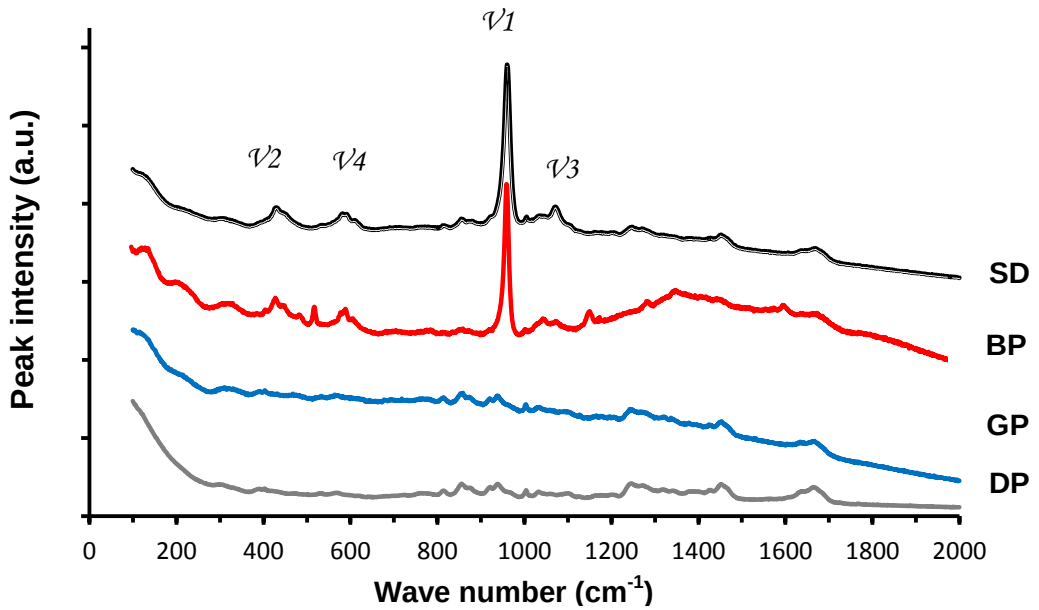

Figure 33: Normalised Raman spectra obtained for demineralised dentine discs after storage for 8 weeks in PBS with the Biodentine (BP), in PBS with GIC (GP), in PBS without cement (DP), in addition to sound dentine (SD). The Raman peaks representing the phosphate's vibrational modes (v1, v2, v3, and v4) in sound dentine (SD) were only detectable in the BP group. No apatite peaks was detectable in the dentine of the other groups.

4.4 Discussion:

Tetracycline labelling has been successfully applied in the study of in-vitro mineralisation models of bone (Treharne & Brighton 1979) as well as dental tissues (Moseley *et al.* 2003), and therefore was selected as a labelling agent in the current study. Combining this labelling technique with the two-photon fluorescence microscopy for the mineralisation detection has enabled deep tissue imaging of mineral formation within the organic matrix structure of demineralised dentine, and hence provided better imaging quality with deeper penetration capability (Helmchen & Denk 2005, Theer *et al.* 2003). This technique in comparison with other mineralisation detection techniques has allowed the observation of the different morphological features of this process such as the mineralisation fronts and intra- as well as inter-tubular mineralisation.

Fluorescence emission was strongest in the dentine samples stored with the calcium silicate cement in a PBS solution and Tetracycline (BTP), where Tetracycline-incorporated minerals have formed (Figure 22-a). Such levels of fluorescence were only obtainable in the presence of calcium, phosphate, and Tetracycline, while it was much weaker in the absence of any one of these components (Figure 23). This indicates that Tetracycline labelling was selective for the mineralisation process that involved the formation of calcium phosphate products. This can be demonstrated by the ratio of the fluorescence intensity of dentine stored in phosphate containing medium (BTP) to the fluorescence intensity of dentine stored in phosphate-free medium (BTW) (Figure 24). The high ratio confirms the crucial role of phosphate ions in enhancing the fluorescence through apatite formation, which did not occur in a phosphate-free medium. The fluorescence lifetime measured for both samples indicated that fluorescence is originating from Tetracycline (Figure 25).

The fluorescence intensity exhibited by the dentine samples stored alone in Tetracycline and PBS solution (DTP) or with Biodentine in a Tetracycline-free PBS solution (BP) were almost the same (Figures 22-c & d and Figure 23),

however, the origin of their fluorescence seems to be different as indicated by their different fluorescence lifetimes. The short fluorescence lifetime detected in the former appears to originate from the Tetracycline, which was very close to the fluorescence lifetime of free Tetracycline or the Tetracycline-Ca^{2+} complex. The longer fluorescence lifetime detected in the dentine samples stored with Biodentine in PBS alone (BP) was due to the dentine auto-fluorescence (Figure 25), which has an emission fluorescence spectrum (430-700) that overlaps with the emission filter range under the same excitation wavelength (550 ±20nm) used during the imaging (Thomas *et al.* 2010).

Tetracycline fluorescence lifetime did not differ significantly in its free or chelated forms (Table 5). Hence, the fluorescence lifetimes detected in all the dentine samples that were stored in Tetracycline containing media (BTP, BTW, DTP) were almost similar, regardless of the formation of calcium minerals or not. It is not likely that Tetracycline fluorescence has originated from free fluorophore molecules, rather, it is likely to have originated from tetracycline-incorporated minerals or Tetracycline adsorbed to the dentine matrix proteins (Simpson 1981). Tetracycline might bind directly to the matrix proteins (Bowles & Bokmeyer 2007), or through complexes with divalent cations (Jacobs *et al.* 1964) which could have occurred through chelating the residual calcium that remained after EDTA demineralisation (Solomons & Neuman 1960, Hoerman & Mancewicz 1964). This could explain the appearance of the annular patterns in the BTP, GTP, and GTW groups, and to a lesser extent in the BTW samples, which could reflect the architecture and organisation of the protenious organic matrix of dentine (Figure 32-b). In the dentine samples stored in phosphate-free media (BTW), non-phosphate containing minerals, such as calcium carbonate, might have also formed, which exhibited much less fluorescence intensity.

Complete degradation of demineralised dentine, over a relatively short period of time has not been reported in dentine remineralisation studies with different approaches (Arends *et al.* 1989, Knolt & ten Cate 1991, Saito *et al.* 2003, Gu *et al.* 2011). In the current study, dentine degraded in the samples that were stored in PBS with the calcium silicate cement (BTP and BP groups) where remineralisation has occurred. However, it did not occur in the samples that

were stored in the cement-free media (DTP), PBS-free media (BTW), or the glass ionomer samples (GTP, GTW, GP). Therefore, the calcium silicate cement and the ion-rich PBS solution were both responsible for the degradation of the dentine matrix. The macroscopic (Figure 21) and microscopic (Figures 26, 27, 28, 29, & 30) appearances of the remaining "re-mineralised" dentine demonstrates the preservation of the outer surfaces (not contacting the cement) of the dentine discs. This indicates that the degradation process which affected the organic matrix nearest to the cement has spared the peripheral tissues where the tissues had better chance to remineralise.

We believe that remineralisation and degradation of the organic matrix were both encouraged in the storage media that contained both the PBS and the calcium silicate cement. Therefore, both processes could have been competing; remineralisation was progressing from the outer surfaces of the demineralised dentine disc, while degradation was progressing from the inner surface that contacts the cement. This would suggest a role of the Biodentine cement in the degradation process which could be mediated by the strongly alkaline calcium hydroxide resulting from the cement (Taylor 1997). Enzymatic degradation, mediated by the activity of matrix metalloproteinases (MMPs), is not likely with the current experimental conditions, which include antagonising factors for the activity of these enzymes such as; Tetracycline (Osorio *et al.* 2011), high pH (Tjäderhane *et al.* 1998) Zinc-free (Tezvergil-Mutluay *et al.* 2010), and EDTA demineralisation of dentine (Carvalho *et al.* 2000, Pashley *et al.* 2004).

Remineralisation on the other hand is believed to have been encouraged on the outer surface of the dentine discs, as reported before by Mukai & ten Cate (2002), Inaba *et al.* (1996), and Liu *et al.* (2011b). The outer tissues were more exposed to the ion-rich mineralising solution and furthest from the cement, which might have encouraged surface nucleation followed by inward crystal growth as a result of the surface gradient effect of the surrounding ions (Kawazaki *et al.* 2000). Therefore it could be concluded that the mineralisation did not occur as a result of residual mineral nuclei growth as suggested by (Klont & ten Cate 1991); rather it took place through de-novo nucleation on the

outer surface (Kawazaki *et al.* 2000), which explains why the mineralisation was limited to the outer surface and did not proceed deeper.

Preservation of the remineralised dentine could suggest that collagen was mineralised to an extent that was sufficient to prevent further hydrolysis, especially under the amplified hydrolysing conditions that led to the fast degradation of the rest of the "unmineralised" dentine. However, we cannot confirm the extent of remineralisation, and whether intra-fibrillar remineralisation of collagen has occurred, which is required to protect the exposed collagen fibrils in demineralised dentine from hydrolysis (Hashimoto *et al.* 2000, Uskoković & Bertassoni 2010, Tay & Pashley 2009, Pashley *et al.* 2004).

Achieving a full thickness remineralisation, would require this process to be faster and diffuse. This could be obtained by adding biomimetic analogues (Dai *et al.* 2011), which substitute the action of non-collagenous matrix proteins that are normally involved in the natural biomineralization process. These substitutes are suggested to provide diffused nucleation sites to encourage metastable crystals to precipitate within the gap zone of collagen fibrils (Tay & Pashly 2008), therefore protecting them from further hydrolysis and restore their functional properties (Betrassoni *et al.* 2009). Despite the claim that the absence of these substitutes would prevent the remineralisation (Li & Chang 2008), in the current study mineralisation was detectable in the matrix of totally demineralised dentine without the use of any biomimetic substitute (Zhang *et al.* 2012). This further indicates that the dentine mineralisation resulted from novel nucleation sites, although residual phosphate and matrix phosphoproteins after EDTA demineralisation cannot be totally excluded (Saito *et al.* 1998, Saito 2003).

The highly fluorescent structures detected inside the dentinal tubules in both longitudinal (Figures 26 & 27) and cross sections (Figure 28) indicate intra-tubular mineralisation. Similar structures were reported in remineralised carious dentine (Takuma & Kurahashi 1962, Lester & Boyde 1968). Tubular occlusion was also detected in in-vitro dentine remineralisation within 50 microns from the surface of demineralised dentine (Qi *et al.* 2012, Arends *et al.* 1990), and in

sound dentine underneath mineral trioxide aggregate (MTA) filling (Dreger *et al.* 2012).These structures were speculated to be real mineral crystallisation, or less probably calcifying odontoblastic processes or bacteria (Lester & Boyde 1968). Our findings support that they could form inside the dentinal tubules due to intra-tubular crystallisation, although their appearance would suggest the calcification of the odontoblastic process, especially with the hollow centre of these structures (Figure 27); however, having the odontoblastic process surviving all the preparation procedures including cutting, demineralisation and ageing would make this assumption scantily possible.

The appearance of 0.5 to 1 µm sized highly fluorescent spherules in the inter-tubular dentine matrix might indicate apatite deposition within the matrix. The formation of apatite spherules by calcium silicate cements (Figures 27 & 28) has been reported when the hydrated cement was stored in PBS (Tay *et al.* 2007) or simulated body fluid (SBF) (Chen *et al.* 2009) solutions. These spherules were characterised as calcium deficient apatites (Tay *et al.* 2007), which formed after the pH of the ageing solution had reached its maximum alkaline status as a result of calcium hydroxide production from the cement (Taylor 1997). This has encouraged the transformation of the amorphous phase of calcium phosphate into apatite crystalline (Tay *et al.* 2007). The apatite microspheres were also detectable on the surface of collagenous scaffolds that were mineralised using biomimetic approaches (Lickorish *et al.* 2004, Li & Chang 2008, Liu *et al.* 2011b, Gu *et al.* 2011, Zhang *et al.* 2012). The arrangement of these structures in organised patterns might have been assisted by the dentine organic matrix acting as a template for the crystal growth (Klont & ten Cate 1991) and even controlling the mineralisation process (Ozawa *et al.* 2008). Acicular crystalline structures, similar to our findings (Figure 30), were also reported by Zhang *et al.* 2012.

The mineralisation inside the dentine matrix stored with Biodentine in phosphate rich media (BTP and BP groups) was further confirmed by the results of the back scattered electron SEM imaging, which revealed the dense mineral content of the detected microstructures (Figure 31). The fact that the same microscopic features of dentine remineralisation were equivalently detectable by

both the two-photon fluorescence microscope and the back scattered electron SEM supports the equivalent efficiency of both techniques, but with much less effort required for sample preparation in the former.

Detecting the characteristic phosphate peaks of hydroxyapatite in the Raman spectra of re-mineralised dentine (BP group) (Figure 33) is indicative of the nature of the mineralisation induced by Biodentine in a phosphate rich medium, which confirms its bioactivity (Sarkar *et al.* 2005, Tay *et al.* 2007). The exact position of the apatite peaks detected in both sound and remineralised dentine was very similar. Therefore, the formation of other calcium phosphate minerals such as; amorphous calcium phosphate (ACP), octacalcium phosphate (OCP), dicalcium phosphate dehydrate (DCPD), or tricalcium phoshphate (TCP) could be excluded. This is based on the absence of the v1 bands of these salts which are located respectively at 952-955 cm^{-1} (Sauer *et al.* 1994, Crane *et al.* 2006) 957 cm^{-1} (Sauer *et al.* 1994), 985 cm^{-1} (Sauer *et al.* 1994), and 970 cm^{-1} (Koutsopoulos 2002). OCP is not expected to form in the highly alkaline conditions of the storage media; rather, the alkaline conditions will drive the transformation of amorphous calcium phosphate into hydroxyapatite, or other anion substituted apatites (Tay *et al.* 2007).

In comparison with the glass ionomer cement, the calcium silicate cement - Biodentine exhibited a higher potential in inducing remineralisation of totally demineralised dentine. This was indicated by the higher ratio in the fluorescence intensity between the samples stored with Biodentine in phosphate-rich and phosphate-free media. In addition, no mineralisation features, such as the intra- and inter-tubular mineralisation were observed in the dentine samples stored with GIC (Figure 32), and no phosphate minerals were detectable (Figure 33). These findings are in agreement with Kim *et al.* (2010), who reported the failure of GIC to induce remineralisation in totally demineralised dentine in similar conditions, but with the use of both biomimetic and non-biomimmetic approaches. This contrasts with previous studies that indicated the remineralisation of caries affected dentine under the influence of GIC (Miyauchi *et al.* 1978, Ngo *et al.* 2006, Lee *et al.* 2008) although different dentine substrates were used.

The variation in the results between our findings and the previous studies could be due the differences in the GIC's effect on the partially demineralised caries affected dentine in comparison with totally demineralised dentine used in the current study (Kim *et al.* 2010). This difference could be attributed to the fact that the GIC might not be able to induce homogenous remineralisation, rather it requires pre-existent nucleation sites, which could exist in the dentine that is partially demineralised as in the caries affected dentine. When applied on partially demineralised dentine, the freshly mixed GIC paste undergoes ion exchange processes with the wet dentine underneath (Ngo *et al.* 2006, Sennou *et al.* 1999). These processes involve the diffusion of calcium/strontium ions into the hypomineralised matrix, accompanied by polyalkenoic acids that will induce further demineralisation (Sennou *et al.* 1999), which eventually create an ion rich layer followed by mineral deposition on pre-existent nuclei. However in the absence of nucleation sites, no mineral deposition will occur (Kim *et al.* 2010).

4.5 Conclusions:

Combining the Tetracycline labelling with the two-photon fluorescence microscopy provided a selective and high quality imaging technique, which was comparable in quality to back scattered electron SEM, but with the additional ability of subsurface observation of the mineralisation inside the organic matrix of demineralised dentine. This technique has also enabled the visualisation of the morphological feature of the dentine matrix remineralisation that was induced by the calcium silicate cement, which proved its remineralising ability as confirmed by the Raman results. The calcium silicate based dental cement-Biodentine exhibited higher potential to induce mineralisation in totally demineralised dentine in comparison with the glass ionomer cement.

Chapter 5 Discussion

Optical imaging techniques have been commonly involved in the study of restorative materials (Grant 1967, Watson *et al.* 1998) and their relation to the dental tissues (Watson *et al.* 1991, Sidhu & Watson 1998, Sauro *et al.* 2012).These techniques rely on the interaction between light and matter in various forms, therefore they provide unique capabilities with minimal or no distortion imposed to the samples during examination. In the current work, confocal microscopy combined with fluorescence labelling techniques was useful in the study of dentine cement interfaces by comparing their different morphological features. This technique allowed subsurface imaging of the interfaces (Watson & Boyde 1987), and therefore enabled an accurate allocation of the fluorophore-labelled fluids. The morphological characterisation of the interfaces was contrasted by Raman chemical mapping, which along with spectral analysis, has enabled the modelling of the infiltration of the cements into the sound dentine. Raman spectroscopy has also reliably detected and quantified the change in calcium carbonate resulting from the carbonation of calcium silicate cements.

For the study and characterisation of Biodentine, Raman spectroscopy was useful to identify the constituents of the cement's powder and hydration products. The fact that this technique does not require sample preparation has made it a favourable choice for the study of cementitious materials in general (Ibáñez *et al.* 2007). Raman results demonstrated the production of hydrated calcium silicate phases and calcium hydroxide, which are the main hydration products of ordinary Portland cement. However, in comparison with ordinary Portland cement and MTA, hydration products such as calcium aluminium sulphate (ettringite), were not detected. This is predictable due to the absence of calcium sulphate and aluminium oxide in the Biodentine, which could be attributed to the production technique based on lab preparation, unlike MTA and other calcium-silicate based dental cements which are produced through clinckering (Darvell & Wu 2011).

On hydration of the calcium-silicate cement, the production and release of calcium hydroxide is believed to be responsible for its activity (Holland 1999), which mediates its action on the surrounding dental tissues (Camilleri 2007, 2008). Confocal imaging of the sound dentine beneath the Biodentine has indicated the formation of a structurally altered layer within the interfacial dentine. We found that the caustic effect of the strongly alkaline calcium hydroxide was a selective process affecting primarily the organic component of dentine (Andreasen 2002). When applying the cement on wet dentine, the calcium hydroxide leaches out into the dentine, leading to the swelling of collagen fibrils as a result of water absorption (Bowes 1950, Kemp & Tristram 1971), which appeared in the confocal images in the form of a dye infiltrated zone, especially in the deep dentine. This was confirmed by the reduced, or even absent second harmonic generation signal (SHG) originating from the dentine within the mineral infiltration zone (MIZ) when imaged using a two-photon fluorescence microscope, indicating changes in the collagen conformation (Sun *et al.* 2006). Unlike in the dentine underneath the glass ionomer cement, where the SHG signal was not affected.

The diffusion of calcium hydroxide into the wet dentine was found to be associated with mineral transfer in the form of calcium carbonate detected using Raman spectroscopy. The mineral transfer occurs while the caustic etching is taking place leading to the formation of the MIZ. Our Raman findings confirmed the production of calcium carbonate as a result of the carbonation process that affected the dental cement, similar to construction cements (Roy *et al.* 1999). Intraoral conditions such as the presence of a carbonate/bicarbonate buffering system in the saliva had a prominent effect on calcium carbonate production. Carbonation started shortly after mixing of the cement, which was demonstrated by the prompt and continuous deposition of calcium carbonate on the surface of the hydrated cement just after mixing. Therefore, it was possible to consider the carbonate's Raman peak as a representative peak for the Biodentine, which was used to trace the cement's penetration into the dentine.

Aiming to understand the nature of the relation between the dentine and the calcium silicate based restorative material-Biodentine, glass ionomer cement

(GIC) was chosen as a control material for comparison. This choice was based on the similarity between the two cements in terms of clinical applications and their water based nature (Nicholson 1998). Although other calcium silicate based dental cements; such as mineral trioxide aggregate (MTA), might have been more relevant for direct comparison, none of these cements has been indicated for coronal restorations (Torabinejad & Chivian 1999).

In comparison with the calcium silicate based cement, the GIC acted differently on the interfacial sound dentine. Due to the acidic nature of the material, the dye infiltrated layer that appeared just beneath the cement was due to the demineralising effect of the acid, which was manifested by the scalloped appearance of this layer in the confocal images. The dye was infiltrating deeper towards the pulp in areas corresponding to the highly mineralised peri-tubular dentine, inversely to the dye distribution in the MIZ of the calcium silicate based cement. Raman mapping of the GIC interface with dentine confirmed the penetration of the polyalkenoic acids into the dentine. The acidic action on the interfacial dentine is associated with ion exchange between the two substrates. Ions like Al^{+3}, Sr^{+2}, Si^{+4}, F^{-1} diffuse out of the cement towards the dentine, while Ca^{+2} and PO_4^{-3} diffuse into the cement from dentine (Sennou *et al.* 1999). This ion exchange associated with the acidic demineralisation of dentine is the inverse action of calcium silicate cements on interfacial dentine.

On demineralised dentine, calcium hydroxide has also played an important role in the remineralising potential of the Biodentine. Calcium hydroxide provided a major source of calcium to induce the formation of apatite structures in the presence of phosphate ions. Calcium hydroxide also provided the alkaline conditions which favoured biomineralisation and formation of the apatite over other non-apatitic forms of calcium phosphate; such as octa-calcium phosphate (Tay *et al.* 2007). This was confirmed by the detection of highly fluorescent microstructures within the matrix of inter-tubular dentine, as well in the opened dentinal tubules using the two-photon fluorescence microscopy in conjugation with tetracycline labelling. These structures were not detectable in the demineralised dentine under the GIC. Raman imaging confirmed the formation of apatite structures in the demineralised dentine stored with the calcium silicate

cement, but not with GIC. The use of the two-photon fluorescence microscopy proved to be both useful and selective for the observation of dentine remineralisation deep inside the demineralised matrix, and equivalent in efficiency to back scattered electron microscopy.

In conclusion, calcium silicate based dental restorative material-Biodentine has demonstrated an interactive relationship with both sound and demineralised dentine. This interaction is mediated by an alkaline caustic effect on dentine's organic component associated with mineral transfer. Both factors provide an appropriate environment for dentine remineralisation, which was detectable in the presence of phosphate rich media. Clinically, the use of a coronal restorative material with bioactive potential could be beneficial for the minimal invasive management of dental caries.

Chapter 6 Future Work

In-vitro investigation of the remineralising potential of calcium silicate based dental restorative materials on caries affected dentine.

This study would allow a closer simulation for the clinical situation, and expected to provide a better view for the remineralising effect of calcium silicate cements, where the dentine will not be totally depleted of minerals. For this purpose caries affected dentine will be used instead of the totally demineralised dentine using the same experimental set-up which we used on totally demineralised dentine. Carious third molars which are indicated for extraction will be collected directly after obtaining the proper consent from the patients. Caries infected dentine will be excavated chemically using Carisolv® (MediTeam Dental. Göteborg-Sweden) after preparing a cavity to access the carious lesion. On one of the proximal walls of the cavity, a diamond cylindrical bur will be used to prepare a flat proximal wall for the cavity that will create a right angle with its floor; this angle will be used later as reference point for the imaging. The root of each tooth will be cut, and the crown will be then sectioned from the middle of the cavity along its long axes into two halves using a water cooled wafering blade. Samples will be then cleaned in an ultrasonic bath with deionised water for 5 minutes. One half will be filled with a calcium silicate based dental cement (Biodentine), while the other half will be filled with glass ionomer cement GC IX. Each half will be then mounted and the sectioned surface of the tooth will be tightened against a plastic matrix using a specially designed small vise to prevent any leakage of the cement during application. Cements will be applied directly after proper mixing as per manufacturer's instructions, and samples will be stored in an incubator for 1 hour at 37°C temperature and 100% humidity. Samples will be then stored in a solution of phosphate buffered saline (PBS) with 0.015% tetracycline under the same temperature. Solutions will be changed every 2 days. Control groups will be prepared in which no tetracycline or PBS or both will be added. Two-photon fluorescence microscope will be used to image the caries affected dentine just underneath the cement. Five fluorescence and FLIM images will be obtained for

each sample at two stages. The first images will be taken before storage at certain points, where the coordination of these points will be recorded and saved. After 8 weeks of storage in the solutions, samples will be polished lightly to remove any surface precipitation, and the same points imaged before will be re-imaged. The change in the fluorescence intensity and fluorescence lifetime will be measured.

Mechanical characterisation of the interface between calcium silicate based dental cements and dentine using the nanoindentation test.

Studying and characterising the mechanical properties of the dentine under this type of cements would provide more information about the nature of the interface between the two substrates. Applying the nanoindentation test would enable the detection of changes in dentine elastic modulus and surface hardness. This would provide further understanding of the interface in light of the suggested mechanism of action of Biodentine on wet dentine which involves both alkaline etching and mineral transfer.

In-vivo investigation of the therapeutic effects of calcium silicate based dental restorative material used as a pulp capping material.

This study will be aiming to evaluate the pulpal therapeutic effects of Biodentine when applied directly or indirectly on the diseased pulps. Being a rich source of calcium with antimicrobial effects would allow this cement to encourage healing of the pulp, which could be also associated with dentine bridge formation. Using in-vivo tomographic imaging such as the cone beam computed tomography (CBCT), would allow the observation of any changes in the hard tissue formation or any changes affecting the apical bone. This could be also associated with evaluating pulpal blood flow.

Publications

RESEARCH REPORTS
Biomaterials & Bioengineering

A.R. Atmeh[1], E.Z. Chong[1], G. Richard[2], F. Festy[1], and T.F. Watson[1]*

[1]Biomaterials, Biomimetics and Biophotonics, King's College London Dental Institute, Floor 17 Tower Wing, Guy's Hospital, London Bridge, London SE1 9RT, UK; and [2]Septodont, Saint Maur des Fossés Cedex, France; *corresponding author, timothy.f.watson@kcl.ac.uk

J Dent Res X(X):xx-xx, XXXX

Dentin-cement Interfacial Interaction: Calcium Silicates and Polyalkenoates

ABSTRACT

The interfacial properties of a new calcium-silicate-based coronal restorative material (Biodentine™) and a glass-ionomer cement (GIC) with dentin have been studied by confocal laser scanning microscopy (CLSM), scanning electron microscopy (SEM), micro-Raman spectroscopy, and two-photon auto-fluorescence and second-harmonic-generation (SHG) imaging. Results indicate the formation of tag-like structures alongside an interfacial layer called the "mineral infiltration zone", where the alkaline caustic effect of the calcium silicate cement's hydration products degrades the collagenous component of the interfacial dentin. This degradation leads to the formation of a porous structure which facilitates the permeation of high concentrations of Ca^{2+}, OH^-, and CO_3^{2-} ions, leading to increased mineralization in this region. Comparison of the dentin-restorative interfaces shows that there is a dentin-mineral infiltration with the Biodentine, whereas polyacrylic and tartaric acids and their salts characterize the penetration of the GIC. A new type of interfacial interaction, "the mineral infiltration zone", is suggested for these calcium-silicate-based cements.

KEY WORDS: Biodentine, glass-ionomer cement, interfaces, Raman, confocal microscopy, second harmonic generation.

DOI: 10.1177/0022034512443068

Received December 12, 2011; Last revision February 23, 2012; Accepted February 25, 2012

INTRODUCTION

Torabinejad first developed mineral trioxide aggregate (MTA) as a surgical root repair material in 1993 (Lee *et al*., 1993). Subsequently, significant interest has been shown in MTA, due to its biocompatibility (Camilleri *et al*., 2004) and potential bioactivity (Tay *et al*., 2007). More recently, a new calcium-silicate restorative material called Biodentine™ has been produced by Septodont (Saint Maur des Fosses, France), to be used not only as an endodontic repair material but also as a coronal restorative material for dentin replacement.

Biodentine (henceforth used in the text for brevity) is composed of a highly purified tricalcium silicate powder that contains small proportions of dicalcium silicate, calcium carbonate, and a radiopaquer. It is dispensed in a fixed powder:liquid proportion, providing a shorter setting time of 12 min (manufacturer's data sheets), compared with the 3 to 4 hrs of MTA (Torabinejad *et al*., 1995). Because of components similar to those of Portland Cement, it may be assumed that Biodentine sets through a hydration reaction that involves dissolution of calcium silicate granules to produce calcium hydroxide and calcium silicate hydrates, which form the matrix that holds unhydrated granules and contains water-filled micro-spaces where the calcium hydroxide distributes, which provides the high alkalinity (Taylor, 1997; Tsivilis *et al*., 2002; Kjellsen and Justnes, 2004; Camilleri *et al*., 2011). However, the setting reactions involved in the complex mixture of Biodentine have not been fully investigated.

Glass-ionomer cements (GIC) are also water-based restorative materials. GIC setting, however, is an acid-base reaction that involves the formation of polyalkenoate salts as a result of the acid attack on fluoroaluminosilicate glass fillers. Being of an acidic nature, GICs are considered self-etching cements, and on wet dentin, trigger an ionic exchange with the interface, accompanied by water movement between the two substrates (Watson, 1999).

The null hypothesis is that the water-based cements in this study have identical cement and mineral diffusion into the dentin.

MATERIALS & METHODS

For the evaluation of the interface between human dentin and Biodentine/GIC, we used confocal reflection and fluorescence microscopy to observe interface micropermeability (Watson *et al.*, 2008), two-photon auto-fluorescence and second-harmonic-generation (SHG) imaging to detect collagen denaturation (Chen *et al.*, 2007), SEM for microstructural characterization, and micro-Raman spectroscopy for chemical mapping of the interfaces (Martinez-Ramirez *et al*., 2006; Ibáñez *et al*., 2007).

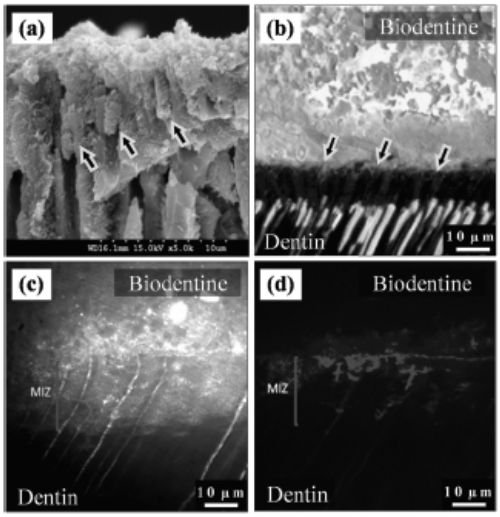

Figure 1. Interfacial characteristics. (a) SEM micrograph of fractured dentin beneath a Biodentine restoration. Tag-like structures were detected forming within the dentinal tubules (arrows). (b) Fluorescence-mode CLSM image showing the cement tags, which appear on the interfacial surface of the fluorescein-labeled Biodentine (above) after it was pulled away from dentin due to desiccation. 63x/1.4NA OI. (c) Reflection-mode TSM image for the dentin/Biodentine interface. The mineral infiltration zone (MIZ) appears as a band of highly reflective dentin beneath the interface, indicating a change in dentin's mineral content within this zone. The fluorescence-mode image of the same area (d) shows the distribution of Rhodamine-B dye, which permeated from the pulp chamber into the interface and cement.

Sample Preparation

Occlusal cavities were prepared in 49 teeth extracted after the appropriate informed consent was obtained from the patients (East Central London Research Ethics Committee 1, 10/H0721/55). Cavities were prepared by the use of a high-speed handpiece with a type 012 diamond bur, and standardized to 7 × 4 × 4 mm, and a cavosurface angle of 90°. All teeth were then cleaned for 5 min in an ultrasonic bath. Thirty-one cavities were filled with the Biodentine, mixed as *per* manufacturer's instructions for 30 sec with an amalgamator. In 18 teeth, cavities were filled with a conventional GIC-Fuji IX (GC Corporation, Tokyo, Japan) without the application of dentin conditioner, and cements were applied to the cavities directly after mixing and cavity preparation by means of a plastic instrument and adapted in an amalgam condenser. All samples were kept wet inside an incubator at 37°C for 24 hrs before being labeled and imaged. In each tooth, the root was cut just below the cementum-enamel junction by means of a water-cooled diamond wafering blade (Benetec Limited, London, UK). Additionally, 10 dentin discs of 1 mm thickness were cut from five extracted human teeth; mixed Biodentine was applied on five discs and GIC on the others. The discs were kept for 4 days in distilled water at 37°C before they were fractured perpendicular to the interface and gold-sputter-coated. The fractured surfaces were imaged by scanning electron microscopy (Hitachi S3500N, Hitachi High Technologies, Maidenhead, UK).

Imaging

Samples were divided into four groups:

Micro-permeability group (n = 15): An aqueous 0.25% solution of Rhodamine-B (R6626-Sigma-Aldrich, Dorset, UK) was put in the open pulp chambers of the Biodentine (n = 10) and GIC (n = 5) samples and placed upside-down in a damp environment. The dye was left for 3 hrs to permeate toward the interface.

Double-labeling group (n = 15): Biodentine (n = 10) and GIC (n = 5) cements were mixed with 1 mg of a fluorescein dye powder (F6377 Sigma-Aldrich, Dorset, UK) and applied to cavities one day before the micro-permeability test was conducted.

After being stained, all samples were rinsed with distilled water, sectioned vertically, then ground with carborundum paper up to 1200 grit.

A confocal tandem scanning microscope (TSM) (Noran Instruments, Middleton, WI, USA) was used to image the samples of the first group, with a x60/1.4 numerical aperture (NA) and x100/1.4 NA oil immersion (OI) objective lens with a 546-nm band-pass excitation and a 600-nm long-pass emission filters. Confocal widefield images were recorded with an electron multiplying iXon 885 EM-CCD (Andor Technology, Northern Ireland, UK). Samples of the second group were imaged by confocal laser scanning microscopy (CLSM) Leica TCS SP2 (Leica Microsystems, Heidelberg GmbH, Germany) with an x100/1.4NA OI objective lens in conjunction with 488-nm laser excitation and 530-nm emission filters for the fluorescein dye, and 568-nm laser excitation and 640-nm emission filters for the Rhodamine-B.

From four randomly selected samples of each material, four interfacial images were made *per* sample. Each image was adjusted so that the interface was exactly horizontal, and the average vertical intensity profile was calculated to allow unbiased fluorescence infiltration measurements to be made.

Stain-free group (n = 10): Biodentine (n = 5) and GIC (n = 5) filled teeth were sectioned and prepared for imaging as described above. Using an in-house multi-photon microscope, we performed stain-free imaging for both tissue auto-fluorescence (830-nm excitation and 500-nm emission) and collagen second-harmonic generation (950-nm excitation, 475-nm emission).

Micro-Raman Spectroscopy group (n = 9): Nine samples (6 Biodentine and 3 GIC) were kept in distilled water at 37°C for 8 days. A flat sectioned surface was created by means of a diamond wafering blade to expose the interface between the dentin and the cement, ground as described above and measured 1 and 8 days following cement placement.

For each sample, a Raman map of the material/dentin interface, with a resolution of 0.9 µm across the interface, was recorded with the fast StreamLine™ mapping provided with the inVia micro-Raman spectrometer (Renishaw plc, Wotton-under-Edge, UK). A water immersion x60/1.2NA objective lens Plan Apo VC was used with a 785-nm laser source (25 mW line

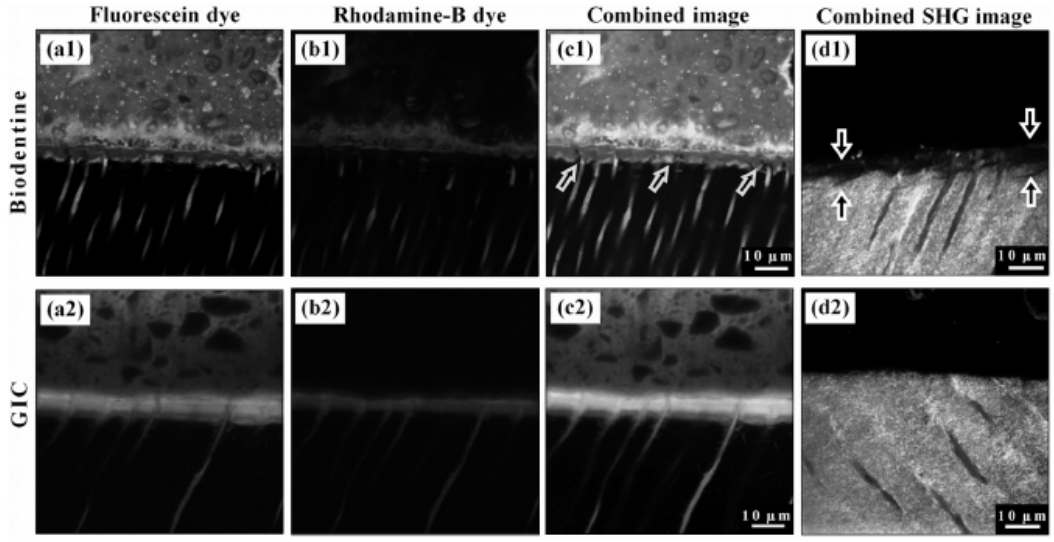

Figure 2. Representative fluorescence-mode CLSM images for the interfaces of Biodentine and GIC cements (upper side of each image) with the dentin (lower side). **(a1)** Distribution of the fluorescein dye labeling the Biodentine cement shows a band of richly dye-infiltrated dentin just beneath the interface. This band cannot be seen with Rhodamine-B micro-permeability **(b1)**, where the dye permeated through this band and diffused into the cement above the interface without any mixing with the fluorescein. This band is believed to be formed as a result of the strong alkaline effect of calcium hydroxide leaching out of the cement, and it corresponds to the MIZ. **(c1)** Dye-deficient areas can be seen within this zone (arrows), which represent the un-affected peritubular dentin. **(a2)** Fluorescein distribution in GIC samples also shows a richly dye-infiltrated dentin band, but this band was formed due to the acidic effect of GIC, which affected both intertubular and peritubular dentin. **(b2)** Rhodamine-B permeating from the pulp has also infiltrated this band, which diffused laterally through the affected tubular walls and mixed with the fluorescein as shown in **(c2)**. **(d1)** Second-harmonic-generation (SHG) signal, originating from the intertubular collagen (cyan), is weak and almost absent in the interfacial dentin beneath the Biodentine (arrows) when superimposed over the dentin's autofluorescence signal (red), which reflects its actual margin. Notice the preserved tubular structure of dentin in this zone, unlike the images for GIC samples **(d2)**, where the SHG signal has the same distribution as the dentin's autofluorescence signal.

illumination) and a 600 lines/mm diffraction grating. All Raman maps were uploaded into in-house curve-fitting software to fit the cements' characteristic peaks, generate intensity line profiles in the crown-pulp direction, and calculate the diffusion lengths.

RESULTS

Tag-like Structures

Representative SEM (Fig.1a) and confocal (Fig.1b) images of Biodentine samples showed tag-like structures within the dentinal tubules just beneath the interface. Fig. 1b shows these tags on the bottom surface of a detached Biodentine filling. There was little evidence of tag-like structures beneath the GIC restorations.

Interfacial Interactions

A representative reflection-mode TSM confocal image for the dentin/Biodentine interface (Fig.1c) shows a bright band, ranging between 5 and 15 µm, noticed within the structure of dentin directly below and along the interface, which indicates a change in the reflective properties of dentin at this area. A fluorescence image of the same area (Fig. 1d) shows the permeability of the dye solution.

Representative CLSM fluorescence images for the double-labeled Biodentine samples show a richly dye-infiltrated layer (6.5 µm ± 0.6 µm wide) positioned just beneath the interface (Fig. 2a1). Fig. 2b1 shows the distribution of Rhodamine-B permeating from the pulp and diffusing into the cement, but barely into the intertubular dentin. Fig. 2c1 is a combined image. Similarly, the GIC samples exhibited a richly dye-infiltrated layer (14.5 µm ± 1.9 µm wide) visible within the structure of dentin in both the fluorescent images (Figs. 2a2, 2b2), which show similar dye distribution when combined (Fig. 2c2). The combined two-photon auto-fluorescence and SHG images of the Biodentine samples showed a band of low SHG signal intensity due to the alteration of the collagen fibers close to the interface by this material (Fig. 2d1), not seen in the GIC samples (Fig. 2d2).

In the SEM images, a band of structurally altered dentin was visible just below the interface in the Biodentine samples (Fig. 3a), but not in the GIC samples (Fig. 3b). Within this 10- to 20-µm-wide band, microstructural alterations were noticeable but were absent on the opposite surfaces of the discs, where no

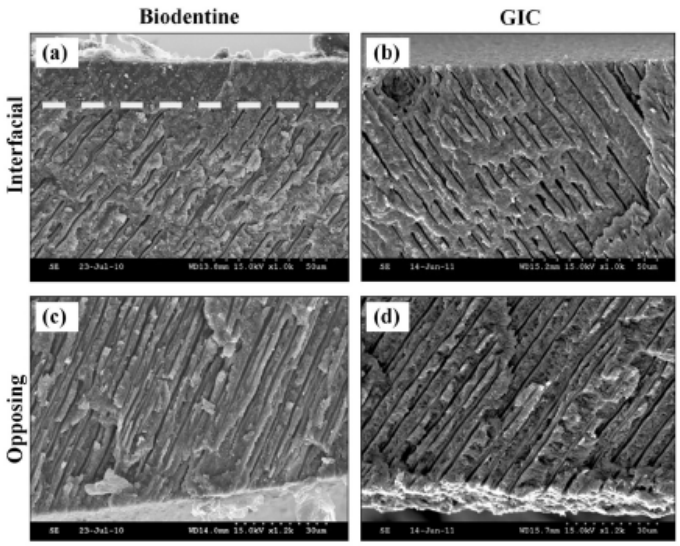

Figure 3. SEM micrographs of the fractured dentin discs which were exposed to Biodentine (**a**) or GIC (**b**). A band of structurally altered dentin extends along the interface, as can be seen by the obliterated dentin tubules above the dotted line in (a), when compared with dentin of the opposite surface of the disc, where no cement was applied (c). (b) No structural changes can be detected in the dentin beneath GIC when compared with dentin of the opposite surface (**d**).

cement was applied (Figs. 3c, 3d). In the surfaces exposed to Biodentine, the dentinal tubules appear blocked and did not open to the surface, unlike the tubules in the clean, unexposed surfaces.

Chemical Mapping

The 1082-cm^{-1} carbonate Raman peak (Fig. 4), representing the stretching mode of the C-O bond in the carbonate group (Martinez-Ramirez *et al*., 2006), was associated with the presence of calcium carbonate, originating either from calcium hydroxide carbonation or present originally in the Biodentine. The GIC's broad peak (Fig. 4), located at 1262 cm^{-1}, corresponds to the overlapping of smaller peaks that represent the polyacrylic (PAA) and tartaric acids and their salts (Young *et al*., 2000). The intensity of both cements' peaks declined at points located beneath the interface, but in different patterns. This declination was gradual throughout the whole depth for the GIC samples but was followed by a sudden drop in the Biodentine samples. The penetration depths of Biodentine and GIC measured 48 ± 10 µm and 51 ± 6 µm, respectively.

DISCUSSION

In the dentin/Biodentine interface, tag-like microstructures were detectable in the fractured samples in both confocal (Fig. 1b) and SEM images (Fig. 1a). These tags have previously been reported in MTA (Reyes-Carmona *et al.,* 2009) and Biodentine (Han and Okiji, 2011). Following hydration, the flowable consistency of the cement aids its penetration through opened dentinal tubules to crystallize over time within their structure (Weller *et al.,* 2008), participating in the mechanical properties of the interface (Reyes-Carmona *et al*., 2010).

However, the confocal images of the Biodentine samples also showed an interfacial layer within the structure of dentin, just beneath the cement. This layer appears both as a highly reflective band (Fig. 1c) and a richly dye-infiltrated band flooded by fluorophores leaching from the cement (Figs. 2a1, 2c1). This layer, which we call the "mineral infiltration zone" (MIZ), may be associated with an altered intertubular microstructure leading to a change in the optical properties of the interfacial dentin. This layer is confirmed by the SEM micrographs that showed the same band of structurally altered dentin immediately beneath the Biodentine (Fig. 3a). The GIC samples (Fig. 3b) and the dentin of the opposite surfaces of the discs (Figs. 3c, 3d), however, did not show such changes.

The MIZ conceptually resembles the inter-diffusion zone in the interface between dentin and adhesives (Ferrari and Davidson, 1996), or the ion exchange layer that appears interfacially between dentin and GIC (Wilson *et al*., 1983) (Fig. 2c2). However, the mechanism for the formation of the MIZ might be different, given the alkaline nature of unset calcium-silicate cements compared with acidic GICs. The MIZ could be attributed to a dual effect of the calcium-hydroxide-releasing cement: first, an alkaline caustic etching, followed by mineral diffusion.

Calcium hydroxide is a highly alkaline material (pH = 13) and could induce a caustic degradation effect on exposed collagen. This effect is mediated by the breakdown of intermolecular bonds in the collagen fibrils, increasing their water absorption and leading to swelling (Bowes, 1950; Kemp and Tristram, 1971). Andersen *et al*. (1992) referred to the same effect in explaining the decrease in the weight of pulpal tissues when exposed to calcium hydroxide. They attributed this change to the breakdown of ionic bonds in proteins and destruction of their tertiary structures. The denaturing effect of calcium hydroxide was also suggested by Andreasen *et al*. (2002) and White *et al*. (2002), who noticed a negative effect of this paste on root mechanical properties. This was confirmed by the reduced, or even absent, second-harmonic-generation signal originating from dentin within the MIZ (Fig. 2d1), indicating changes in the collagen conformation (Sun *et al*., 2006), unlike in GIC samples (Fig. 2d2), where the SHG signal was not affected.

The high alkalinity of hydrated Biodentine could therefore induce a caustic denaturing and permeability of the organic

collagen component of interfacial dentin, explaining the concentration of fluorophores within this zone. This alkaline caustic effect or "caustic etching" has virtually no effect on the highly mineralized peritubular dentin, due to its lower collagen content, and is therefore represented by a dye-deficient area in the MIZ (Figs. 2a1, 2c1).

In the GIC samples, the richly dye-infiltrated layer formed beneath the interface was a result of the demineralizing effect of the PAA and tartaric acids on the inorganic dentin component. This inverse effect showed deeper infiltration of the cement-labeling fluorophore into the higher mineralized peritubular dentin (Figs. 2a2, 2c2), associated with lateral diffusion of the dye permeating from the pulp space through the demineralized peritubular dentin in that zone, leading to mixing of both dyes (Fig. 2c2). This mixing did not appear in the Biodentine samples (Fig. 2c1), where the dye permeating from the pulp failed to diffuse laterally in the MIZ, indicating an intact peritubular dentin.

Formation of an interfacial layer between the dentin and calcium silicate cements was previously reported (Sarkar *et al.*, 2005; Reyes-Carmona *et al.*, 2009; Han and Okiji, 2011). Those authors suggested that this layer forms within the dentin tubules and the interfacial region of the two substrates due to hydroxyapatite formation. Our findings also show that the mineral infiltration zone formed within the intertubular structure of the dentin, and that this layer is rich with carbonate ions. However, no direct comparison should be made, since the samples in our study were kept in distilled water to delineate the effect of the cement alone, unlike the aforementioned studies, which used phosphate-buffered saline solutions.

Infiltration of calcium hydroxide/carbonate into interfacial dentin is associated additionally with mineral transfer, shown by the Raman maps (Fig. 4). The drop in Biodentine's Raman peak toward the pulp was gradual near the interface, corresponding to diffusion, but dropped suddenly at greater depth, suggesting the presence of a diffusion barrier: Calcium carbonate crystallization could be limiting further penetration. Dentin buffering may also explain this sudden drop. In GIC samples, the characteristic Raman peak dropped gradually throughout the whole penetration depth, which is consistent with diffusion products not being hindered by crystallization. This type of cements' diffusion into the intertubular dentin should be differentiated from "tubular diffusion" through the fluid-filled dentinal tubules, and therefore we suggest the term "intertubular diffusion" to describe it.

In summary, a richly dye-infiltrated layer appeared within the dentin under GIC and calcium silicate (Biodentine). However, its formation may be mediated by two opposite processes, one acidic and the other alkaline etching, respectively. Raman spectroscopy confirmed the intertubular diffusion of carbonate from calcium silicate cement into dentin, leading to the formation of the "mineral infiltration zone" with mineral infiltration into the intertubular dentin, following the denaturing effect of the strongly alkaline cement. Comparison of the interfaces shows a dentin-mineral infiltration with the Biodentine, whereas polyacrylic and tartaric acids and their salts characterize GIC penetration. The use of stain-free SHG imaging technologies also indicates modification of the dentin collagen beneath tricalcium-silicate cement, all of which invalidates the null hypothesis regarding the relation of both materials with dentin.

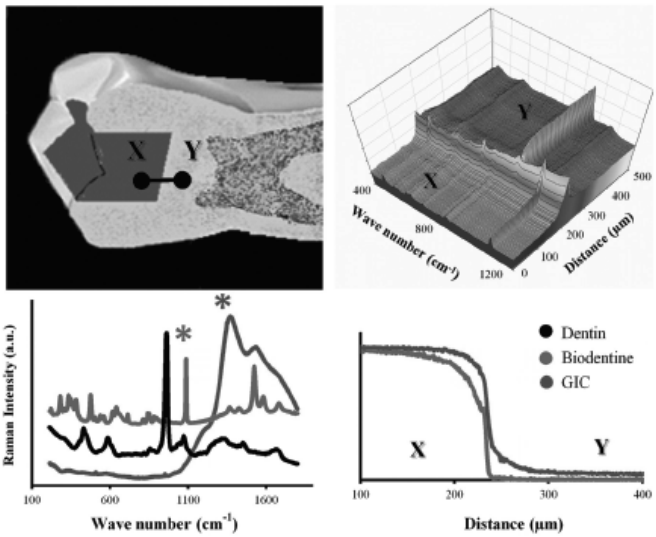

Figure 4. (**upper left**) Raman area maps were obtained for the dentin-cement interface in GIC and Biodentine filled teeth by StreamLine™ scanning in the direction from points X to Y. Raman spectral maps were analyzed with curve-fitting software which averaged each area map into a single line, where each point on that line was represented by an averaged Raman spectrum (**upper right**). From the cements' Raman spectra (**lower left**), representative characteristic peaks [1082 cm^{-1} and 1262 cm^{-1} (marked with asterisks)] were designated for Biodentine and GI cements, respectively. The average penetration depth was derived from the profiles of normalized Raman intensity of each peak, after they were generated from the curve-fitting software (**lower right**).

ACKNOWLEDGMENTS

This research was supported by Septodont. The authors acknowledge support from the Department of Health *via* the National Institute for Health Research (NIHR) comprehensive Biomedical Research Centre award to Guy's & St Thomas' NHS Foundation Trust with King's College London and King's College Hospital NHS Foundation Trust (Grant code, Guy's & St Thomas' NHS Foundation Trust & King's College London NIHR Biomedical Research Centre). This work was also supported by a Wellcome/EPSRC Medical Engineering Centre grant. We thank Peter Pilecki and Dr. Salvatore Sauro for their valuable assistance. The author(s) declare no potential conflicts of interest with respect to the authorship and/or publication of this article.

REFERENCES

Andersen M, Lund A, Andreasen JO, Andreasen FM (1992). In vitro solubility of human pulp tissue in calcium hydroxide and sodium hypochlorite. *Dent Traumatol* 8:104-108.

Andreasen JO, Farik B, Munksgaard EC (2002). Long-term calcium hydroxide as a root canal dressing may increase risk of root fracture. *Dent Traumatol* 18:134-137.

Bowes JH (1950). The swelling of collagen in alkaline solutions; swelling in solutions of bivalent bases. *Biochem J* 46:530-532.

Camilleri J, Montesin FE, Papaioannou S, McDonald F, Pitt Ford TR (2004). Biocompatibility of two commercial forms of mineral trioxide aggregate. *Int Endod J* 37:699-704.

Camilleri J, Cutajar A, Mallia B (2011). Hydration characteristics of zirconium oxide replaced Portland cement for use as a root-end filling material. *Dent Mater* 27:845-854.

Chen M, Chen W, Sun Y, Fwu P, Dong C (2007). Multiphoton autofluorescence and second-harmonic generation imaging of the tooth. *J Biomed Opt* 12:064018.

Ferrari M, Davidson CL (1996). In vivo resin-dentin interdiffusion and tag formation with lateral branches of two adhesive systems. *J Prosthet Dent* 76:250-253.

Han L, Okiji T (2011). Uptake of calcium and silicon released from calcium silicate-based endodontic materials into root canal dentin. *Int Endod J* 44:1081-1087.

Ibáñez J, Artús L, Cuscó R, López Á, Menéndez E, Andrade MC (2007). Hydration and carbonation of monoclinic C2S and C3S studied by Raman spectroscopy. *J Raman Spectrosc* 38:61-67.

Kemp GD, Tristram GR (1971). The preparation of an alkali-soluble collagen from demineralized bone. *Biochem J* 124:915-919.

Kjellsen K, Justnes H (2004). Revisiting the microstructure of hydrated tricalcium silicate—a comparison to Portland cement. *Cement & Concrete Composites* 26:947-956.

Lee SJ, Monsef M, Torabinejad M (1993). Sealing ability of a mineral trioxide aggregate for repair of lateral root perforations. *J Endod* 19:541-544.

Martinez-Ramirez S, Frías M, Domingo C (2006). Micro-Raman spectroscopy in white Portland cement hydration: long-term study at room temperature. *J Raman Spectrosc* 37:555-561.

No Authors Listed (2009). Biodentine Safety Data Sheet. Saint Maur des Fosses, France: Septodont. URL accessed on 3/2/2012 at: http://www.sirowahelsinki.fi/uudet_septodont_pdf/Biodentine_safetydata.pdf.

Reyes-Carmona JF, Felippe MS, Felippe WT (2009). Biomineralization ability and interaction of mineral trioxide aggregate and white Portland cement with dentin in a phosphate-containing fluid. *J Endod* 35:731-736.

Reyes-Carmona JF, Felippe MS, Felippe WT (2010). The biomineralization ability of mineral trioxide aggregate and Portland cement on dentin enhances the push-out strength. *J Endod* 36:286-291.

Sarkar NK, Caicedo R, Ritwik P, Moiseyeva R, Kawashima I (2005). Physicochemical basis of the biologic properties of mineral trioxide aggregate. *J Endod* 31:97-100.

Sun Y, Chen W, Lin S, Jee S, Chen Y, Lin L, *et al.* (2006). Investigating mechanisms of collagen thermal denaturation by high resolution second-harmonic generation imaging. *Biophys J* 91:2620-2625.

Tay FR, Pashley DH, Rueggeberg FA, Loushine RJ, Weller RN (2007). Calcium phosphate phase transformation produced by the interaction of the Portland cement component of white mineral trioxide aggregate with a phosphate-containing fluid. *J Endod* 33:1347-1351.

Taylor HW (1997). Cement chemistry. 2nd ed. London, UK: Thomas Telford Publishing.

Torabinejad M, Hong CU, McDonald F, Pitt Ford TR (1995). Physical and chemical properties of a new root-end filling material. *J Endod* 21:349-353.

Tsivilis S, Chaniotakis E, Kakali G, Batis G (2002). An analysis of the properties of Portland limestone cements and concrete. *Cement & Concrete Composites* 24:371-378.

Watson TF (1999). Bonding glass-ionomer cements to tooth structure. In: Advances in glass-ionomer cements. Davidson CL, Mjör IA, editors. Germany: Quintessence Publishing Co., Inc.

Watson TF, Cook RJ, Festy F, Pilecki P, Sauro SE (2008). Optical imaging techniques for dental biomaterials interfaces. In: Dental biomaterials: imaging, testing and modelling. Curtis RV, Watson TF, editors. Cambridge, UK: CRC Press.

Weller RN, Tay KC, Garrett LV, Mai S, Primus CM, Gutmann JL, *et al.* (2008). Microscopic appearance and apical seal of root canals filled with gutta-percha and ProRoot Endo Sealer after immersion in a phosphate-containing fluid. *Int Endod J* 41:977-986.

White JD, Lacefield WR, Chavers LS, Eleazer PD (2002). The effect of three commonly used endodontic materials on the strength and hardness of root dentin. *J Endod* 28:828-830.

Wilson AD, Prosser HJ, Powis DM (1983). Mechanism of adhesion of polyelectrolyte cements to hydroxyapatite. *J Dent Res* 62:590-592.

Young AM, Sherpa A, Pearson G, Schottlander B, Waters DN (2000). Use of Raman spectroscopy in characterisation of the acid-base reaction in glass-ionomer cements. *Biomaterials* 21:1971-1979.

References

Aaron JE, Makins NB, Francis RM, Peacock M. Staining of the calcification front in human bone using contrasting fluorochromes in vitro. J Histochem Cytochem, 1984; 32: 1251–1261

Alfano RR, Yao SS. Human teeth with and without dental caries studied by visible luminescent spectroscopy. J Dent Res. 1981;60(2):120-2.

Al-Khateeb S, Forsberg CM, de Josselin de Jong E, Angmar-Månsson B.A longitudinal laser fluorescence study of white spot lesions in orthodontic patients.Am J OrthodDentofacialOrthop. 1998;113(6):595-602.

Allred H. The differential staining of peritubular and intertubular matrices in human dentine. Arch Oral Biol. 1968 Jan;13(1):1-12.

Altshuler GB, Belashenkov NR, MartsinovskiGA,Solounin AA. Non-linear transmission and second harmonic generation in dentin in the field of ultrashortNd-laser pulses. Proc. SPIE 1984;6.

Andersen M, Lund A, Andreasen JO, Andreasen FM (1992). In vitro solubility of human pulp tissue in calcium hydroxide and sodium hypochlorite. Dent Traumatol 8:104-108.

Andreasen JO, Farik B, Munksgaard EC. Long-term calcium hydroxide as a root canal dressing may increase risk of root fracture. Dent Traumatol, 2002; 18:134-137.

Antonakos A, Liarokapis E, Leventouri T. Micro-Raman and FTIR studies of synthetic and natural apatites.Biomaterials. 2007 Jul;28(19):3043-54.

Arends J, Ruben JL, Christoffersen J, Jongebloed WL, Zuidgeest TG. Remineralization of human dentine in vitro. Caries Res. 1990;24(6):432-5.

Armstrong WG. Fluorescence characteristics of sound and carious human dentine preparations, Archives of Oral Biology1963a;8(2): 79-90.

Armstrong WG. The presence of ultra violet absorbing material and its relation to fluorescence "quenching" effects in carious dentine. Archives of Oral Biology 1963b;8(2): 223-231.

Armstrong WG, Horsley HJ. Isolation and properties of fluorescent components associated with calcified tissue collagen. Calcif Tissue Res. 1972;8(3):197-210.

Asgary S, Parirokh M, Eghbal MJ, Brink F. A comparative study of white mineral trioxide aggregate and white Portland cements using X-ray microanalysis. Australian Endodontic Journal 2004; 30, 89–92

Asgary S, Parirokh M,Eggbal M, Brink F. Chemical differences between white and gray mineral trioxide aggregate. J Endod, 2005;31:101-103

Awonusi A, Morris MD, Tecklenburg MM. Carbonate assignment and calibration in the Raman spectrum of apatite. Calcif Tissue Int. 2007 Jul;81(1):46-52.

Bachmann L, Zezell DM, Ribeiro AD, Gomes L, Ito AS. Fluorescence spectroscopy of biological tissues- A review. Applied spectroscopy reviews 2006;41(6): 575-590.

Baldwin GC. (1974). An introduction to non-linear optics. Springer, pp 1-5.

Band YB (2006). The interaction of light and matter In: Light and matter: electromagnetism, optics, spectroscopy and lasers. England: John Wily & sons Ltd, pp 177-207.

Banerjee A, Boyde A. Auto-fluorescence and mineral content of carious dentine: scanning optical and backscattered electron microscopic studies. Caries Res.1998;32(3):219-26.

Banerjee A, Sherriff M, Kidd EA, Watson TF. A confocal microscopic study relating the auto-fluorescence of carious dentine to its microhardness. Br Dent J. 1999;187(4):206-10.

Banerjee A, Cook R, Kellow S, Shah K, Festy F, Sherriff M, Watson T. A confocal micro-endoscopic investigation of the relationship between the microhardness of carious dentine and its auto-fluorescence.Eur J Oral Sci. 2010;118(1):75-9.

Barberis P, Merle-Méjean T, Quintard P. On Raman spectroscopy of zirconium oxide films, Journal of Nuclear Materials, 1997;246(2–3): 232-243.

Bardow A, Moe D, Nyvad B, Nauntofte B. The buffer capacity and buffer systems of human whole saliva measured without loss of CO2. Arch Oral Biol. 2000 Jan;45(1):1-12

Belío-Reyes IA, Bucio L, Cruz-Chavez E. Phase composition of ProRoot mineral trioxide aggregate by X-ray powder diffraction. J Endod. 2009 Jun;35(6):875-8

Bensted J. Uses of Raman spectroscopy in cement chemistry. Journal of the American Ceramic Society, 1976;59(3-4): 140-143.

Bertassoni LE, Habelitz S, Marshall SJ, Marshall GW. Mechanical recovery of dentin following remineralization in vitro--an indentation study.J Biomech. 2011 Jan 4;44(1):176-81.

Bertrand MF, Hessleyer D, Muller-Bolla M, Nammour S, Rocca J. Scanning Electron Microscopic Evaluation of Resin–Dentine. Interface After Er:YAG Laser Preparation. Lasers in Surgery and Medicine, 2004;35:51–57.

Billington RW, Williams JA, Pearson GJ. Ion processes in glass ionomer cements, Journal of Dentistry, 2006; 34(8): 544-555.

Billinton N, Knight AW. Seeing the wood through the trees: A review of techniques for distinguishing green fluorescent protein from endogenous auto-fluorescence. Analytical Biochemistry, 2001; 291: 175-197.

Biodentine Data sheet.Septodont (Saint Maur des Fosses- France).December 2009.

BiodentineTM Scientific file (2010). Active Biosilicate TechnologyTM, Septodont, Saint-Maur-des-Fosses Cedex, France, R&D Department.

Bloebaum RD, Skedros JG, Vajda EG, Bachus KN, Constantz BR. Determining mineral content variations in bone using backscattered electron imaging.Bone. 1997 May;20(5):485-90.

Booij M, ten Bosch JJ. A fluorescent compound in bovine dental enamel matrix compared with synthetic dityrosine. Arch Oral Biol. 1982;27(5):417-21.

Borisova EG, Uzunov TT, AvramovLA.Early differentiation between caries and tooth demineralization using laser-induced auto-fluorescence spectroscopy.Lasers Surg Med. 2004;34(3):249-53.

Borisova E, Uzunov T, Avramov L. Laser-induced auto-fluorescence study of caries model in vitro. Lasers Med Sci. 2006 Apr;21(1):34-41.

Boskey AL. Assessment of bone mineral and matrix using backscatter electron imaging and FTIR imaging. Curr Osteoporos Rep. 2006 Jun;4(2):71-5.

Bowes JH, Kenten RH. The swelling of collagen in alkaline solutions. 1. Swelling in solutions of sodium hydroxide. Biochem J. 1950 Jan;46(1):1-8.

Bowles WH, Bokmeyer TJ. Staining of adult teeth by minocycline: binding of minocycline by specific proteins.J Esthet Dent. 1997;9(1):30-4.

Boyd RW (2003).The Non-linear Optical Susceptibility In: Non-linear optics. London: Academic Press, PP 1-65.

Boyd RW and Masters BR (2008).Non-linear Optical Spectroscopy In: Masters BR and So P (ed).Handbook of biomedical non-linear optical microscopy, New York: Oxford university Press, pp 348-375.

Boyde A, Jones SJ. Backscattered electron imaging of dental tissues. Anat Embryol (Berl). 1983;168(2):211-26.

Boyde A, Jones SJ. Back-scattered electron imaging of skeletal tissues.Metab Bone Dis Relat Res. 1983-1984;5(3):145-50.

Boyde, A, Elliott JC, Jones SJ. Stereology and histogram analysis of backscattered electron images: Age changes in bone. Bone 1993;14:205-210.

Brodersen KE. Modelling calcium carbonate deposition from bicarbonate solutions in cracks in concrete. CRACK2 2003,99.

Cai Y, Tang,R (2009). Towards understanding biomineralization: calcium phosphate in biomimetic mineralization process. Front. Mater. Sci. China,Vol.3,No.2,pp.124–131

Camilleri J, Montesin FE, Papaioannou S, McDonald F, Pitt Ford TR. Biocompatibility of two commercial forms of mineral trioxide aggregate. Int EndodJ. 2004 Oct;37(10):699-704.

Camilleri J, Montesin FE, Brady K, Sweeney R, Curtis RV, Pitt Ford TR, The constitution of mineral trioxide aggregate, Dental Materials, 2005;21(4):297-303.

Camilleri, J, Pitt Ford TR. Mineral trioxide aggregate: a review of the constituents and biological properties of the material. Int Endod J, 2006 Oct; 39,747-754

Camilleri J. Hydration mechanisms of mineral trioxide aggregate. International endodontic journal,2007;40:462-470.

Camilleri J. Characterization of hydration products of mineral trioxide aggregate.International Endodontic Journal. 2008; 41, 408– 417

Camilleri J. Characterization and hydration kinetics of tricalcium silicate cement for use as a dental biomaterial. Dent Mater. 2011 Aug;27(8):836-44.

Camilleri J, Cutajar A, Mallia B. Hydration characteristics of zirconium oxide replaced Portland cement for use as a root-end filling material. Dent Mater. 2011 Aug;27(8):845-54.

Carneiro LS, Nunes CA, Silva MA, Leles CR, Mendonça EF.In vivo study of pixel grey-measurement in digital subtraction radiography for monitoring caries remineralization.Dentomaxillofac Radiol. 2009;38(2):73-78.

Carvalho RM, Tay F, Sano H, Yoshiyama M, Pashley DH.Long-term mechanical properties of EDTA-demineralized dentin matrix.J Adhes Dent. 2000 Autumn;2(3):193-9.

Causton BE. The physico-mechanical consequences of exposing glass ionomer cements to water during setting.Biomaterials. 1981 Apr;2(2):1125.

Chang JJ, Yeih Y, Huang R, Chi JM. Mechanical properties of carbonated concrete. Journal of Chinese Institute of Engineers,2003;26(4): 513-522.

Chang CW, Sud D, Mycek MA. Fluorescence Lifetime Imaging Microscopy In: Methods in cell biology, 2007; 81: 495-524.

Chen MH, Chen WL, Sun Y, Fwu PT, Dong CY.Multiphotonauto-fluorescence and second-harmonic generation imaging of the tooth. J Biomed Opt. 2007;12(6):064018.

Chen SY, Hsu CY, Sun CK. Epi-third and second harmonic generation microscopic imaging of abnormal enamel. Opt Express. 2008;16(15):11670-9.

Chen CC, Ho CC, David Chen CH, Wang WC, Ding SJ. In vitro bioactivity and biocompatibility of dicalcium silicate cements for endodontic use.J Endod. 2009 Nov;35(11):1554-7.

Chi JM, Huang R, Yang CC. Effects of carbonation on mechanical properties and durability of concrete using accelerated testing method. Journal of Marine Science and Technology, 2002;10(1): 14-20.

Chia-Yi Chu, Tien-Chun Kuo,Shu-Fang Chang, Yow-Chyun Shyu,Chun-Pin Lin. Comparison of the microstructure of crown and root dentine by a scanning electron microscopic study. J Dent Sci, 2010; 5(1):14−20.

Cláudio A. Rigo da Silvaa, Rubens J. Pedrosa Reisb, Fernando Soares Lameirasc, Wander Luiz Vasconcelosd. Carbonation-Related Microstructural Changes in Long-Term Durability Concrete, Materials Research, 2002;5(3), 287-293.

Clegg RM, Schneider PC (1996). Fluorescence lifetime-resolved imaging microscopy: a general description of lifetime-resolved imaging measurements In. Slavik (ed) In: Fluorescence Microscopy and Fluorescent Probes. New York: Plenium Press, pp 15-20.

Conjeaud, M. and H. Boyer, Some possibilities of Raman microproble in Cement chemistry.Cement and Concrete Research, 1980. 10: 61-70

Crane NJ, Popescu V, Morris MD, Steenhuis P, Ignelzi MA Jr. Raman spectroscopic evidence for octacalcium phosphate and other transient mineral species deposited during intramembranous mineralization. Bone. 2006 Sep;39(3):434-42.

Cuscó R, Guitián F, de Aza S, Artús L. Differentiation between hydroxyapatite and β-tricalcium phosphate by means of μ-Raman spectroscopy, Journal of the European Ceramic Society, 1998; 18(9): 1301-1305,

D'Alpino PH, Pereira JC, Svizero NR, Rueggeberg FA, Carvalho RM, Pashley DH.A new technique for assessing hybrid layer interfacial micromorphology and integrity: two-photon laser microscopy. J Adhes Dent, 2006; 8(5):279-284.

Dai L, Liu Y, Salameh Z, Khan S, Mao J, Pashley DH, Tay FR. Can Caries-Affected Dentin be Completely Remineralized by Guided Tissue Remineralization? Dent Hypotheses. 2011 Jan 1;2(2):74-82.

Dammaschke T, Gerth HUV, Zuchner H, Schafer E. Chemical and physical surface and bulk material characterization of white ProRoot MTA and two Portland cements. Dent Mater, 2005;21:731–738.

Darvell BW, Wu RC. “MTA”—An Hydraulic Silicate Cement: Review update and setting reaction. Dental Materials, 2011; 27(5): 407-422.

Davis GR, Wong FS.X ray microtomography of bones and teeth. Physiol Meas. 1996 Aug;17(3):121-46.

Daw C, Glasser FP. Calcium carbonate efflorescence on Portland cement and building materials. Cement and Concrete Research, 2003;33(1):147-154.

Deb S, Nicholson JW. The effect of strontium oxide in glass-ionomer cements. J Mater Sci Mater Med. 1999 Aug;10(8):471-4.

Deyl Z, Macek K, Adam M, Hancikova O. Studies on the chemical nature of elastin fluorescence. BiochemBiophysActa, 1980; 625: 248-254.

Dreger LA, Felippe WT, Reyes-Carmona JF, Felippe GS, Bortoluzzi EA, Felippe MC. Mineral trioxide aggregate and Portland cement promote biomineralization in vivo. J Endod. 2012 Mar;38(3):324-9.

Eisenmann DR, Yaeger JA. In-vitro mineralization of hypomineralized dentine induced by strontium and fluoride in the rat. Arch Oral Biol. 1972 Jun;17(6):987-99.

Elbaum R, Tal E, Perets AI, Oron D, Ziskind D, Silberberg Y, Wagner HD. Dentin micro-architecture using harmonic generation microscopy. J Dent. 2007;35(2):150-5.

Evans G, Raman Analysis Speeds into Biomedicine, Biophotonics; Feb, 2008.

Ferrari M, Davidson CL. In vivo resin-dentine interdiffusion and tag formation with lateral branches of two adhesive systems. J ProsthetDent, 1996; 76:250-253.

Foreman PC.The excitation and emission spectra of fluorescent components of human dentine. Arch Oral Biol. 1980;25(10):641-7.

Forsten L. Fluoride release and uptake by glass-ionomers and related materials and its clinical effect. Biomaterials, 1998;19(6):503-508

Fratzl P, Schreiber S, Roschger P, Lafage MH, Rodan, G, Klaus hofer K. Effects of sodium fluoride and alendronate on the bone mineral in minipigs: A small-angle X-ray scattering and backscattered electron imaging study. J Bone Miner Res, 1996;11:248-253.

Fujimoto D. Evidence for natural existence of pyridinoline crosslink in collagen. BiochemBiophys Res Commun. 1980;93(3):948-53.

Funteas UR, Wallace JA, Fochtman EW. A comparative analysis of Mineral Trioxide Aggregate and Portland cement. Aust Endod J, 2003 Apr;29(1):43-44.

Fusayama T. Two layers of carious dentin; diagnosis and treatment. Oper Dent. 1979 Spring;4(2):63-70.

Gilchrist F, Santini A, Harley K, Deery C. The use of micro-Raman spectroscopy to differentiate between sound and eroded primary enamel. Int J Paediatr Dent. 2007 Jul;17(4):274-80.

Glasser J, Fonda GR.The Fluorescence of Double Salts of Calcium Phosphate. J. Amer. chem. Soc 1938; 60: 722.

Grant AA. The use of optical and electron microscopy in the study of dental materials. Aust Dent J. 1967 Oct;12(5):429-32.

Griffiths BM, Watson TF, Sherriff M.The influence of dentine bonding systems and their handling characteristics on the morphology and micropermeability of the dentine adhesive interface. J Dent, 1999; 27(1):63-71.

Griffiths BM, Naasan M, Sherriff M, Watson TF Variable polymerisation shrinkage and the interfacial micropermeability of a dentin bonding system. J Adhes Dent. 1999; 1(2):119-131.

Gu L, Kim YK, Liu Y, Ryou H, Wimmer CE, Dai L, Arola DD, Looney SW, Pashley DH, Tay FR. Biomimetic analogs for collagen biomineralization. J Dent Res. 2011 Jan;90(1):82-7.

Guangsheng He, Song H. Liu (1999). Second-order non-linear wave mixing In: Physics of non-linear optics. Singapore: World Scientific, pp35.

Hafström-Björkman U, Sundström F, ten Bosch JJ.Fluorescence in dissolved fractions of human enamel.ActaOdontol Scand. 1991;49(3):133-8.

Han L, Okiji T. Uptake of calcium and silicon released from calcium silicate-based endodontic materials into root canal dentine. Int Endod J. 2011 Dec;44(12):1081-7.

Hartles RL, Leaver AG. The fluorescence of teeth under ultraviolet irradiation.Biochem J. 1953;54(4):632-8.

Hashimoto M, Ohno H, Kaga M, Endo K, Sano H, Oguchi H. In vivo degradation of resin-dentin bonds in humans over 1 to 3 years. J Dent Res. 2000 Jun;79(6):1385-91.

Helmchen F, Denk W. Deep tissue two-photon microscopy. Nature Methods.2005;12(2):932-40.

Hibst R, Robert P, Adrian L. Detection of occlusal caries by laser fluorescence: basic and clinical investigations. Medical Laser Application, 2001; 16(3): 205-213.

Hoerman KC, Mancewicz SA. Fluorometric demonstration of tryptophan in dentin and bone protein. J Dent Res. 1964 Mar-Apr;43:276-80.

Hoerman KC, Balekjian AY. Some quantum aspects of collagen. Fed Proc. 1966 May-Jun;25(3):1016-21.

Holland GR. Extensive and coincident side branching of dentinal tubules. Anat Anz, 1982;152(2):171-178.

Holland GR. Morphological features of dentine and pulp related to dentine sensitivity. Arch Oral Biol, 1994; 39: S3-S11.

Holland R, de Souza V, Nery MJ, Otoboni Filho JA, Bernabé PF, Dezan Júnior E. Reaction of rat connective tissue to implanted dentin tubes filled with mineral trioxide aggregate or calcium hydroxide. J Endod. 1999 Mar;25(3):161-6.

Howard W. Robertsa, Jeffrey M. Toth, David W. Berzins, David G. Charlton. Mineral trioxide aggregate material use in endodontic treatment: A review of the literature. Dent Mater, 2008; 24:149–164.

Horie K, Ushiki H, Winnik FM (2000). Molecular Photonics: fundamentals and practical aspects. Tokyo: Kodanha.

Ibáñez J, Artús L, Cuscó R, López Á, Menéndez E, Andrade MC. Hydration and carbonation of monoclinic C2S and C3S studied by Raman spectroscopy. J. Raman Spectrosc, 2007; 38: 61–67.

Ignatova M, Voccia S, Gabriel S, Gilbert B, Cossement D, Jerome R, Jerome C. Stainless steel grafting of hyperbranched polymer brushes with an antibacterial activity: synthesis, characterization, and properties. Langmuir. 2009 Jan 20;25(2):891-902.

Inaba D, Ruben J, Takagi O, Arends J. Effect of sodium hypochlorite treatment on remineralization of human root dentine in vitro. Caries Res. 1996;30(3):218-24.

Inoué S (2006).Confocal imaging In: Pawley JB (ed). Handbook of biological confocal microscopy (3rd ed). Berlin: Springer, pp 1-16.

Islam I, Chng HK, Yap AU.X-ray diffraction analysis of mineral trioxide aggregate and Portland cement. Int Endod J. 2006 Mar;39(3):220-5.

Jacobs R, Harris WH, Katz EP, Glimcher MJ. The interaction between tetracycline and reconstituted guinea-pig-skin collagen in vitro.Biochim Biophys Acta. 1964 Jun 8;86:579-87.

Kabasawa M,Ejiri S,Hanada K, Ozawa H. Observations of Dental Tissues Using the Confocal Laser Scanning Microscope. Biotechnic & Histochemistry, 1995; 70(2): 66-69.

Kagayama M, Sasano Y, Sato H, Kamakura S, Motegi K, Mizoguchi I. Confocal microscopy of dentinal tubules in human tooth stained with alizarin red Anat Embryol (Berl), 1999 Mar;199(3):233-238.

Kao FJ. The use of optical parametric oscillator for harmonic generation andtwo-photon UV fluorescence microscopy.Microsc Res Tech. 2004;63(3):175-81.

Kawano F, Hanawa T, Kon M, Oka K, Tomotake Y, Asaoka K, Ichikawa T, Matsumoto N. Estimation of residual stress in dental porcelain by laser-Raman spectroscopy.Dent Mater J. 1998 Mar;17(1):41-50.

Kawasaki K, Ruben J, Stokroos I, Takagi O, Arends J.The remineralization of EDTA-treated human dentine. Caries Res. 1999 Jul-Aug;33(4):275-80.

Kawasaki K, Ruben J, Tsuda H, Huysmans MC, Takagi O. Relationship between mineral distributions in dentine lesions and subsequent remineralization in vitro. Caries Res. 2000 Sep-Oct;34(5):395-403.

Kemp GD, Tristram GR. The preparation of an alkali-soluble collagen from demineralized bone. Biochem J. 1971 Oct;124(5):915-9.

Kim BM, Eichler J, Da Silva LB. Frequency doubling of ultrashort laser pulses in biological tissues. Appl Opt. 1999;38(34):7145-50.

Kim BM, Eichler J, Reiser KM, Rubenchik AM, Da Silva LB. Collagen structureand non-linear susceptibility: effects of heat, glycation, and enzymatic cleavage on second harmonic signal intensity. Lasers Surg Med. 2000;27(4):329-35.

Kim YK, Yiu CK, Kim JR, Gu L, Kim SK, Weller RN, Pashley DH, Tay FR. Failure of a glass ionomer to remineralize apatite-depleted dentin. J Dent Res. 2010 Mar;89(3):230-5.

Kirkpatrick RJ, Yarger, McMillan PF, Ping Yu, Tong CX. Raman spectroscopy of C-S-H, tobermorite, and jennite, Advanced Cement Based Materials,1997;5(3):93-99.

Kjellsen K, Justnes H. Revisiting the microstructure of hydrated tricalcium silicate—a comparison to Portland cement. Cement & Concrete Composites, 2004; 26:947–956.

Klont B, ten Cate JM. Remineralization of bovine incisor root lesions in vitro: the role of the collagenous matrix. Caries Res. 1991;25(1):39-45.

Ko, ACT, Hewko M, Leonardi L, Sowa MG, Dong CCS, Williams P, Cleghorn B. Ex vivo detection and characterization of early dental caries by optical coherence tomography and Raman spectroscopy. Journal of biomedical optics, 2005; 10(3): 031118-031118.

König K, Schneckenburger H, Hibst R. Time-gated in vivo auto-fluorescence imaging of dental caries. Cell MolBiol (Noisy-le-grand). 1999; 45(2): 233-9.

König K, Hibst R, Flemming G, SchneckenburgerH.Laser-induced auto-fluorescence of caries. Proc. SPIE, 1993; 1880: 125-131.

Koutsopoulos S. Synthesis and characterization of hydroxyapatite crystals: a review study on the analytical methods. J Biomed Mater Res. 2002 Dec 15;62(4):600-12.

Kumari L, Li W, Wang D. Monoclinic zirconium oxide nanostructures synthesized by a hydrothermal route. Nanotechnology. 2008 May 14;19(19):195602.

LaBella F, Keeley F, Vivian S, Thornhill D. Evidence for dityrosine in elastin.BiochemBiophys Res Commun. 1967;26(6):748-53.

Lakowicz JR (2006). Introduction to fluorescence In: Principles of fluorescence spectroscopy, New York: Springer, Volume 1, pp1-26

Laurent P, Camps J, De Méo M, Déjou J, About I. Induction of specific cell responses to a Ca(3)SiO(5)-based posterior restorative material. Dent Mater. 2008 Nov;24(11):1486-94.

Laurent P, Camps J, About I. Biodentine(TM) induces TGF-β1 release from human pulp cells and early dental pulp mineralization. Int Endod J. 2012 May;45(5):439-48.

Learmonth RP, Kable SH, Ghiggino KP (2009).Basics of fluorescence.Gloyds EM (ed) In: Fluorescence applications in biotechnology and life science. New Jersy: Wily-Blackwell, pp1-26.

Lee SJ, Monsef M, Torabinejad M. Sealing ability of a mineral trioxide aggregate for repair of lateral root perforations. J Endod, 1993; 19(11): 541-544.

Lee HS, Berg JH, García-Godoy F, Jang KT. Long-term evaluation of the remineralization of interproximal caries-like lesions adjacent to glass-ionomer restorations: a micro-CT study. Am J Dent. 2008 Apr;21(2):129-32.

Leiendecker AP, Qi YP, Sawyer AN, Niu LN, Agee KA, Loushine RJ, Weller RN, Pashley DH, Tay FR. Effects of Calcium Silicate-based Materials on Collagen Matrix Integrity of Mineralized Dentin. J Endod. 2012 Jun;38(6):829-33.

Leroy GG, Penel NL, Bres. Human tooth enamel: a Raman polarized approach. Applied spectroscopy, 2002; 56(8): 1030-1034.

Lester KS, Boyde A. Some preliminary observations on caries ("remineralization") crystals in enamel and dentine by surface electronmicroscopy.Virchows Arch Pathol Anat Physiol Klin Med. 1967;344(2):196-212.

Li X, Chang J. Preparation of bone-like apatite-collagen nanocomposites by a biomimetic process with phosphorylated collagen. J Biomed Mater Res A. 2008 May;85(2):293-300.

Lickorish D, Ramshaw JA, Werkmeister JA, Glattauer V, Howlett CR. Collagen-hydroxyapatite composite prepared by biomimetic process. J Biomed Mater Res A. 2004 Jan 1;68(1):19-27.

Lin P, Lyu H, Hsu CS, Chang C, Kao JF. Imaging carious dental tissues with multiphoton fluorescence lifetime imaging microscopy .Biomed Opt Express. 2011; 2(1): 149–158.

Liu Y, Kim YK, Dai L, Li N, Khan SO, Pashley DH, Tay FR. Hierarchical and non-hierarchical mineralisation of collagen. Biomaterials. 2011a Feb;32(5):1291-300.

Liu Y, Mai S, Li N, Yiu CK, Mao J, Pashley DH, Tay FR. Differences between top-down and bottom-up approaches in mineralizing thick, partially demineralized collagen scaffolds. Acta Biomater. 2011b Apr;7(4):1742-51.

Liu Y, Li N, Qi Y, Niu LN, Elshafiy S, Mao J, Breschi L, Pashley DH, Tay FR. The use of sodium trimetaphosphate as a biomimetic analog of matrix phosphoproteins for remineralization of artificial caries-like dentin. Dent Mater. 2011c May;27(5):465-77.

Long DA (1977).Raman Spectroscopy.McGraw Hill Higher Education

Mancewicz SA, Hoerman KC. Characteristics of insoluble protein of tooth and bone.i.fluorescence of some acidic hydrolytic fragments. Arch Oral Biol. 1964;9:535-44.

Martinez-Ramirez S, Frías M, and Domingo C. Micro-Raman spectroscopy in white portland cement hydration: long-term study at room temperature. Journal of Raman Spectroscopy, 2006; 37(5): 555-561.

Martínez-Ramírez S, Fernández-Carrasco L (2011). Raman Spectroscopy: Application to Cementitious Systems In: Doyle SG (ed). Construction and Building: Design, Materials, and Techniques, Nova Science Publishers, pp 233-24.

Matsumoto H, Kitamura S, Araki T. Auto-fluorescence in human dentine in relation to age, tooth type and temperature measured by nanosecond time-resolved fluorescence microscopy. Arch Oral Biol. 1999 Apr;44(4):309-18.

Matsushita F, Aono Y, Shibata S. Carbonation degree of autoclaved aerated concrete.Cement and Concrete Research. 2000;30: 1741-1745.

McClure. Demonstration of calcification fronts by in vivo and in vitro Tetracycline labelling, J. Clin. Pathol.1982; 35:1278–1282.

McConnell G, Girkin JM, Ameer-Beg SM, Barber PR, Vojnovic B, Ng T, Banerjee A, Watson TF, Cook RJ. Time-correlated single-photon counting fluorescence lifetime confocal imaging of decayed and sound dental structures with a white-light supercontinuum source. J Microsc. 2007;225(Pt 2):126-36.

Mendis BR, Darling AI. Distribution with age and attrition of peritubulardentine in the crowns of human teeth. Arch Oral Biol. 1979;24(2):131-9.

Mertz J (2008). Applications of Second-Harmonic Generation Microscopy In: Masters BR and So P (eds). Handbook of biomedical non-linear optical microscopy. Oxford university Press.

Mjör IA, Nordahl I. The Density and Branching of Dentinal Tubules in Human Teeth. Archs oral Biol, 1996;41:401-412

Morgan J. Introduction to geometrical and physical optics.American Journal of Physics, 1953; 21: 696.

Moseley R, Waddington RJ, Sloan AJ, Smith AJ, Hall RC, Embery G. The influenceof fluoride exposure on dentin mineralization using an in vitro organ culturemodel. Calcif Tissue Int. 2003 Nov;73(5):470-5.

Mukai Y, ten Cate JM. Remineralization of advanced root dentin lesions in-vitro. Caries Res. 2002;36(4):275-80.

New G (2011). Introduction In: Introduction to nolinear optics. Cambridge Cambridge University Press, pp 1-18.

Ngo HC, Mount G, Mc Intyre J, Tuisuva J, Von Doussa RJ. Chemical exchange between glass-ionomer restorations and residual carious dentine in permanent molars: an in vivo study. J Dent. 2006 Sep;34(8):608-13.

Nicholson JW. Chemistry of glass-ionomer cements: a review. Biomaterials. 1998 Mar;19(6):485-94

Oida T, Sako Y, Kusumi A. Fluorescence lifetime imaging microscopy (flimscopy). Methodology development and application to studies of endosome fusion in single cells.Biophysical Journal, 1993; 64(3): 676-685

Oliveira MG, Xavier CB, Demarco FF Pinheiro AL, Costa AT, Pozza DH. Comparative chemical study of MTA and Portland cements. Braz Dent J 2007;18:3–7.

Onishi T, Umemura S, Yanagawa M, Matsumura M, Sasaki Y, Ogasawara T, Ooshima T. Remineralization effects of gum arabic on caries-like enamel lesions.Arch Oral Biol. 2008;53(3):257-60.

Osorio R, Yamauti M, Osorio E, Ruiz-Requena ME, Pashley DH, Tay FR, Toledano M. Zinc reduces collagen degradation in demineralized human dentin explants. J Dent. 2011 Feb;39(2):148-53.

Ozawa H, Hoshi K, Amizuka N. Current Concepts of Bone Biomineralization . J. Oral Biosci. 2008 , 50: 1-14.

Panayotov I, Tassery H, Martin M, Cloitre T, Cuisinier FJ, Gergely C, Levallois BN. Non Linear Optical Microscopy Study of Sound and Carious Dentin. In: CED-IADR-; Sep 2011; Budapest, Hungry. Abstract 0551, pp 59.

Pashley DH, Tay FR, Yiu C, Hashimoto M, Breschi L, Carvalho RM, Ito S. Collagen degradation by host-derived enzymes during aging. J Dent Res. 2004 Mar;83(3):216-21.

Pérard M, Tricot-Doleux S, Pellen-Mussi P, Meary F, Pérez F.Evaluation of the cytotoxicity of pulp floor perforation filling materials by using in parallel 2d and 3d culture models. Bull Group Int Rech Sci Stomatol Odontol. 2011; 50(2): 42-43.

Petersson LG, Kambara M. Remineralisation study of artificial root caries lesions after fluoride treatment. An in vitro study using electric caries monitor and transversal micro-radiography.Gerodontology. 2004 Jun;21(2):85-92.

Potgieter-Vermaak SS, Potgieter JH, Van Grieken R, The application of Raman spectrometry to investigate and characterize cement, Part I: A review, Cement and Concrete Research, 2006; 36(4): 656-662.

Qi YP, Li N, Niu LN, Primus CM, Ling JQ, Pashley DH, Tay FR. Remineralization of artificial dentinal caries lesions by biomimetically modified mineral trioxide aggregate. Acta Biomater. 2012 Feb;8(2):836-42.

Reid SA,Boyde A. Changes in the mineral density distribution in human bone with age: Image analysis using backscattered electrons in the SEM. J Bone Miner Res 2:13-22; 1987.

Reyes-Carmona JF, Felippe MS, Felippe WT. Biomineralization ability and interaction of mineral trioxide aggregate and white portland cement with dentine in a phosphate-containing fluid. Journal of Endodontics, 2009; 35(5): 731-736.

Rietdorf J, Gadella TWJ. Fluorescence lifetime imaging microscopy (FLIM).AdvBiochemEngin/Biotechnol, 2005; 95: 143-175.

Rivera EM, Yamauchi M. Site comparisons of dentine collagen cross-links from extracted human teeth. Arch Oral Biol. 1993 Jul;38(7):541-6.

Roschger P, Plenk H Jr, Klaushofer K, Eschberger J. A new scanning electron microscopy approach to the quantification of bone mineral distribution: Backscattered electron image grey-levels correlated to calcium Ke~-line intensities. Scann Microsc 9:75-88: 1995.

Roy SK, Poh KB, Northwood DO.Durability of concrete -accelerated carbonation and weathering studies.Building and Environment 1999; 34: 597-606.

Saito, T, Yamauchi, M, Crenshaw, MA. Apatite Induction by Insoluble Dentin Collagen. J Bone Miner Res, 1998; 13: 265–270.

Saito T, Toyooka H, Ito S, Crenshaw MA. In vitro study of remineralization of dentin: effects of ions on mineral induction by decalcified dentin matrix. Caries Res. 2003 Nov-Dec;37(6):445-9.

Sakoolnamarka R, Burrow MF, Prawer S, Tyas MJ. Raman spectroscopic study of noncarious cervical lesions. Odontology, 2005; 93(1): 35-40.

Sarkar NK, Caicedo R, Ritwik P, Moiseyeva R, Kawashima I. Physicochemicalbasis of the biologic properties of mineral trioxide aggregate.J Endod. 2005Feb;31(2):97-100.

Sathyanarayana DN (2005). Raman Spectroscopy In: Vibrational Spectroscopy: Theory And Applications. New Delhi: New Age Int, pp 294- 347.

Sato-Berrú RY, Vázquez-Olmos A, Fernández-Osorio AL, Sotres-Martínez S. Micro-Raman investigation of transition-metal-doped ZnO nanoparticles. Journal of Raman Spectroscopy, 2007;38(9): 1073-1076.

Sauer GR, Zunic WB, Durig JR, Wuthier RE. Fourier transforms Raman spectroscopy of synthetic and biological calcium phosphates. Calcif Tissue Int. 1994 May;54(5):414-20.

Sauro S, Toledano M, Aguilera FS, Mannocci F, Pashley DH, Tay FR, Watson TF, Osorio R. Resin-dentin bonds to EDTA-treated vs. acid-etched dentin using ethanol wet-bonding. Dent Mater, 2010;26(4):368-379.

Sauro S, Thompson I, Watson TF. Effects of common dental materials used in preventive or operative dentistry on dentin permeability and remineralization. Oper Dent. 2011 Mar-Apr;36(2):222-30.

Sauro S, Watson TF, Thompson I, Banerjee A. One-bottle self-etching adhesives applied to dentine air-abraded using bioactive glasses containing polyacrylic acid: an in vitro microtensile bond strength and confocal microscopy study. J Dent. 2012 Nov;40(11):896-905.

Sawyer AN, Nikonov SY, Pancio AK, Niu LN, Agee KA, Loushine RJ, Weller RN, Pashley DH, Tay FR. Effects of calcium silicate-based materials on the flexural properties of dentin. J Endod. 2012 May;38(5):680-3.

Schembri M, Peplow G, Camilleri J. Analyses of Heavy Metals in Mineral Trioxide Aggregate and Portland Cement. J Endod, 2010 ; 36(7):1210-1215

Schmitt MO, Schneider S. Spectroscopic investigation of complexation between various Tetracyclines and Mg2+ or Ca2+. Phys Chem Comm, 2000;3:42-55.

Schneider S, Schmitt MO, Brehm G, Reiher M, Matousek P, Photochem MT. Photobiol. Fluorescence kinetics of aqueous solutions of Tetracycline and its complexes with Mg2+ and Ca2+. Sci., 2003,2, 1107-1117.

Sennou HE, Lebugle AA, Grégoire GL. X-ray photoelectron spectroscopy study of the dentin-glass ionomer cement interface. Dent Mater. 1999 Jul;15(4):229-37

Sidhu SK, Watson TF. Interfacial characteristics of resin-modified glass-ionomer materials: a study on fluid permeability using confocal fluorescence microscopy. J Dent Res, 1998; 77(9): 1749-1759.

Sidhu SK, Pilecki P, Cheng PC, Watson TF.The morphology and stability of resin-modified glass-ionomer adhesive at the dentin/resin-based composite interface. Am J Dent, 2002; 15(2):129-136.

Silva, CA, Reis RJP, Lameiras FS, Vasconcelos WL.Carbonation-Related Microstructural Changesin Long-Term Durability Concrete. Materials Research ,2002;5(3): 287-293.

Skinner HC, Nalbandian J. Tetracyclines and mineralized tissues: review and perspectives. Yale J Biol Med. 1975 Nov;48(5):377-97.

So PC (2001). Two-photon Fluorescence Light Microscopy. In: eLS. John Wiley & Sons Ltd, Chichester. http://www.els.net [doi: 10.1038/npg.els.0002991]

Solomons CC, Neuman WF. On the mechanisms of calcification: theremineralization of dentin. J Biol Chem. 1960 Aug;235:2502-6.

Song J, Mante F, Romanow WJ, Kim S. Chemical analysis of powder and set forms of Portland cement, gray ProRoot MTA, white ProRoot MTA, and gray MTA-Angelus. Oral Surg Oral Med Oral Pathol Oral Radiol Endod, 2006;102:809-815.

Song KB, Choi YH, Jeong SH, Seol HJ, Kim HI, Kwon YH. Detection of incipient carious lesions formed on human teeth in vitro using ultraviolet laser. Photomed Laser Surg. 2005;23(5):498-503.

Spencer P, Wang Y, Walker MP, Wieliczka DM, Swafford JR. Interfacial chemistryof the dentin/adhesive bond. J Dent Res. 2000 Jul;79(7):1458-63.

Spitzer D, ten Bosch JJ.The total luminescence of bovine and human dental enamel.Calcif Tissue Res. 1976;20:201-8.

Spitzer D, ten Bosch JJ. Luminescence quantum yields of sound and carious dental enamel. Calcif Tissue Res. 1977;24(3):249-51.

Stookey GK. Quantitative light fluorescence: a technology for early monitoring of the caries process. Dent Clin North Am. 2005 Oct;49(4):753-70,

Stübel H. Die FluoreszenztierischerGewebe in ultraviolettemLicht. Arch GesPhysiol 1911; 142:1–14.

Sun Y, Chen WL, Lin SJ, Jee SH, Chen YF, Lin LC, So PT, Dong CY.Investigating mechanisms of collagen thermal denaturation by high resolution second-harmonic generation imaging.Biophys J. 2006;91(7):2620-5

Sundström F, Fredriksson K, Montán S, Hafström-Björkman U, Ström J. Laser-induced fluorescence from sound and carious tooth substance: spectroscopic studies. Swed Dent J. 1985;9(2):71-80.

Suzuki M, Kato H, Wakumoto S. Vibrational analysis by Raman spectroscopy of the interface between dental adhesive resin and dentin. J Dent Res. 1991 Jul;70(7):1092-7.

Szabo, Trombitas, and Szabo.Scanning electron microscopy of the walls of tubules in human coronal dentine. Arch Oral Biol, 1985; 30(10):705-710.

Tanumiharja M, Burrow MF, Cimmino A, Tyas MJ. The evaluation of four conditioners for glass ionomer cements using field-emission scanning electron microscopy. J Dent. 2001 Feb;29(2):131-8.

Takuma S, Kurahashi Y. Electron microscopy of various zones in a cariouslesion in human dentine. Arch Oral Biol. 1962 Jul-Aug;7:439-53.

Tapp E, KovácsK, Carroll R. Tetracycline Staining of Tissues in Vitro. Biotechnic & Histochemistry, 1965; 40(4):199-203.

Tarrida M, Madon M, Le Rolland B, Colombet P. An in-situ Raman spectroscopy study of the hydration of tricalcium silicate, Advanced Cement Based Materials, 1995;2(1):15-20.

Tay FR, Pashley DH, Rueggeberg FA, Loushine RJ, Weller RN. Calcium phosphate phase transformation produced by the interaction of the portland cement component of white mineral trioxide aggregate with a phosphate-containing fluid. J Endod. 2007 Nov;33(11):1347-51.

Tay FR, Pashley DH. Guided tissue remineralisation of partially demineralised human dentine. Biomaterials. 2008 Mar;29(8):1127-37.

Tay FR, Pashley DH.Biomimetic remineralization of resin-bonded acid-etched dentin. J Dent Res. 2009;88(8):719-24.

Taylor H. (1997). Cement Chemistry (2nd ed). London: Thomas Telford Publishing.

Ten Cate JM, Buus JM, Damen JM. The effects of GICrestorations on enamel and dentin demineralization and remineralization ADR December 1995 9: 384-388.

Tezvergil-Mutluay A, Agee KA, Hoshika T, Carrilho M, Breschi L, Tjäderhane L, Nishitani Y, Carvalho RM, Looney S, Tay FR, Pashley DH. The requirement of zinc and calcium ions for functional MMP activity in demineralized dentin matrices. Dent Mater. 2010 Nov;26(11):1059-67.

Theer P, Hasan MT, Denk W. Two-photon imaging to a depth of 1000 microm in living brains by use of a Ti:Al2O3 regenerative amplifier. Opt Lett. 2003;28(12):1022-4

Thomas HF, Carella P. A Scanning Electron Microscope Study of Dentinal Tubules from Un-erupted Human Teeth. Arch Oral Biol, 1983; 28: 1125-1130.

Thomas SS, Mohanty S, Jayanthi JL, Varughese JM, Balan A, Subhash N. Clinical trial for detection of dental caries using laser-induced fluorescence ratio reference standard. J Biomed Opt. 2010;15(2):027001.

Thomas SS, Jayanthi JL, Subhash N, Thomas J, Mallia RJ, Aparna GN. Characterization of dental caries by LIF spectroscopy with 404-nm excitation. Lasers Med Sci. 2011;26(3):299-305.

Tiede E, Chomse H. (1934).Ber.dtch. chem. Ge8.676, 1988.(Cited in Chem. Abstr.(1935), 29, 1473.

Tjäderhane L, Larjava H, Sorsa T, Uitto VJ, Larmas M, Salo T The activation and function of host matrix metalloproteinases in dentin matrix breakdown in caries lesions. J Dent Res 1998.77:1622-1629.

Torabinejad M, Hong CU, McDonald F, Pitt Ford TR. Physical and chemical properties of a new root-end filling material. J Endod, 1995;21:349–353.

Torabinejad M, Chivian N. Clinical applications of mineral trioxide aggregate. J Endod, 1999; 25(3): 197-205.

Tramini P, Pélissier B, Valcarcel J, Bonnet B, Maury L. A Raman spectroscopic investigation of dentin and enamel structures modified by lactic acid. Caries Res. 2000 May-Jun;34(3):233-40.

Treharne RW, Brighton CT.The use and possible misuse of Tetracycline as a vital stain. Clin Orthop Relat Res. 1979;(140):240-6.

Tsatsas BG, Frank RM. Ultrastructure of the dentinal tubular substances near the dentineo-enamel junction.Calcif.Tiss. Res,1972; 9: 238–242.

Tsuda H, Ruben J, Arends J. Raman spectra of human dentin mineral. Eur J Oral Sci. 1996 Apr;104(2 (Pt 1)):123-31.

Uskoković V., Bertassoni L.E. Nanotechnology in Dental Sciences: Moving towards a Finer Way of Doing Dentistry. Materials. 2010; 3(3):1674-1691.

Van der Veen MH, ten Bosch JJ. The influence of mineral loss on theauto-fluorescent behaviour of in vitro demineralised dentine. Caries Res.1996;30(1):93-9.

Van Meerbeek B, Mohrbacher H, Celis JP, Roos JR, Braem M, Lambrechts P, Vanherle G. Chemical characterization of the resin-dentin interface by micro-Raman spectroscopy. J Dent Res. 1993 Oct;72(10):1423-8.

Villat C, Tran XV, Pradelle-Plasse N, Ponthiaux P, Wenger F, Grosgogeat B, Colon P. Impedance methodology: A new way to characterize the setting reaction of dental cements. Dent Mater. 2010 Dec;26(12):1127-32.

Vollenweider M, Brunner TJ, Knecht S, Grass RN, Zehnder M, Imfeld T, Stark WJ.Remineralization of human dentin using ultrafine bioactive glass particles.Acta Biomater. 2007 Nov;3(6):936-43.

Walls AW. Glass polyalkenoate (glass-ionomer) cements: a review. J Dent. 1986 Dec;14(6):231-46.

Watson TF, Boyde A. Tandem scanning reflected light microscopy: applications in clinical dental research. Scanning Microsc. 1987 Dec;1(4):1971-81.

Watson TF. A confocal optical microscope study of the morphology of the tooth/restoration interface using Scotchbond 2 dentine adhesive. J Dent Res, 1989 ; 68(6):1124-1131

Watson TF, Boyde A. Confocal light microscopic techniques for examining dental operative procedures and dental materials. A status report for the American Journal of Dentistry, 1991; 4(4):193-200.

Watson TF, Billington RW, Williams JA. The interfacial region of the tooth/glass ionomer restoration: a confocal optical microscope study. Am J Dent, 1991; 4(6):303-310.

Watson TF and de J Wilmot DM.A confocal microscopic evaluation of the interface between Syntac adhesive and tooth tissue. J. Dent, 1992; 20: 302-310.

Watson TF. Fact and artefact in confocal microscopy. ADR, 1997; 11: 433.

Watson TF, Pagliari D, Sidhu SK, Naasan MA. Confocal microscopic observation of structural changes in glass-ionomer cements and tooth interfaces. Biomaterials. 1998 Mar;19(6):581-8.

Watson TF (1999). Bonding glass-ionomer cements to tooth structure. In: Advances in glass-ionomer cements. Davidson CL, Mjör IA, editors. Germany: Quintessence Publishing Co. Inc.

Watson TF, Cook RJ, Festy F, Pilecki P, Sauro SE (2008). Optical imaging techniques for dental biomaterials interfaces. In: Dental biomaterials: imaging, testing and modelling. Curtis RV, Watson TF, editors. Cambridge, UK: CRC Press.

Webb H. Confocal optical microscopy. Rep. Prog. Phys, 1996; 59: 427–471.

Wehrmeister, U., Soldati, A. L., Jacob, D. E., Häger, T. and Hofmeister, W. (2010), Raman spectroscopy of synthetic, geological and biological vaterite: a Raman spectroscopic study. J. Raman Spectrosc., 41: 193–201.

Weller RN, Tay KC, Garrett LV, Mai S, Primus CM, Gutmann JL, Pashley DH, Tay FR. Microscopic appearance and apical seal of root canals filled with gutta-percha and ProRoot Endo Sealer after immersion in a phosphate- containing fluid. Int Endod J, 2008; 41:977–986.

White JD, Lacefield WR, Chavers LS, Eleazer PD. The effect of three commonly used endodontic materials on the strength and hardness of root dentin. J Endod , 2002; 28:828-830.

Wilson AD, Prosser HJ, Powis DM. Mechanism of adhesion of polyelectrolyte cements to hydroxyapatite.J Dent Res,198362:590-592.

Xu J, Butler IS, Gibson DF, Stangel I. High-pressure infrared and FT-Raman investigation of a dental composite. Biomaterials. 1997 Dec;18(24):1653-7.

Xu R (2001). Light scattering In: Particle Characterization: Light Scattering Methods. Dordrech: Kluwer Academic, pp 56.

Yadav LDS (2005). Raman spectroscopy In:Organic spectroscopy. New Delhi: Kluer Academic, pp124.

Yiu CK, Tay FR, King NM, Pashley DH, Sidhu SK, Neo JC, Toledano M, Wong SL.Interaction of glass-ionomer cements with moist dentin. J Dent Res. 2004 Apr;83(4):283-9.

Yoshiyama M, Masada J, Uchida A, Ishida H. Scanning electron microscopic characterization of sensitive vs. insensitive human radicular dentin. J Dent Res. 1989 Nov;68(11):1498-502.

Young AM, Sherpa A, Pearson G, Schottlander B, Waters DN. Use of Raman spectroscopy in characterisation of the acid-base reaction in glass-ionomer cements. Biomaterials, 2000; 21:1971-1979.

Zezell DM, Ribeiro AC, Bachmann L, Gomes AS, Rousseau C, Girkin J. Characterization of natural carious lesions by fluorescence spectroscopy at 405-nm excitation wavelength. J Biomed Opt. 2007;12(6):064013.

Zhang X, Neoh KG, Lin CC, Kishen A. Remineralization of partially demineralized dentine substrate based on a biomimetic strategy. J Mater Sci Mater Med. 2012 Mar;23(3):733-42.

Zipfel WR, Williams RM, Christie R, Nikitin AY, Hyman BT, Webb WW. Live tissue intrinsic emission microscopy using multiphoton-excited native

fluorescence and second harmonic generation. Proc Natl Acad Sci U S A. 2003;100(12):7075-80.